Numerical Studies of a Plasma Accelerator Driven Free Electron Laser

A thesis submitted to The Department of Physics
University of Strathclyde /University of Princess Nourah Bint Abdulrahman
for the degree of Doctor of Philosophy

Badriah Mesfer Alotaibi

October 8 , 2019

Abstract

The Free Electron Laser (FEL) is a unique source of tunable, coherent light, that is particularly important towards and into the x-ray region of the spectrum. After the achievement of FEL lasing that is based on conventional acceleration utilizing radio-frequency cavities, a significant challenge is the creation of an compact FEL working with an electron bunching accelerated via plasma-based accelerators. However, electron beams produced by some plasma accelerators with large normalized emittance, significant levels of energy spread and energy chirp are a major challenge towards driving FELs. Novel plasma-based acceleration and injection methods, such as beam driven under dense Plasma photocathode Wake-Field Acceleration (PWFA), promises electron beams with ultra-low normalized emittance, high peak currents and low energy spreads. The plasma photocathode injection method is an advanced plasma based electron injector which releases electrons directly inside a PWFA by selectively laser-ionizing a neutral background gas. A 250 MeV electron beam from a PWFA with a fs-scale duration, mm-mrad normalized emittance and with a natural negative energy chirp is investigated.

This thesis uses simulations to explore the capability of a plasma photocathode to drive an FEL and to investigate the effects of the electron beam energy chirp on lasing. It is shown that removing the energy chirp is a key to enable the high quality beams to achieve FEL lasing. The beam is first used as delivered – with relatively high chirp and then with the chirp removed. The VSim code is used to model the plasma accelerator, and the Puffin code for the FEL process. A dynamically evolving current profile, due to energy chirp changing the electron pulse current profile, induces ballistic bunching at moderate energies. This bunching can generate significant coherent radiation via the process of Coherent Spontaneous Emission (CSE). While this CSE is seen to drive some FEL-induced electron bunching at the radiation wavelength, the dynamic evolution of the energy chirped pulse dampens out any high-gain FEL bunching interaction. When the beam energy chirp was removed numerically, the FEL was shown to lase via the high-gain FEL interaction and exponential gain was demonstrated. Therefore, if the energy chirp of the beam can be reduced experimentally, and on-going research is suggesting this is possible, this opens the prospect of a future PWFA FEL operating in the high-gain regime.

Acknowledgements

Many appreciations and thanks must be given to my supervisors, Dr Brian McNeil (Department of Physics, University of Strathclyde, Glasgow, G4 0NG United Kingdom) and Dr. Sherif Mohamed Khalil (Plasma Physics & Nuclear Fusion Department, NRC, Atomic Energy Authority, Cairo, Egypt), for their patient guidance, enthusiastic encouragement, valuable and constructive suggestions and useful critiques of this research work . Thanks to my university Princess Nourah Bint Abdulrahman University in Riyadh for the funding that made this PhD possible. I must also thank Dr. Piotr Traczykowski for his support and kindness. Thanks to Dr. Lawrence Campbell for helping me in my early studies.

We gratefully acknowledge the support of the(i) King Abdullah University of Science and Technology (KAUST), http://kaust.edu.sa , and (ii) KAUST Supercomputing Laboratory (KSL) Thuwal, Saudi Arabia, for their help in offering me and my colleague Reem, the facilities and resources in running the Shaheen program (Code). A lot of thanks should be given to my family, children, husband, friends and family, too for their encouragement and support.

Contents

List of Figures

Chapter 1

Introduction

1.1 Free Electron Lasers

The Free Electron Laser [1] (FEL) is defined as a unique radiation resource showing many advantages over the conventional atomic lasers because an FEL is tunable over a much broader spectral range into the hard X-ray. This is because the physics of FEL operation differs greatly from the principles of operation of a conventional laser. In an FEL, the process of radiation generation is not based on electrons that are bounded in a gain medium but uses a particle accelerator which provides electrons propagating freely in space. This allows one of the largest limitations of conventional lasers, the quantized gain media that limits the available wavelength range. FELs function in all spectral regions from the far-infrared into hard X-rays. Limited reflectivity of mirrors at the shortest wavelengths are not an obstacle to the FEL as it can start from noise in an amplifier mode of operation. In an FEL a highly relativistic electron beam propagates through an undulator, which is a structure of periodic magnetic dipoles. In the undulator the electrons are forced by the magnetic field onto a sinusoidal path, guiding the emission of synchrotron radiation along the beam path. The radiation wavelength depends on the period length of the magnetic undulator, the strength of the undulator field and the energy of the electrons. It is therefore more tunable when compared to conventional lasers. Doppler frequency up-shifting of the emitted radiation allows FELs to generate radiation in short-wavelength similar to X-rays. Because the electrons travel at near the speed of light, they propagate within the radiation field emitted by other electrons and can interact with this field because of their transverse motion in its electric field.

This interaction leads to an energy exchange between electrons and the radiation and thus the energy of electrons modulate on the scale of the radiation wavelength. Because the trajectory of a charged particle inside a magnetic field is energy dependent, microbunching at the radiation wavelength occurs when the energy modulation becomes converted into a density modulation. The emission process occurs from incoherent to coherent while it is making propagation through the undulator for a sufficiently long interaction distance. The power of the radiation grows exponentially along the undulator and reaches a maximum before the microbunching is smeared out because of the energy dependent trajectories cause the bunch to disperse.

FELs can generate coherent X-ray pulses with a multi-GW peak power and a duration of a few femtoseconds. They are the brightest source of X-ray synchrotron radiation known at this time [2]. Because of these radiation properties, FELs are known as fourth generation of light sources instead of the temporally incoherent third generation synchrotrons.

1.2 Acceleration of electron in plasma

There is a need for researchers to reduce the cost and size of FELs by applying new accelerator techniques. One of these techniques being plasma accelerator (PA). One important application of plasma accelerator is to drive FEL. The potential advantages are offering higher peak currents and the high acceleration gradient. Some Laser driven PAs (LPA) methods offer electron beams that have a smaller transverse emittance, a higher energy per unit length, higher currents and shorter pulse durations than the conventional Radio Frequency (RF) accelerator. Tajima and Dawson were behind the central concept of the LPA [3]. The electrons are accelerated due to the strong electric field within plasma. The possibility of utilizing these accelerators for the sources of light is due to their potential to provide high-energy bunches with similar, or better qualities to conventional RF accelerators. This may lead to a dramatic decrease in both the cost and size of these facilities, and means that they can be more easily housed in industrial, university, or medical laboratories. Researchers would have much more readily available access to intense femtosecond pulses of short wavelength radiation which would dramatically lower the cost to already over-stretched funding bodies. A great many fields of science would be greatly affected by this type of commoditization. Synchrotron radiation production from laser-accelerated electrons has already been seen at soft X-ray wavelengths [4,5]. This is likely to be raised to higher quality of electron beam in the near future. Because of the size of the plasma wake in which they are accelerated, the electron bunches are intrinsically of femtosecond duration, and the corresponding kiloampère peak currents suggest that operation in the FEL regime may be a possibility [6,7].

In this thesis we used simulated electron pulses generated from laser plasma acceleration (LPA), by using VSim code[8], and the Trojan Horse technique (TH) or plasma photocathode were used to make the beam suitable for FELs [9,10].

1.3 FEL Simulation Codes

A free-electron laser (FEL) relies upon the self-amplified spontaneous emission (SASE) process. Linear theory design is characterized by parameters based upon the abilities of the existing linear accelerator and the simulations. Codes used in the design include GENESIS [11], GINGER [12], FAST [13] etc.

FEL simulation codes, such as GENESIS, GINGER, MEDUSA, RON, and TDA3D, show good agreement with each other e.g. in the length of undulator to reach complete FEL saturation. In this thesis the Puffin code [14,15] is used to simulate the FEL interaction. Unlike other codes Puffin is an unaveraged 3D mathematical model and uses parallel CPU methods to model the FEL. In the ‘averaged codes’ the electric field and the electron distribution is averaged over a resonant radiation wavelength and the beam current is assumed constant over each radiation wavelength. This averaging means that the averaged

codes cannot model CSE effects or changes in the electron pulse current due to beam dynamic.

Puffin is a more flexible code without such averaging and was developed to test advanced FEL principles and has led researchers to gain a greater understanding of some new FEL techniques. The Puffin code has undergone much progress and extended its functionality since the start of this thesis. Puffin is currently under active development and an official release will be tagged soon [15]. Puffin is reviewed in chapter 2.

1.4 Outline of the thesis

Chapter 2 will discuss the main FEL theory and extract a set of simplified differential equations to characterize the FEL interaction in the magnetic field and electron motion. Some characteristics of the FEL and conditions to allow the high gain FEL interaction possible are derived to cover the models used such as Puffin. Some descriptions of the modifications of Puffin will be described, which permit a more realistic undulator field to be modeled.

Chapter 3 An overview of the particles of a "compact source of light" plasma accelerator are described. A comparison is described between RF linacs and a plasma accelerator, with a focus on the Trojan Horse technique. The main concept of the beam transport and matching between plasma accelerator and FEL are given, including natural undulator focusing. The effect of electron beam energy spread that hinders coherent FEL radiation generation is explained. The theory of correlated energy spread is also explained and overviewed.

Chapter 4 Novel energy chirp FEL methods will then be elaborated upon in the fourth chapter, with a description of energy chirp impact on FEL performance. Review some methods that remove the energy chirp are also discussed.

Chapter 5 This chapter consists of Start-to-End Simulations which shows all carried steps to deal with a chirped electrons pulse created from plasma accelerator. The electron pulse was generated by a plasma accelerator code VSim and the plasma photocathode method was utilized to make the beam more suitable for application to FELs.

Chapter 6 A summary of results, together with an overview of future work towards realizing a FEL driven by an electron beam from a plasma accelerator with a photocathode.

Chapter2

Theory of the FEL

2.1 Introduction

A free-electron laser (FEL), is defined as a type of laser that uses very-high-speed (relativistic) electrons. These electrons move freely inside an undulator or a wiggler magnetic structure, hence the lasing medium in this system are the free electrons. The free-electron laser has the widest frequency bandwidth of any laser kind, and currently ranges from microwaves to the hard X-ray. In the Free Electron Laser (FEL) a magnetic undulator couples a radiation field to a relativistic electron pulse. This electron-radiation-field coupling leads to a collective instability (a collective feed-back loop), which exponentially amplifies a small initial radiation field.

Figure 2.1 demonstrates the structure of a planar undulator. It consists of two rows of alternating polarity dipole magnets, where the north poles are brown and the south poles are blue poles. This arrangement of magnets produces a sinusoidal magnetic field through the undulator axis. There are two feature regimes of FELs low gain and high gain. In the low-gain regime, the radiation field is amplified and an undulator is placed inside a cavity. Electron pulses pass many times through the cavity where the radiation builds up. The cavity length ensures coincidence between the electron pulses and the radiation each round-trip of the cavity until saturation is reached. In the high-gain regime, radiation is amplified to the level of saturation through one pass of the undulator.

An energy modulation in the electron pulse is produced by the radiation field. This energy modulation is changed into a density modulation by the natural dispersion action of the undulator. This density modulation is described as electron microbunching. The microbunches are periodic at the resonant radiation wavelength. Consequently, they could emit coherently at the resonant wavelength and radiation collectively. The radiation field increases the level of microbunching growing in a collective feed-back loop. In low gain FELs [16,17], this makes the FEL lasing off-resonance condition. In contrast, in high gain FELs [1] the phase of the radiation field develops gradually. This effectively converts the electron microbunches into a phase where the radiation field could be amplified.

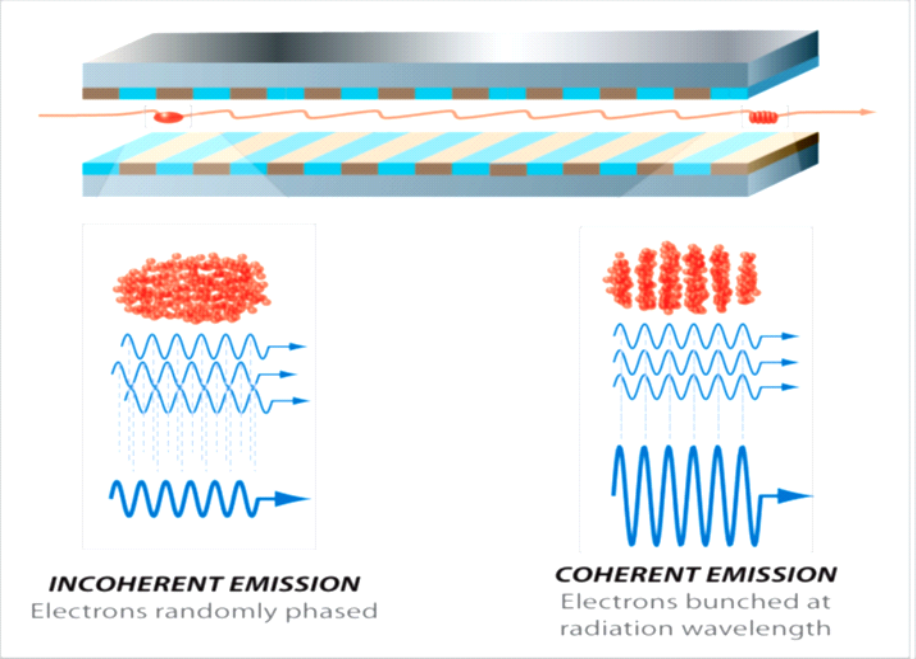

Figure 2.1: shows two sets of alternating dipole magnets in the undulator. The electron pulse radiates through the undulator. As it combines with the radiation field, it bunches the beam at the resonant wavelength. The coherent emission exponentially amplifying the radiation by electron bunches .This figure is from [1].

To find the average resonance condition, consider the radiation travelling at the speed of light c, and the electron at $c\bar{\beta}_z < c$, where $\bar{\beta}_z = \frac{\bar{v}_z}{c}$ is the speed $\bar{v}_z$ of the electron in the direction z as a fraction of c averaged over an undulator period . It will be more useful to consider the average resonant wavelength due to there will be a spread of electron energies (and velocities v_{zj}). For example when the electron pulse has a correlated energy chirp that lead to have correlated resonant frequency. Always the radiation which is emitted by the electron is seen travel ahead of these electron and when a whole number of radiation wavelengths $\lambda_r$propagate ahead of the electron in the time it takes the electron to travel one undulator period $\lambda_u$the constructive interference will occur.

$$\frac{\lambda_u}{c\bar{\beta}_z} = \frac{n\lambda_r + \lambda_u}{c} \qquad (2.1)$$

After which we find the equation for FEL resonance,

$$\lambda_r = \frac{\lambda_u}{n}\left(\frac{1-\bar{\beta}_{zj}}{\bar{\beta}_{zj}}\right) \qquad (2.2)$$

There are two major points to achieve a high quality photon beam [18]. First, a low emittance, high quality electron beam by the advanced particle accelerators allows the

focusing of the beam more tightly to ensure it could be matched to the radiation waist size and the electron transverse size. Next, devolvement of the undulator or wiggler. These unique devices are built up from linear alternating magnets with periodic magnetic dipole field.

The best way to understand the FEL process is by reviewing and discussing the basic theory of FEL.

2.2 Electron motion and magnetic field in the undulator

2.2.1 FEL Spontaneous Emission

To begin, we discuss the important undulator component of the FEL. The undulator is the main core of the FEL. There are two main types of undulators used to produce radiation. They usually either have a "planar" or "helical" magnetic field along the axis of the undulator. The electrons take either a sinusoidal or helical path respectively, which cause the electrons to emit linearly or circularly polarized radiation. In this thesis we used a planar undulator. Figure 2.2 shows a schematic of a planar undulator with the electron passing through it and emitting resonant wavelength radiation.

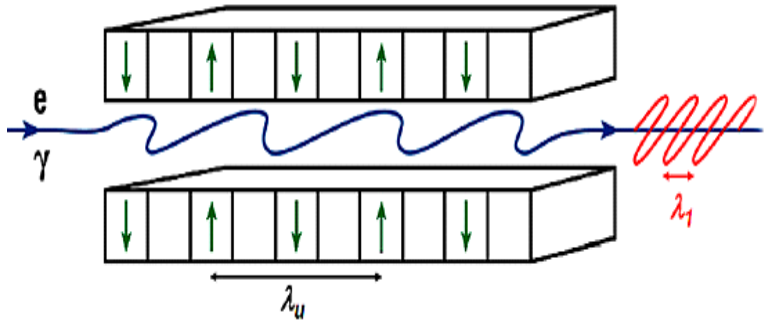

Figure 2.2: Schematic of a planar FEL undulator with the electron propagating and emitting resonant wavelength radiation [2].

First we derived the trajectory of the electron pulse through the helical undulator due to helical undulator allows the simpler description of the FEL interaction because there is no 'jitter' along the propagation z-axis. Close to the center of the undulator, the magnetic field can be described as equation (2.3) [16,17]. The electron pulse takes a helical path through the undulator due to force it by the helical magnetic field is given by,

$$\boldsymbol{B_u} = \frac{B_\circ}{2}\left(\boldsymbol{u}e^{-ik_u z} + c.c.\right) \qquad (2.3)$$

Where $(c.c.)$ is a complex number, and $\boldsymbol{u}$ is the undulator polarization , $\boldsymbol{u} = u_x\hat{\mathbf{x}} + iu_y\hat{\mathbf{y}}$, and in the case of the helical undulator $u_{x,y} = 1$.

$$\boldsymbol{B_u} = \frac{B_\circ}{2}\left[\left(u_x\hat{\mathbf{x}} + iu_y\hat{\mathbf{y}}\right)e^{-ik_uz} + \left(u_x\hat{\mathbf{x}} - iu_y\hat{\mathbf{y}}\right)e^{ik_uz}\right] \quad (2.4)$$

$$\boldsymbol{B_u} = \frac{B_\circ}{2}\left[(u_x\hat{\mathbf{x}})(e^{ik_uz} + e^{-ik_uz}) + \left(-iu_y\hat{\mathbf{y}}\right)(e^{ik_uz} - e^{-ik_uz})\right] \quad (2.5)$$

After applying Euler's relations $2\cos(k_uz) = e^{ik_uz} + e^{-ik_uz}$ and

$$2i\sin(k_uz) = e^{ik_uz} - e^{-ik_uz}$$

$$\boldsymbol{B_u} = B_\circ[\hat{\mathbf{x}}\cos(k_uz) + \hat{\mathbf{y}}\sin(k_uz)] \quad (2.6)$$

Equation (2.6) shows the magnetic field of the helical undulator however, in the case of the planner undulator, the magnetic field is as ,

$$\boldsymbol{B_u} = \frac{B_\circ}{2}\left[\left(-iu_y\hat{\mathbf{y}}\right)(e^{ik_uz} - e^{-ik_uz})\right] \quad (2.7)$$

When the relativistic electrons beam passes along this undulator, the effect of the Lorentz-force causes the alternating magnetic field to deflect them into a sinusoidal path in the case of plannar undulator or helical path in helical undulator. The oscillating electrons then radiate spontaneous undulator radiation. The Lorentz force equation [19] describes the forces of a moving charged particle in any electric and magnetic field:

$$F_j = -e(\boldsymbol{E} + c\beta_J \times \boldsymbol{B}_u) \quad (2.8)$$

In the absence of magnetic fields and the radiation pulse's electric field we calculate the transverse motion of the electron pulses, we can simplify the FEL equations by this assumption. We first assume the electric field of the radiation pulse is small and does not affect the electron pulse's perpendicular momentum.

$$\boldsymbol{F_j} = -ec\beta_j \times \boldsymbol{B_u} \quad (2.9)$$

The relativistic momentum is $p_j = \gamma_j mc\beta_j$ from Newton's third law, where $v_j = c\beta_j$

$$\frac{d\gamma_j\beta_j mc}{dt} = -e(c\beta_j \times \boldsymbol{B_u}) \quad (2.10)$$

$$mc\left(\beta_j\frac{d\gamma_j}{dt} + \gamma_j\frac{d\beta_j}{dt}\right) = -e\left(c\beta_j \times \boldsymbol{B_u}\right) \quad (2.11)$$

We neglect the electric field zero due to energy exchange can be assumed $\frac{d\gamma}{dt} = 0$. This assumption comes from the fact that a magnetic field can't change charged particle's energy. This fact will be demonstrated later, now equation (2.11) becomes,

$$mc\gamma_j \frac{d\beta_j}{dt} = -e\left(c\beta_j \times \boldsymbol{B_u}\right) \qquad (2.12)$$

$$\frac{d\beta_j}{dt} = -\frac{e}{mc\gamma_j}(c\beta_j \times \boldsymbol{B_u}) \qquad (2.13)$$

After calculating the cross product $\beta_j \times B_u$,

$$\beta_j \times \boldsymbol{B_u} = -\hat{\mathbf{x}}\beta_{zj}B_\circ \sin(k_u z) + \hat{\mathbf{y}}\beta_{zj}B_\circ \cos(k_u z) + \hat{\boldsymbol{z}}\left(\beta_{xj}B_u - \beta_{yj}B_u\right)$$

Recombining with (2.13)

$$\frac{d\beta_j}{dt} = -\frac{e}{m\gamma_j}\left(-\hat{\mathbf{x}}\beta_{zj}B_\circ \sin(k_u z) + \hat{\mathbf{y}}\beta_{zj}B_\circ \cos(k_u z) + \hat{\boldsymbol{z}}\left(\beta_{xj}B_u - \beta_{yj}B_u\right)\right) \quad (2.14)$$

The individual components are:

$$\frac{d\beta_{xj}}{dt} = \frac{e}{m\gamma_j}(\beta_{zj}B_\circ \sin(k_u z))$$

$$\frac{d\beta_{yj}}{dt} = -\frac{e}{m\gamma_j}(\beta_{zj}B_\circ \cos(k_u z))$$

$$\frac{d\beta_{zj}}{dt} = -\frac{e}{m\gamma_j}(\beta_{xj}B_y - \beta_{yj}B_x)$$

After that we ignoring the z-component, and using

$$\frac{d}{dt} = c\beta_{zj}\frac{d}{dz}$$

to transform the derivatives into z

$$\frac{d\beta_{xj}}{dz} = \frac{e}{mc\gamma_j}(B_\circ \sin(k_u z))$$

$$\frac{d\beta_{yj}}{dz} = -\frac{e}{mc\gamma_j}(B_\circ \cos(k_u z))$$

After integrating these equations then give,

$$\beta_{xj} = -\frac{e}{k_u mc\gamma_j}(B_\circ \cos(k_u z)) \qquad (2.15)$$

$$\beta_{yj} = -\frac{e}{k_u mc\gamma_j}(B_\circ \sin(k_u z)) \qquad (2.16)$$

We can be defined the scaled undulator parameter as,

$$a_u = -\frac{e}{k_u mc} B_\circ \qquad (2.17)$$

$$\beta_{xj} = -\frac{a_u}{\gamma_j}(\cos(k_u z)) \qquad (2.18)$$

$$\beta_{yj} = -\frac{a_u}{\gamma_j}(\sin(k_u z)) \qquad (2.19)$$

The electron velocity vector is :

$$\beta_j = -\frac{a_u}{\gamma_j}(\cos(k_u z)\hat{\mathbf{x}} + \sin(k_u z)\hat{\mathbf{y}}) + \beta_z \hat{\boldsymbol{z}} \qquad (2.20)$$

In the case of planar undulator , equation(2.25) become,

$$\beta_{xj} = -\frac{a_u}{\gamma_j}(\cos(k_u z)) \qquad (2.21)$$

2.2.2 FEL Electron Bunching

The electrons will exchange energy with the field when an electron beam copropagates with a radiation field, either an externally injected seed or the spontaneous radiation from other electrons, because the undulator provide the transverse oscillation[17].

Once again we look at the Lorentz force equation (2.8), to describe an electron's energy exchange with an electromagnetic field, this case considering only the electric field vector and neglecting the magnetic field and, as

$$(2.22)\boldsymbol{F} = \frac{d}{dt}(\gamma m v) = -e\,\boldsymbol{E}$$

Then multiplying both sides by v which gives ,

$$(2.23)\boldsymbol{v}.\frac{d}{dt}(\gamma m\boldsymbol{v}) = -e\,\boldsymbol{v}.\boldsymbol{E}$$

$$(2.24)\frac{d\gamma}{dt}\boldsymbol{v}.\boldsymbol{v} + \gamma\frac{dv}{dt}.\boldsymbol{v} = -\frac{e}{m}\,\boldsymbol{v}.\boldsymbol{E}$$

$$(2.25)\frac{d\gamma}{dt}\boldsymbol{v}.\boldsymbol{v} + \frac{\gamma}{2}\frac{d\boldsymbol{v}^2}{dt} = -\frac{e}{m}\,\boldsymbol{v}.\boldsymbol{E}$$

From the definition of the relativistic factor equation (2.26) and differentiating this with respect to t, we find,

$$(2.26)\gamma = \sqrt{1+\gamma^2\beta^2}$$

Then we differentia (2.26) with respect to t , to find

$$(2.27)\frac{d\gamma}{dt}\boldsymbol{v}.\boldsymbol{v} + \frac{\gamma}{2}\frac{d\boldsymbol{v}^2}{dt} = -\frac{d\gamma}{dt}c^2$$

$$(2.28)\frac{d\gamma}{dt} = -\frac{e}{mc^2}\,\boldsymbol{v}.\boldsymbol{E}$$

ignoring the field in the y and z directions by assuming a planar undulator, then we obtain

$$(2.29)\frac{d\gamma}{dz} = -\frac{e}{mc}\,\beta_x\boldsymbol{E_x}$$

and equation (2.30) calculated the electron speed in x is as

$$(2.30)\beta_{xj} = -\frac{e}{k_u mc\gamma_j}(B_\circ\cos(k_u z))$$

and also, the radiation field takes the following form,

$$(2.31)\boldsymbol{E} = \hat{\mathbf{x}}|\xi_\circ|\cos(k_r z - \omega_r t + \Phi)$$

where Φ is the phase of the slowly varying complex field envelope,$|\xi_\circ|$ is the complex field envelope , ω_r and k_r are angular frequency and the radiation wavenumber respectively. So from equation (2.29)

$$(2.32)\frac{d\gamma}{dz} \propto -\frac{a_u|\xi_\circ|}{\gamma}\cos(k_u z)\,(\cos(k_r z - \omega_r t + \Phi))$$

$$(2.33)\frac{d\gamma}{dz} \propto -\frac{a_u|\xi_\circ|}{\gamma}(\cos(k_r + k_u)z - \omega_r t + \Phi) + \cos(k_r - k_u)z - \omega_r t + \Phi))$$

We defined the combined ponderomotive well when the electron energy change varies with respect to the phase of the electron, as

$$\theta = (k_r + k_u)z - \omega_r t + \Phi \qquad (2.34)$$

So when equation (2.35) satisfied, the resonant FEL wavelength is satisfied and this allows a continuous slow energy exchange between the electrons and radiation, and equation (2.35) is equivalent to equation (2.2),

$$\frac{d\theta}{dt} = 0 \qquad (2.35)$$

We will define the resonance condition in terms of the undulator by $\bar{\beta}_z$ an expression of the undulator parameters by rearranging the definition of γ,

$$\beta_z^2 = 1 - \beta_\perp^2 - \frac{1}{\gamma^2} \qquad (2.36)$$

Where $\beta_\perp^2 = \beta_x^2 + \beta_y^2$, for planar undulator we used equation (2.18) expression,

$$\beta_z^2 = 1 - \frac{a_u^2}{\gamma^2}\cos^2(k_u z) - \frac{1}{\gamma^2} \qquad (2.37)$$

$$\rightarrow \bar{\beta}_z = \left(1 - \frac{1}{\gamma^2}\left(\frac{a_u^2}{2} + 1\right)\right)^{1/2} \qquad (2.38)$$

$$\lambda_r = \lambda_u\left(\left(1 - \frac{1}{\gamma^2}\left(\frac{a_u^2}{2} + 1\right)\right)^{-1/2} - 1\right) \qquad (2.39)$$

$$\left(1 - \frac{1}{\gamma^2}\left(\frac{a_u^2}{2} + 1\right)\right)^{-1/2} \approx 1 + \frac{1}{2\gamma^2}\left(\frac{a_u^2}{2} + 1\right) - \frac{3}{8\gamma^4}\left(\frac{a_u^2}{2} + 1\right)^2 \ldots$$

Since typically $\gamma = 1000$ we dropping all terms after the second, then the equation becomes

$$\lambda_r = \frac{\lambda_u}{2\gamma^2}\left(1 + \frac{a_u^2}{2}\right) \qquad (2.40)$$

This term $\frac{a_u^2}{2}$ is calculated for the peak magnetic field of planar undulator. However for a helical undulator this term is not halved since the electron oscillates in both x and y from equation (2.41), and equation (2.42) represents the resonance expression for the case of a helical undulator.

$$(2.41)\beta_{\perp} = \frac{a_u}{\gamma_j}(\cos(k_u z)\hat{\mathbf{x}} - \sin(k_u z)\hat{\mathbf{y}})$$

$$\lambda_r = \frac{\lambda_u}{2\gamma^2}(1 + a_u^2) \qquad (2.42)$$

In the resonant wavelength expression $\gamma_r = \langle\gamma_j\rangle$. This condition shows that the resonant wavelength decreases with the electron pulse's resonant energy γ_r for gain wavelength by a factor $1/\gamma^2$. Also, the FEL can tune the resonant wavelength by varying a_u , the undulator parameter, and λ_u the undulator period, where B_u is the peak undulator magnetic field.

So at the resonant energy over many undulator periods electrons will remain at the same phase in the ponderomotive field, and from equation (2.33) the electron energy will be modified by the radiation field and electrons will gain energy and lose energy. This modulation of energy is resulting in a physical bunching in phase space. This bunching changes the amplitude and phase of the radiation field and leads to amplification of the field coherently, which called the FEL lasing process.

2.3 1D FEL equations

From Maxwell equations which describe radiation field bunches electrons equation (2.8) or bunched electrons drive radiation equation (2.43) [1]

$$(2.43)\nabla^2 \boldsymbol{E} - \frac{1}{c^2}\frac{\partial^2 \boldsymbol{E}}{\partial t^2} = \mu_{\circ}\frac{\partial \boldsymbol{J}}{\partial t}$$

Where $J_{\perp} = J.\hat{\mathrm{e}}^* = J_{\mathrm{x}} - iJ_{\mathrm{y}}$ is the transverse current density,

$J_{\perp} = -ec\ \sum_{j=1}^{N}\beta_{\perp}\delta\left(z - z_j(t)\right)$, the delta function tranforms as

$$\delta\left(z - z_j(t)\right) = \frac{\delta(t-t_j)}{\beta_{zj}c} = 2k_r\rho_{FEL}\frac{\delta(\bar{z}_1 - \bar{z}_{1j})}{\beta_{zj}}$$

Since:

$\bar{z} = 2k_u\rho z$ and $\bar{z}_1 l_g = \frac{z - c\bar{\beta}_z t}{(1-\bar{\beta}_z)} => \bar{z}_1 = -{ct}/{l_c}$.

After solving these equations we deduce the following equations (FEL interaction equations[16,17]. The radiation field bunches the electrons equation via (2.44) and (2.45)

and the bunched electrons drive the radiation equation (2.46), via the bunching equation (2.47) [16,17] :

$$(2.44)\frac{d\theta_j}{d\bar{z}} = p_j$$

$$(2.45)\frac{dp_j}{d\bar{z}} = -\left(Ae^{i\theta_j} + c.c\right)$$

$$(2.46)\frac{\partial A}{\partial \bar{z}} + \frac{\partial A}{\partial \bar{t}} = b(\bar{z}, \bar{t})$$

$$(2.47)b(\bar{z}, \bar{t}) = \frac{I(\bar{t})}{I_{pk}}\left|\frac{1}{N}\sum_{j=1}^{N} e^{-i\theta_j(\bar{z})}\right|_{\bar{t}}$$

where $\theta_j = (k_r + k_u)z_j - \omega_r t$ is ponderomotive force phase space , $p_j = \frac{\gamma_r - \gamma_j}{\rho_{FEL}\gamma_r}$ is the scaled energy change, and $\rho_{FEL}|A|^2 \equiv \frac{P_{rad}}{P_{beam}}$ is the efficiency of the high-gain FEL amplifier and for interaction characterized by FEL parameter, ρ is the FEL Pierce parameter is given by $\rho_{FEL} = \frac{1}{\gamma_r}(\frac{a_u\omega_u}{4ck_u})^{2/3}$, typically $\rho_{FEL}\sim 10^{-3} - 10^{-4}$, $|A|^2$ is the scaled EM field intensity,.

We will now use the FEL interaction's equations to investigate the high-gain regime by solving them with initial conditions, uniform distribution of phases $\theta_j = (0,2\pi]$, weak initial EM field $A \ll 1$, $p_j = \delta$, where δ is the initial detuning on the electron energy, and observe how the EM field and electrons evolve in the steady-state approximation (linear analysis). Steady state assumes a continuous e$^-$beam limit where the electron 'pulse' forms a uniform current which has no beginning or end. In this case one can see that the radiation field can only be a function of the distance through the undulator and no pulse effects can be present. Steady-state approx., no pulses so from equation (2.19) there is no 'time' dependence so that $\frac{\partial A}{\partial \bar{t}} = 0$ and $b(\bar{z})$ only.

$$\frac{db}{d\bar{z}} = iP - i\delta b \qquad (2.48)$$

$$\frac{dP}{d\bar{Z}} = -A + i\delta P \qquad (2.49)$$

$$\frac{dA}{d\bar{z}} = b \qquad (2.50)$$

where $P = \langle p_1 e^{-(\theta_0 + \delta z)}\rangle$and $b = -i\langle \theta_1 e^{-(\theta_0 + \delta z)}\rangle$.

Now we have the final form of linearized equations. There are 3 coupled linear differential equations. We using Laplace transforms to solve them[17].

First we assume resonance $\delta = 0$ that then differentiating linear equations are (2.30 ,2.26), we look for solutions equation (2.32)

$$\frac{d^2A}{d\bar{z}^2} = \frac{db}{d\bar{z}} = -iP \qquad (2.51)$$

$$\frac{d^3A}{d\bar{z}^2} = -i\frac{db}{d\bar{z}} = iA \qquad (2.52)$$

$$A(\bar{z}) = A_0 e^{i\lambda\bar{z}} \qquad (2.53)$$

Figure 2.3 shows a schematic of the solution away from resonance $\delta \neq 0$, the dispersion relation is

$$f(\lambda) = \lambda^3 - \delta\lambda^2 - 1 = 0 \qquad (2.54)$$

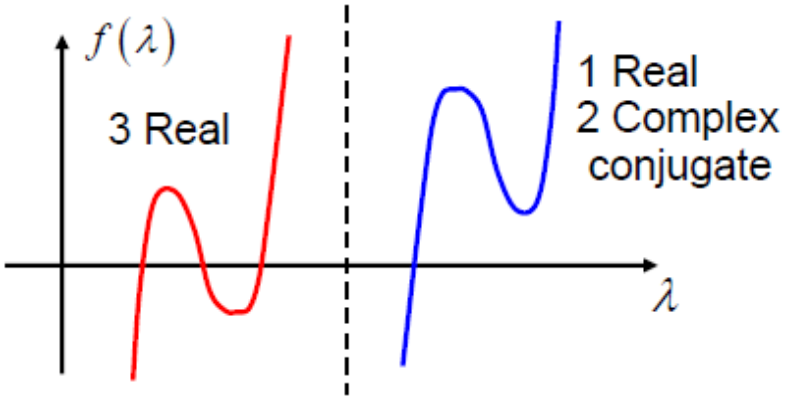

Figure 2.3: shows a schematic of the different solutions of the FEL equations when $\delta \neq 0$.

solution for $\delta = 0$ is equation (2.54) for real parts give oscillatory solutions , but for imaginary parts give $\left(-i\frac{\sqrt{3}}{2}\right)$ exponential growth for $\bar{z} > 1$ and $\left(i\frac{\sqrt{3}}{2}\right)$ exponential decay figure 2.4.

$$A(\bar{z}) = \frac{A_0}{3}\sum_j e^{i\lambda_j\bar{z}} \text{ for } \lambda_j = \left[-1; \left(\frac{1}{2} + i\frac{\sqrt{3}}{2}\right); \left(\frac{1}{2} - i\frac{\sqrt{3}}{2}\right)\right] \qquad (2.5)$$

where $\bar{z} = \frac{z}{l_g} = \frac{4\pi\rho z}{\lambda_u}$ is the scaled position in undulator

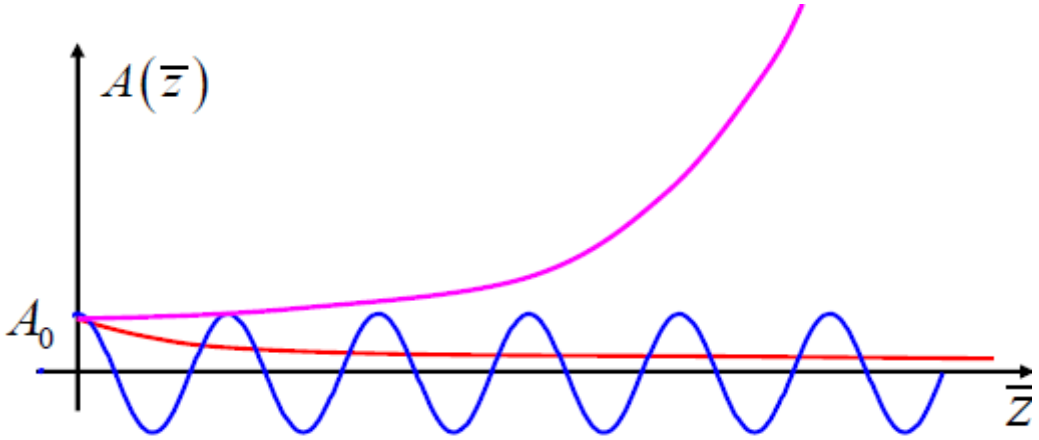

Figure 2.4: shows a schematic of the different solutions of the FEL equations when $\delta = 0$, (blue) real part with oscillatory solutions, (red) imaginary parts with the exponential decay, and last curve is the exponential growth.

2.4 Some Properties of the FEL

There are also other significant properties to the scale of amplification of FELs and their radiation:

Saturation

Saturation is nonlinear process which stop FEL lasing. The saturation power is described as [19]

$$P_{sat} \approx \rho_{FEL} P_{beam} \qquad (2.56)$$

$P_{beam}$is the power of electron beam which given by $P_{beam} = \frac{\gamma mc^2 I_{peak}}{e}$. This equation shows that the Pierce parameter ρ_{FEL} measures the efficiency of an FEL. The saturation length can be approximated by this equation when the undulator length reaches maximum power [2]:

$$L_{sat} \approx \frac{\lambda_u}{\rho_{FEL}} \qquad (2.57)$$

In conclusion, the Pierce parameter ρ_{FEL} should be large in order to augment the saturation power. On the contrary, lasing requires that we find a small value to decrease the bandwidth of the FEL. We must establish a balance between radiation and saturation power.

Bandwidth

A vital characteristic of FEL radiation is bandwidth $\sigma_{\omega,sat}$. The ability of the free-electron laser's bandwidth to amplify detuned radiation needs to be taken into account seeing as it is not based on interference only in contrast to bandwidth of the undulator radiation. We can approximate the FEL bandwidth by ρ_{FEL} the Pierce parameter:

$$\frac{\sigma_{\omega,sat}}{\omega_l} \approx \rho_{FEL} \qquad (2.58)$$

Cooperation length

Cooperation length is also a key characteristic of an FEL. It is defined as the distance slipped by a photon with respect to the electron over one gain length during the bunch propagation [20]:

$$l_c = \frac{L_{g,1D}}{\lambda_u}\lambda_l \qquad (2.59)$$

Emittance

The one dimensional theory is not included in this concept as it is defined as a parameter that characterizes the transverse beam phase space. As all real electron beams have a finite transverse size and a transverse momentum spread there is a change in the beam envelope along the setup. Particle beam size is characterized by its emittance and strength of focusing channel given be beta function [2]. Emittance can be roughly described as an area or volume in the particles' phase space see figure 2.5. For each spatial direction there are two phase space variables for a particle and these are x, p_x, y, p_y, z, and p_z with time as the independent variable. These coordinates correspond to the particle's position and momentum components.

With respect to an ideal particle, the coordinates are frequently assumed to be the errors in position and momentum. An ideal particle, for instance, would lie along the ideal trajectory through the machine and would have no transverse momentum component, $p_x = 0$. Longitudinally, the energy or momentum of a particle can be defined as different from the ideal (non-zero) momentum or energy [21].

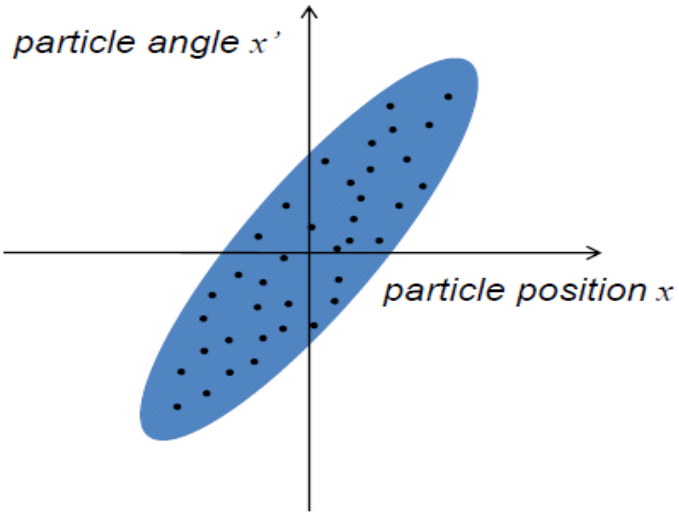

Figure 2.5: shows the definition of Emittance [21].

Normalized emittance

The idea of fixed emittance can still be used if the emittance is scaled according to the beam energy $\epsilon_n = \epsilon(\beta\gamma)$. Here, beam energy defines the relativistic parameters of β and γ. The normalized emittance ϵ_n, then stabilizes as a beam changes energy [21].

Energy Spread

Energy spread is considered an important aspect of all free-electron lasers. The third-order differential does not touch upon this effect. As mentioned in chapter 3, one effect of emittance is limiting the matched beam radius and the interaction coupling in the 1D FEL parameter. Another effect is introducing an energy spread in the resonant energies of the electron beams. This spread exhibited by [21]:

$$\sigma_\epsilon = \frac{\epsilon_n a_u^2 k_u^2 \beta}{4\gamma_r(1+a_u^2)} \qquad (2.60)$$

where σ_ϵ is the resonant effective energy spread due to the emittance. The total effective energy spread given by

$$\sigma_{eff} = \sqrt{\sigma_\gamma^2 + \sigma_\epsilon^2} \qquad (2.61)$$

σ_γ is the homogenous energy spread . The energy spread requirement is a big challenge in plasma accelerator driven FEL..

Some important conditions to have a high gain FEL interaction are [1,2,19]

$$\sigma_\gamma/\gamma \leq \rho_{FEL} \qquad (2.62)$$

Homogenous energy spread and resonant energy spread are less than the FEL Pierce coupling parameter due to ρ_{FEL} is the gain bandwidth [2].

Also, we have another condition,

$$\epsilon_n \leq \frac{\gamma\lambda_r}{4\pi} \qquad (2.63)$$

2.5 Modelling computers

The FEL simulation codes are very important in designing FEL facilities and understanding the theory of FEL physics. There are also several codes that have been used as to compare in experiments that perform these tasks extremely well. In this section we will discuss the modelling computer programs that we used in the simulation and analysis of the data by code simulations. We will start with the Ming Xie estimates without the need for FEL simulation using electrons and fields. To optimize the FEL performance, this was the first step used over the calculations. Then we moved on to a FEL simulation code.

2.5.1 Ming Xie's Fit

One widely used scaling is the 'Ming Xie' formalism [22,23]. This combines many degrading effects of importance for short-wavelength FEL. The basis of this scaling an interpolation of a variational approximation of the evolution of the fundamental mode. The Ming Xie scaling is suitable for short-wavelength systems. This formalism allows us to obtain quick estimates of performance for short-wavelength FELs without using simulations. It is an extremely valuable tool prelim set-up optimizations and parameter scans. For laser-plasma based set-ups, especially those operating in, or close to the bunch length limited regime, this extended scaling is of particular interest. The underlying basic concept is the scaling of 1D gain length due to contribution from energy spread n_γ , emittance n_ϵ , and diffraction n_d. The 3D gain length using this formalism in these conditions is given by [2]:

$$L_{g,3d} = L_{1d}\left(1 + \Lambda\left(n_\gamma + n_\epsilon + n_d\right)\right) \qquad (2.64)$$

Where Λ is the scaling parameter as a function of $\left(n_\gamma + n_\epsilon + n_d\right)$. The degradation factor is a function of the three scaled parameters characterizing the impact of:

Energy spread

$$n_\gamma = 4\pi\left(\frac{L_{1d}}{\lambda_u}\right)\sigma_{\Delta,rms} = \frac{1}{\sqrt{3}}\frac{\sigma_{\Delta,rms}}{\rho_{FEL}} \qquad (2.65)$$

a spread in the radiation wavelength causes by an electron beam with slice energy spread $\sigma_{\Delta,rms}$, according to the resonance equation (2.14) condition. To have a good lasing the slice energy spread need to be strictly smaller than the Pierce parameter [1,2,24]

$$\sigma_{\Delta,rms} < \gamma\rho_{FEL} \qquad (2.65)$$

where $\sigma_{\Delta,rms}$ is the uncorrelated (slice) energy spread

Emittance

$$n_\epsilon = \left(\frac{L_{1d}}{\beta_{av}}\right)\left(\frac{4\pi\epsilon_n}{\lambda_r\gamma}\right) \qquad (2.66)$$

Where ϵ_n is the normalized transverse emittance which related to the electron divergence ($\epsilon_n = \gamma\epsilon$), β_{av} and represents an abstract formulation of the electron beam envelope. It is the average Twiss β -function.

Diffraction

$$n_d = \frac{L_{1d}}{Z_R} = \frac{L_{1d}\lambda_r}{2\pi\sigma_r^2} \qquad (2.67)$$

Where Z_R is the radiation Rayleigh length. This parameter takes the transverse radiation field diffraction. The saturation power for a specific parameter set can be approximated by using the electron beam power P_{beam}.

$$P_{sat} \approx 1.6\rho_{FEL}\left(\frac{L_{1,D}}{L_{g,3D}}\right)P_{beam} \qquad (2.68)$$

2.5.2 Puffin Code

As previously mentioned in section (3.1) , there are several FEL simulation codes; for example Genesis[11]. It is probably the most widely used FEL code today. This code reduces the computation time by making several limiting assumptions. Of these, one of the most important is period averaging.

As with all FEL simulators that average the interaction equations over a radiation wavelength, Genesis is not able to model any sub-period phenomena like, for example, coherent spontaneous emission (CSE). The range of frequencies that can be modelled is also limited.

The simulations presented in this thesis were performed using the unaveraged Puffin, (Parallel Unaveraged FEL Integrator) FEL simulation code. It is written mostly in Fortran 90, using MPI and Open MP. The initial publication, describing the first version of the code, was in 2012 [14] . It defined this code as the first 3D unaveraged, broadband FEL computer simulation code. This includes 3D modelling of the electron beam and radiation field using an unavaraged system of equations in a variably polarized, modular undulator. Puffin therefore simulates the interaction of 6D electron beams (3 dimensions in momentum space and 3 spatial dimensions) and 3D radiation fields. As Puffin integrates in a 6D phase space this can be computationally intensive. To compensate for this, Puffin is used in Fortran 90 under the MPI-standard. MPI standard (Message Passage interface). MPI allows Puffin to run on a supercomputer across several computational nodes. In this thesis we used Shaheen [25], a Cray XC40 supercomputer installed at King Abdullah University of Science and Technology (KAUST) since June 2015.

Another reason to run Puffin on a high performance machine, is that Puffin's 6D phase space can require a large amount of local memory (10-100GB). These typically greatly exceed the space available on (average) desktop computers. It is better to run Puffin on a cluster to minimize computation time, even in the 1D limit. Computation may be reduced from days to hours and local computing power is freed up. Since its inception, Puffin has been used in several publications, e.g. [26,27], with slight changes in the algorithm(s). The code has evolved over time and is now able to perform in more realistic scenarios with more flexible input. Initially, Puffin was published with an OS license and it was developed on Github [28]. We used Puffin code to obtain the results given in chapters 4-6.

Also, in this thesis we used Paraffin code to match the electron beam to natural focusing channel [2] using the script in [29]. Besides that, we used some scripts to prepare the electron beam to become suitable to be used with Puffin. As the original macroparticles distribution from the plasma accelerator is too sparse, and doesn't possess enough macroparticles per resonant wavelength, a procedure of up-sampling the beam and applying proper noise characteristics was used via the JDF scripts [30,31]. The procedure uses cumulative distribution function to obtain the original beam parameters. The new beam with much higher density of microparticles with the correct noise statistics is then created. The newly created beam parameters, such as current, emittance, energy spread etc., are almost unchanged when compared to those of the original beam of macroparticles from the plasma accelerator.

2.6 Outline of FEL equations

The up-to-date system of equations are written in terms of the normalized magnetic fields b_z (longitudinal) and $b_\perp = b_x - ib_y$(transverse), where the magnetic field is

$B_u(x,y,z) = B_0(b_x\hat{x} + b_y\hat{y} + b_z\hat{z}$ with $B_\circ$ being the peak magnetic field . The equations are[14,15]

$$\left[\frac{1}{2}\left(\frac{\partial^2}{\partial\bar{x}^2}+\frac{\partial^2}{\partial\bar{y}^2}\right)-\frac{\partial^2}{\partial\bar{z}\partial\bar{z}_2}\right]A_\perp = -\frac{1}{\overline{n_p}}\frac{\partial}{\partial\bar{z}_2}\sum_{j=1}^{N}\frac{\overline{p_{\perp_J}}}{\Gamma_j}(1+\eta p_{2j})\delta^3(\bar{x_j},\bar{y_j},\overline{z_{2J}}) \tag{2.69}$$

$$\frac{d\bar{p}_{\perp j}}{d\bar{z}} = \frac{1}{2\rho}\left[i\alpha b_\perp - \frac{\eta p_{2j}}{k^2}A_\perp\right] - ik\frac{\bar{p}_j}{\Gamma_j}(1+\eta p_{2j})\alpha b_z \tag{2.70}$$

the development of electron axial coordinates are presented by

$$\frac{d\Gamma_j}{d\bar{z}} = -\rho_{FEL}\frac{(1+\eta p_{2j})}{\Gamma_j}(\bar{p}_j A_\perp^* + c.c.) \tag{2.71}$$

$$\frac{d\bar{z}_{2j}}{d\bar{z}} = p_{2j} \tag{2.72}$$

$$\frac{d\bar{x}_j}{d\bar{z}} = \frac{2\rho_{FEL}k}{\sqrt{\eta}\Gamma_j}(1+\eta p_{2j})R(\bar{p}_j) \tag{2.73}$$

$$\frac{d\bar{y}_j}{d\bar{z}} = -\frac{2\rho_{FEL}k}{\sqrt{\eta}\,\Gamma_j}(1+\eta p_{2j})3(\bar{p}_j) \tag{2.74}$$

where

$$\bar{z}_{2j} = \frac{ct_{j-}z}{l_c}, \qquad \bar{z} = \frac{z}{l_g},$$

$$\bar{p}_\perp = \frac{p_\perp}{mca_{u0}}, \qquad A_\perp = \frac{ekl_g}{\gamma_0 mc^2}E_\perp,$$

$$(\bar{x}+\bar{y}) = \frac{(x,y)}{\sqrt{l_g l_c}}, \qquad l_g = \frac{\lambda_w}{4\pi\rho_{FEL}},$$

$$l_c = \frac{\lambda_r}{4\pi\rho_{FEL}}, \qquad \Gamma_j = \frac{\gamma_j}{\gamma_0},$$

$$\rho_{FEL} = \frac{1}{\gamma_0}\left(\frac{a_{uo}\omega_p}{4ck_u}\right)^{2/3}, \qquad a_{u0} = \frac{eB_0}{mck_u},$$

$$k = \frac{a_{u0}}{2\rho_{FEL}\gamma_0}, \qquad b_\perp = b_x - ib_y,$$

$$\eta = \frac{1-\beta_{z0}}{\beta_{z0}}\ , \qquad \eta p_{2j} = \frac{1-\beta_{zj}}{\beta_{zj}}\ ,$$

a_{u0} is the peak undulator parameter, $\beta_{z0} = \frac{v_{z0}}{c}$ shows the velocity of reference particle with energy γ_0 averaged and $b_{x,y,z} = B_{x,y,z}/B_0$ are the scaled magnetic fields in *x*, *y* and *z*, respectively, and B_0 is the peak on-axis magnetic field.

Chapter3

Plasma accelerator driven FEL

3.1 Introduction

Particle accelerators have applications across many disciplines and they are also important to scientists studying the physics of high energies. The underlying goal is to use a strong electric field to accelerate charged particles. However, a common limitation is that the material wall tends to break down when the fields exceed 10 to 100 MV/m [32,33]. To circumvent this obstacle, kilometer-long accelerators are created so the system can withstand higher energies. Another problem of the conventional accelerator is the high cost which rules it out as a viable solution. In an attempt to bypass the issue, in the late 1970s Tajima & Dawson proposed an alternative to the conventional accelerator. Their concept modeled laser-generated plasma wakes to accelerate the particles [3]. Their efforts resulted in cost savings and a more efficient design. Figure 3.1 shows in the case of a) we want 1mm to get => 100 MeV with Electric field > 100 GV/m, and (b) in RF cavity we need 1 m to get => 100 MeV Gain with Electric field < 100 MV/m [34]. A framework for this model began taking shape in the 1980s. The main benefit of the model was the plasma's ability to withstand electric fields surpassing 100 GV/m without significant degradation of its ability of accelerate the electron. Likewise, the interaction between the plasma and a laser beam generates the accelerating electric field. This thesis will only concentrate on the plasma photocathode that was used to allow the beam suitable for FELs [9,10,18]. It is a promising scheme in the plasma acceleration mechanism which makes an electron bunch with ultra-low emittance and high brightness. Figure 3.2 shows a plasma photocathode technique [35].

Plasma Cavity

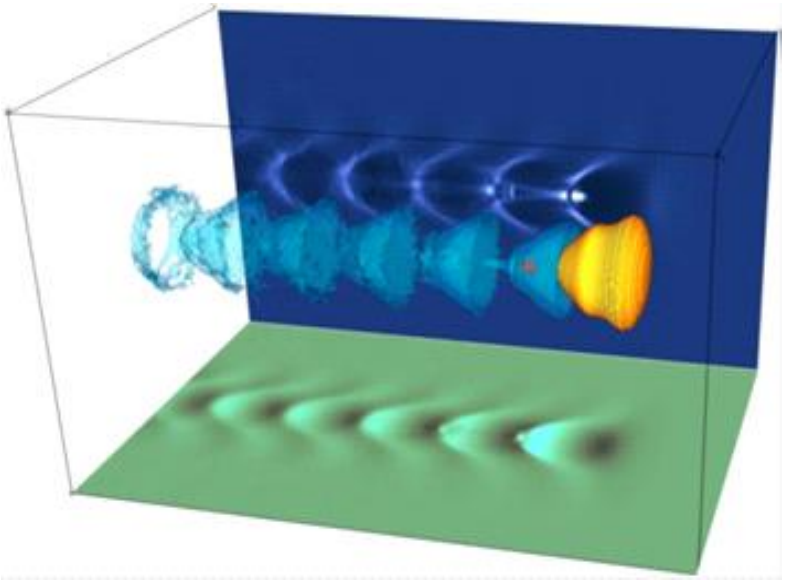

RF Cavity

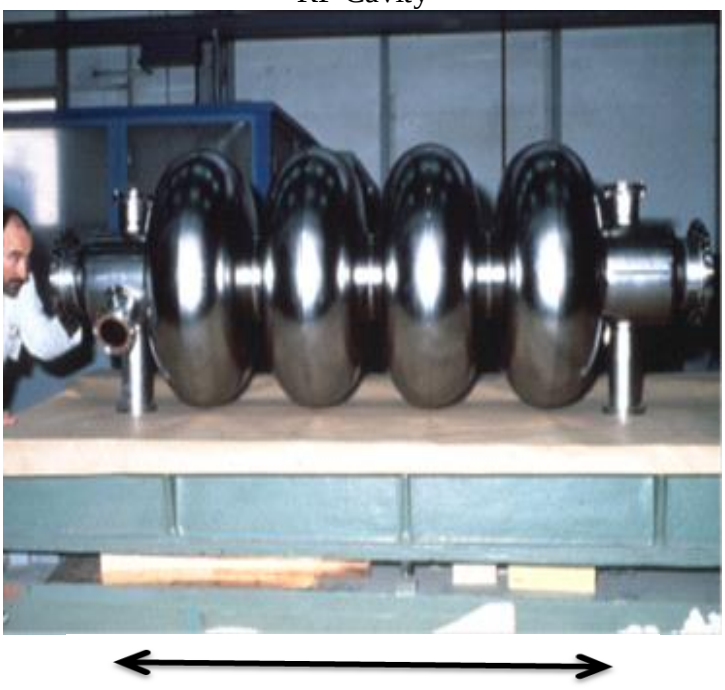

Figure 3.1: comparison between a) plasma accelerator and, b) RF linacs [34].

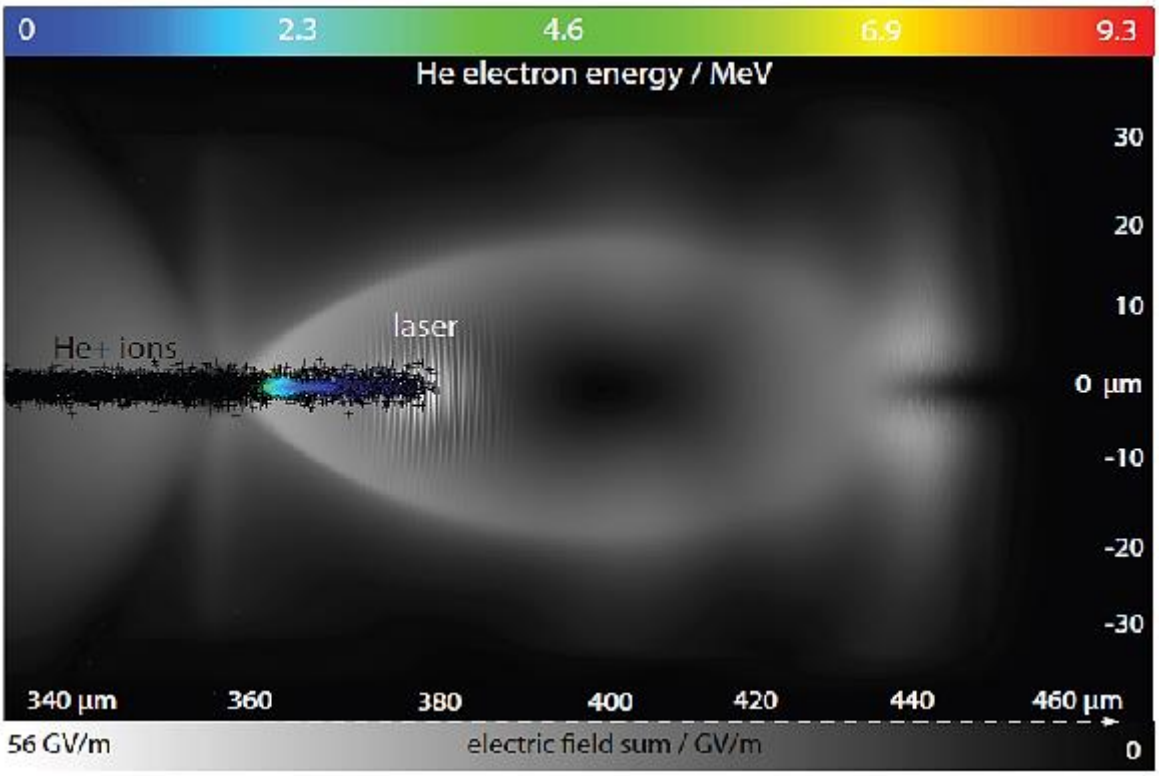

Figure 3.2: indicates screening of the generated beam space charge forces within the initial phase of the acceleration via HIT medium ions on axis [35].

3.2 Plasma photocathode

The plasma photocathode approach [9, 10, 36] is a method which has been developed to overcome the limitations of the laser plasma accelerator. It uses tunneling ionization of a higher ionization threshold gas or component in the plasma by a focused laser pulse directly into the plasma wave. This 'plasma photocathode' can be made in electron-beam driven plasma wakefield accelerators (PWFA) as well as, in principle, laser-driven plasma wakefield accelerators (LWFA). PWFA-based plasma photocathodes combine natural advantages of PWFA, such as dark-current-free and phase-constant operation, and long acceleration lengths with far-reaching decoupling between the plasma medium which supports the wakefield (e.g. hydrogen as low-ionization threshold (LIT) medium) and the one that supports the plasma photocathode medium (e.g. helium as the higher-ionization-threshold HIT medium). From figure 3.2 we can see the black crosses which indicate that the HIT ions, indicates that when the electrons have reached a considerable energy of a few MeV, the screening phase can be effective [35]. In this way, an electron driver beam sets up a hydrogen-based plasma wave, while a synchronized laser pulse is focused inside the bubble. The laser intensity is such that it exceeds the tunneling ionization threshold of helium only about the focus. It is helped by the strong nonlinear rates of ionization scaling. This way, the laser pulse releases electrons confined in the hydrogen plasma bubble, and with very small residual transverse momentum due to the

relatively low intensities and ponderomotive potential of the plasma photocathode laser pulse. This leads to a well confined initial transverse phase space and so a low emittance of the produced electron bunches. The multi- GV/m electric plasma wakefields then rapidly accelerate and compress the released helium electrons and help reduce emittance growth caused by space charge. This allows production of electron bunches with ultralow normalized emittance $\epsilon_n$and high-current I and thus in theory ultrahigh 5D-brightness $B_{5D} = \frac{I_P}{\epsilon_{n,x}\epsilon_{n,y}}$, exceeding those obtainable from conventional accelerators by orders of magnitude. In addition, methods are under development [18,37] which can further reduce the energy spread of bunches produced by plasma photocathodes via tailored beam-loading in phase-constant PWFA's, which promise to decrease the energy chirp substantially to obtain high 6D-brightness electron beam production as drivers for next-generation light sources. The driver electron beam employed to excite the hydrogen PWFA based accelerator structure where the central plasma photocathode mechanism can be realized, may come from a linac, but also may come from a compact laser wakefield accelerator, as many characteristics of LWFA electron beam output such as high current and charge density and modest energy spread and emittance are not prohibitive for driving a PWFA stage [10, 38]. The natural synchronization of the plasma photocathode laser pulse with the laser pulse-generated electron beam drive beam is an advantage of this compact, all-optical solution [10, 38].

3.3 Beam Matching

Compact laser plasma accelerators are capable of generating high energy electron beams with a high peak current and a low emittance. However, a large energy spread and divergence are common downfalls of the plasma accelerator. This outcome is related to the increasing energy spread hindering the potential applications for the coherent radiation generation of free-electron laser FEL. The effect of beam energy spread on FELs is best understood by examining the undulator resonant wavelength equation (2.7). A spread in the average beam energies, results in a spread of the resonant condition equation (2.40) and a reduction in FEL gains condition (2.28) [39]. Under ideal conditions, the minimal requirement for getting high gain FEL is:

$$(3.1)\ \sigma_\delta = \frac{\sigma_\gamma}{\gamma_r} \leq \rho_{FEL} = \left[\frac{1}{16}\frac{I_{peak}}{I_A}\frac{K^2[JJ]^2}{\gamma_r^3\sigma_x^2k_u^2}\right]^{1/3}$$

where , σ_γ is the energy spread, ρ_{FEL} is the Pierce parameter [10] , I_{peak} is the beam peak current, $[JJ] = [J_o(\xi) - J_1(\xi)]$ with $\xi = K^2/(4 + 2K^2)$ is set of Bessel functions for a planar undulator, $I_A \approx 17$ kA is the Alfven current, $k_u = 2\pi/\lambda_u$ and σ_x is the average r.m.s transverse beam size in the undulator. The large energy spread and the large

divergence of the beam generated from a plasma accelerator resulted in extremely low gains with respect to the undulator length. There are many techniques for manipulation to deal with the realistic high energy spread and high divergence [40-43].

LPA beams have quite large divergence and energy spread due to the difficulties in controlling the injection process. Determination of the estimated growth rate, saturation length, equivalent input power and saturation power requires the parameter ρ as seen above. So far ρ has only been defined via the electron beam density n_{pk}.

When the beam current is known, estimates of real quantities can be obtained after determination of the transverse structure of the beam to calculate n_{pk} .

The normalized emittance of the beam ε_n can be used to determine the radius of an electron beam when matched to a linear transverse focusing channel [2].

$$(3.2)\quad r_b = \sqrt{\frac{\varepsilon_n \beta}{\gamma_r}}$$

where β is the $\beta-$function for the focusing channel [20].The $\beta-$function is the inverse of the betatron wavevector $\beta = k_\beta^{-1} = \lambda_\beta / 2\pi$[2].

Where λ_β is the betatron wavelength. As it propagates through the channel a beam maintains a quasi-constant radius when matched to the constant strength focusing channel of the undulator field.

The beam envelope may oscillate as it propagates through the undulator and the beam radius will not remain constant if the beam is not matched and/or the strength of the focusing channel is not constant.

Previous numerical studies [44] show that l_g (FEL gain length) is optimized for a matched beam and from here on the matching is assumed. In this thesis we matched the beam using the natural focusing of the undulator [2] .

In the absence of any external focusing system, such as a FODO quadropole system, the natural focusing β function is given by:

$$\beta = \frac{f\gamma_r}{a_u k_w} \qquad (3.3)$$

where the focusing parameter $f = 1$ for a helical undulator in both the x and y directions of the transverse plane. For a planar undulator with at pole faces $f = 1$ in the plane of the undulator field.

3.4 Electron Beam Requirements

This section further explores how the quality of the electron beam effects XFEL performance. This information enables one to deduce the minimum requirements for the beam properties.

1-Primarily, the undulator configuration for a specific resonance wavelength is used to determine the electron beam energy requirement.

2-Slice energy spread is an important factor; it has to satisfy the condition presented in equation (2.62). The results can be used to extrapolate the upper boundary range $\sigma_{\Delta,rms} < 0.1 - 0.5\%$ with a degree of certainty. The range may vary due to the configuration and precision of the undulator used.

3-The potential range of required norm. emittance is dependent upon the energy spread.

4-Preferably, the peak current should exceed 1 kA and fall within a 2−4 kA range. However, more realistic simulation in section 3.5 gives current to 9 kA [45,46]

The electron beam quality plays an important role in FEL laser gains. Current, transverse size, divergence (i.e., emittance), charge, energy, and energy spread play a role in these gains.

The magnetic field period and strength are important properties of the undulator. As gains increase, the undulator length required to reach saturation decreases. Additionally, as beam quality increases, the final output power increases as well [47].

3.5 Energy spread Simulation

A study was first carried out for a range of parameters using the Ming Xie formalism - see section (2.5.1). These analytical calculations of FEL performance which do not need any significant computation, estimates important parameters such as the gain length, while taking into account many electron beam and 3D effects, such as radiation diffraction. The estimates obtained are a quick and useful way for optimizing FEL output and other parameters such as the gain length.

The FEL simulation code Puffin was also used in a steady-state mode, which has periodic boundary conditions applied over one wavelength of the radiation field/electron beam [48]. Full 3D-Puffin simulations were used to model a LPA driven FEL which assumed Gaussian distributions for the electron pulse duration and other electron parameters. An electron bunch with LPA–like parameters as given in Table.1 was used here for different values of uncorrelated energy spreads 0.0-1.0% [45,46].

Parameters	Value Parameters
Normalized emittance (ϵ_n)	0.2 mm mrad
Normalized beam energy (γ)	600 MeV
Peak current (I_{peak})	9.6 kA
Bunch charge current (Q)	40 pC
RMS energy spread (σ_γ)	(0.0, 0.25, 0.5, 0.75, 1.0)%

Table 3.1: Output parameters from LPA.

The Ming Xie formalism of [22,23] was used to determine the effect of many beam parameters in Table.1, such as electron beam emittance and energy spread on the undulator length to allow high power saturated radiation output. Figure 3.3 shows contour plots of **(a)** Pierce parameter ρ_{FEL} **(b)** RMS transverse sizes of the electron beam $\sigma_{x,y}$ and **(c)** resonant wavelength against λ_u and a_u using the parameters of Table 3.1. This resulted in the parameters of Table 3.2 being chosen.

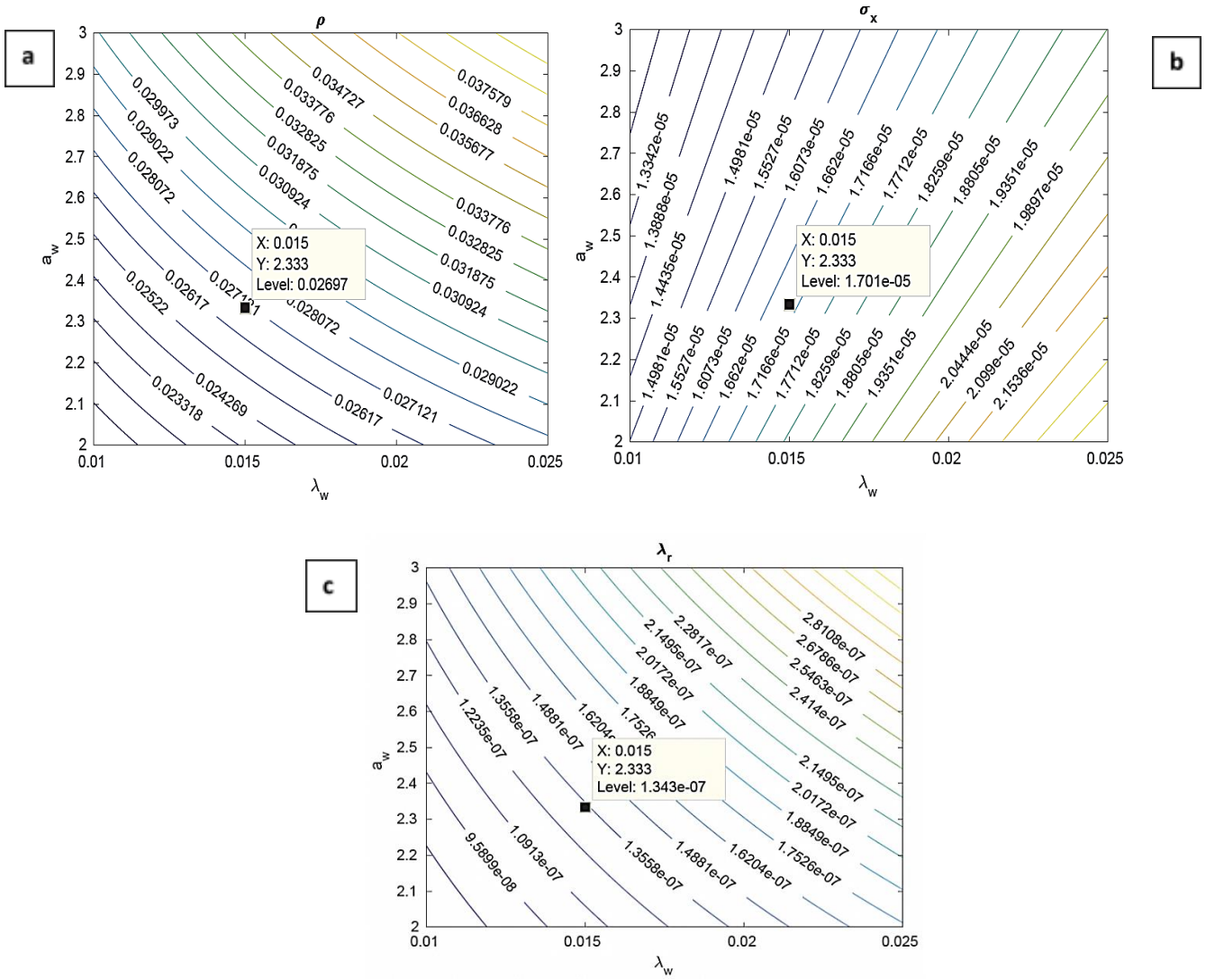

Figure 3.3: Contour plots of (a) ρ_{FEL} , (b) $\sigma_{x,y}$and (c) λ_r against undulator period λ_u and undulator parameter a_u and SI units are used.

Parameters	Value Parameters
ρ_{FEL}	0.0269
L_{sat}	0.83 m
λ_r	1.34×10^{-7} m=134 nm
$\sigma_{x,y}$	1.7×10^{-5} m

Table 3.2: Output parameters from Ming Xie formalism.

These parameters were then used in the Puffin simulation code in steady-state mode. L_{sat} is the saturation length, which can be approximated by $L_{sat} \approx 20 l_g$ [49]. Figure 3.4 shows a comparison between the radiation energy of different values of energy spreads σ_γ in

steady state mode. For energy spread σ_γ/γ much less than ρ_{FEL} the saturation power is not significantly affected.

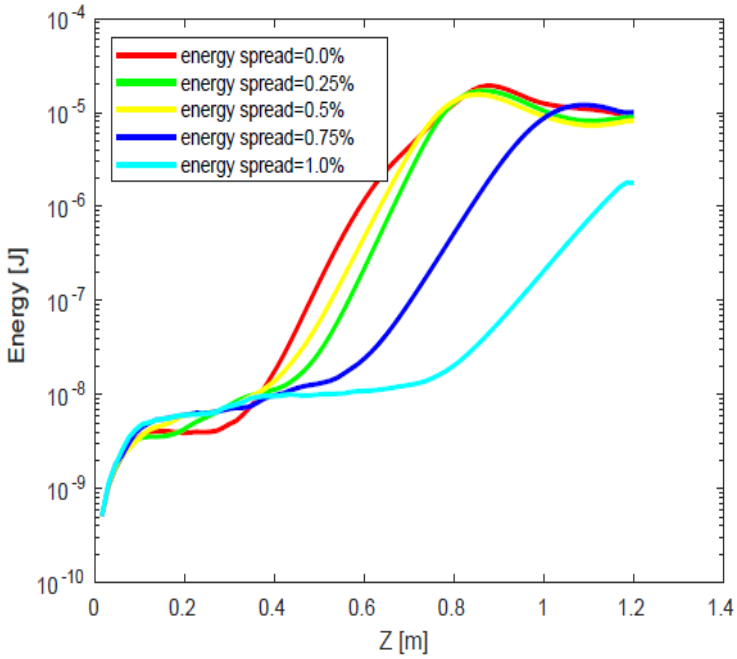

Figure 3.4: The radiation energy as a function of distance z through the undulator for different values of energy spread.

3.5.1 3D Laser-Wakefield Accelerator (LWA) driven FEL

After running Puffin in periodic (steady state) mode as above, it is seen that beam energy spreads of $\sigma_\gamma =$ (0.25%-0.5%) give a reasonable gain. A full Gaussian current electron pulse beam for these values of energy spreads are now simulated. A beam of peak current $I_{peak} = 9.8$ kA, charge of $Q = 40$ pC, and unchirped energy of 600 MeV was used [45,46]. A planar undulator period of $\lambda_u = 15$ mm with an undulator pole gap of $g = 2.5$ mm was chosen to give an undulator parameter of $a_u = 2.3$ [45,46]. These beam and undulator parameters give an FEL parameter of ρ_{FEL}=0.0269 as above with a resonant wavelength $\lambda_r = 134\, nm$ .The electron bunch length is calculated as $\sigma_e = \frac{cQ}{\sqrt{2\pi} I_{peak}} = 0.5\mu m$ which is similar to that of one cooperation length $l_c = \frac{\lambda_r}{4\pi\rho_{FEL}} = 0.4\, \mu m$ [14], so that the radiation output will then be in the weak superradiant mode of operation to give a single, short radiation pulse output [26,50].

Figure 3.5 shows the total radiated energy in the FEL for the Gaussian electron bunch.

Figure3.6 shows that if we have a sufficiently low value of energy spread then a relatively high peak energy can be achieved in a short undulator. Note that as the energy spread

approaches $\sigma_\gamma/\gamma \geq \rho_{FEL}$, then the peak energy reduces and the saturation length increases as expected.

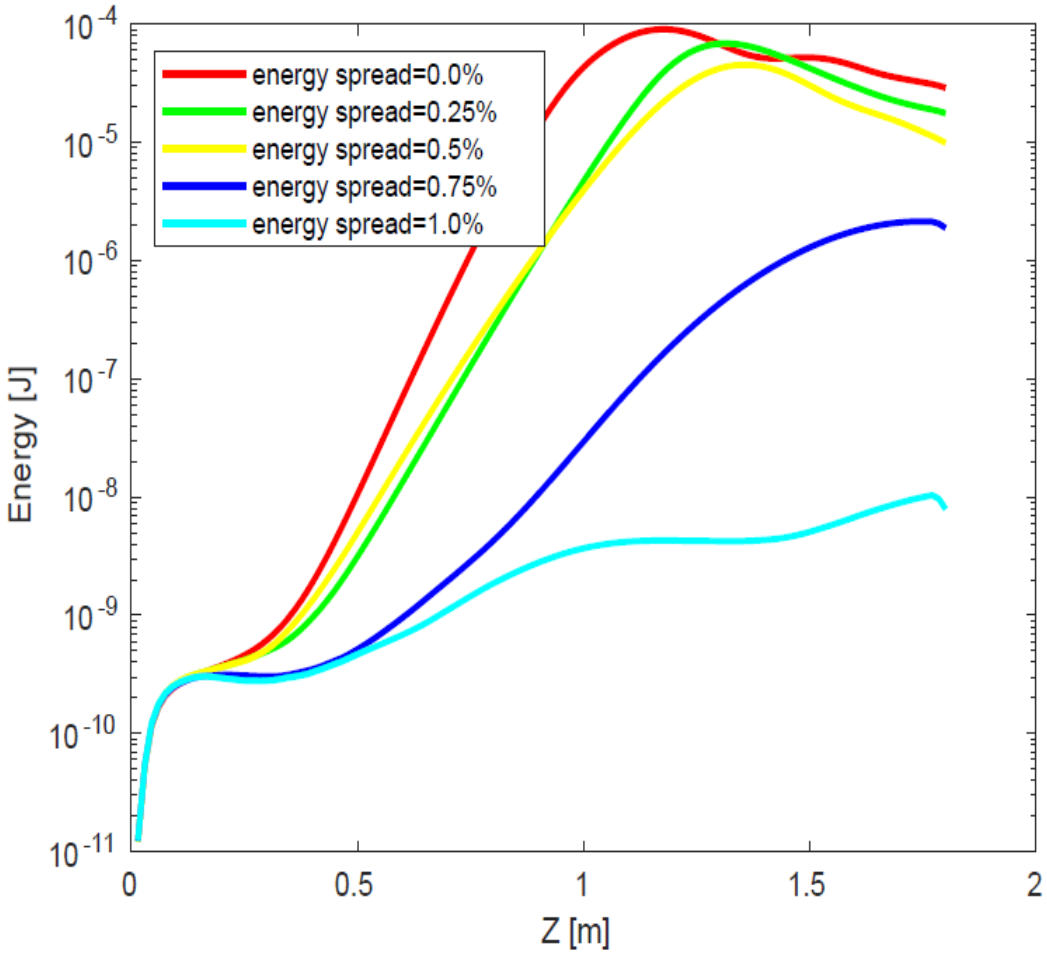

Figure 3.5: 3D Puffin simulation showing radiation energy as a function of distance z through the undulator in Gaussian distribution.

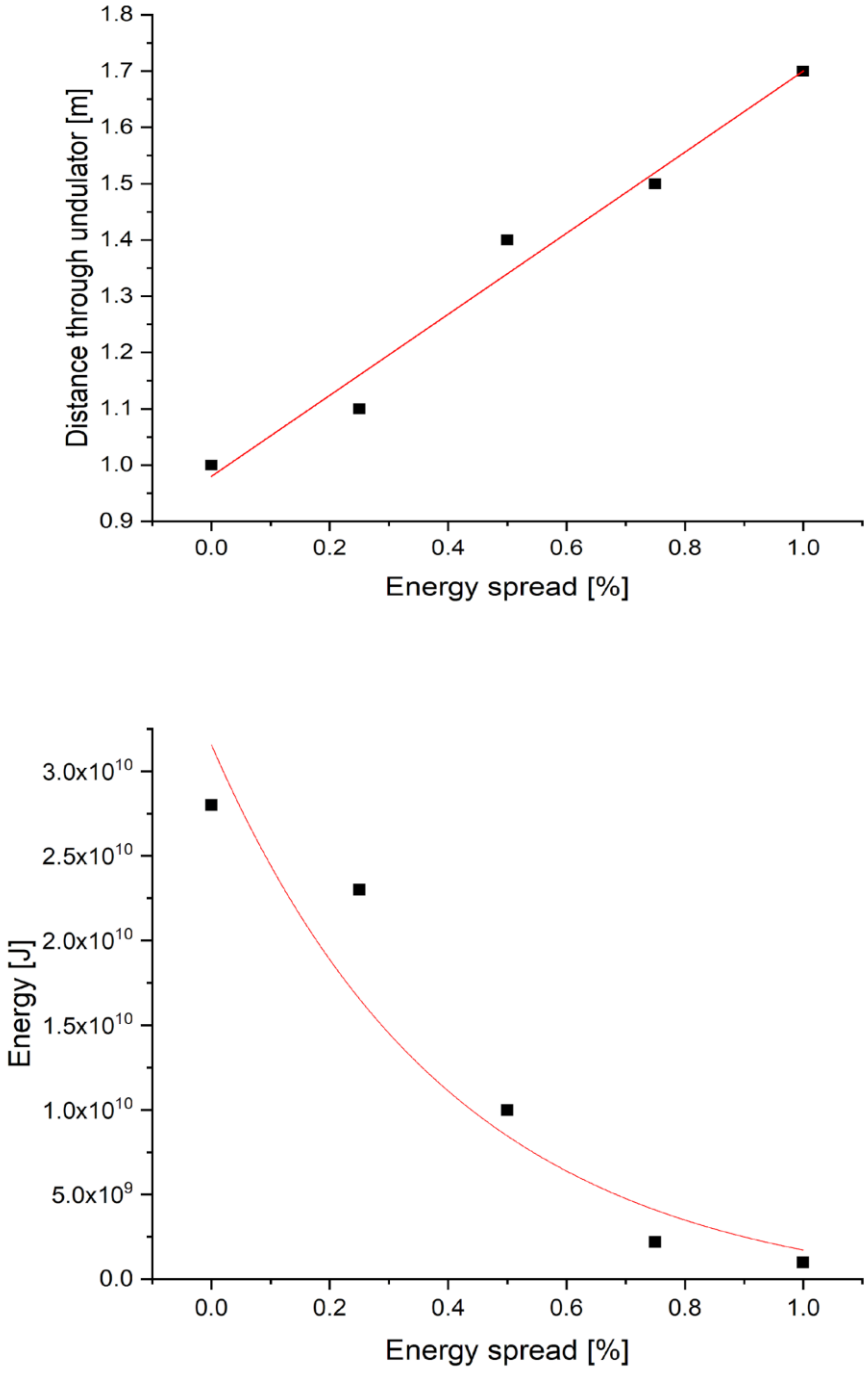

Figure 3.6: Energy [J] as a function of energy spread and undulator distance as a function of energy spread through the undulator in Gaussian distribution.

Figure 3.7 shows the scaled intensity spectrum ($|\tilde{A}|^2$) plotted as function of scaled frequency ω/ω_r for two values of energy spread σ_γ =0.25% and 0.5% , for z = 1.05m through the undulator . Maximum gain is seen at ω/ωr ≈ 0.99 for 0.25% and at $\omega / \omega_r \approx$ 0.97 for 0.5%. This is in broad agreement with small shift from resonance ($\omega / \omega_r = 1$) for the peak that occurs due to the effect of the emittance ($\epsilon_n = \beta\gamma\varepsilon_{rms}$) [13], where $\varepsilon_{rms} = \frac{\lambda_r}{4\pi}$ is the rms emittance [4].

Figure 3.8 shows the temporal power of the pulse as a function of $(ct - z)$ at saturation (z=1.05 m) for energy spread $\sigma_\gamma =$ (0.25% and 0.5%), clearly showing the reduced power when $\sigma_\gamma \geq \rho_{FEL}$. Large energy spread will lead to reduce the bunching.

Next, we will look to start-to-end FELs simulations using LPA in the range of soft X-ray (XFEL) between 1-10 nm [26,51]. This needs a high quality beam with high peak current, high energy and small transverse emittance within a relatively short undulator. This can be challenging in propagating, conditioning and matching the electron beams into the undulator due to the relatively large energy spreads and divergence of the electrons at the LPA exit [52].

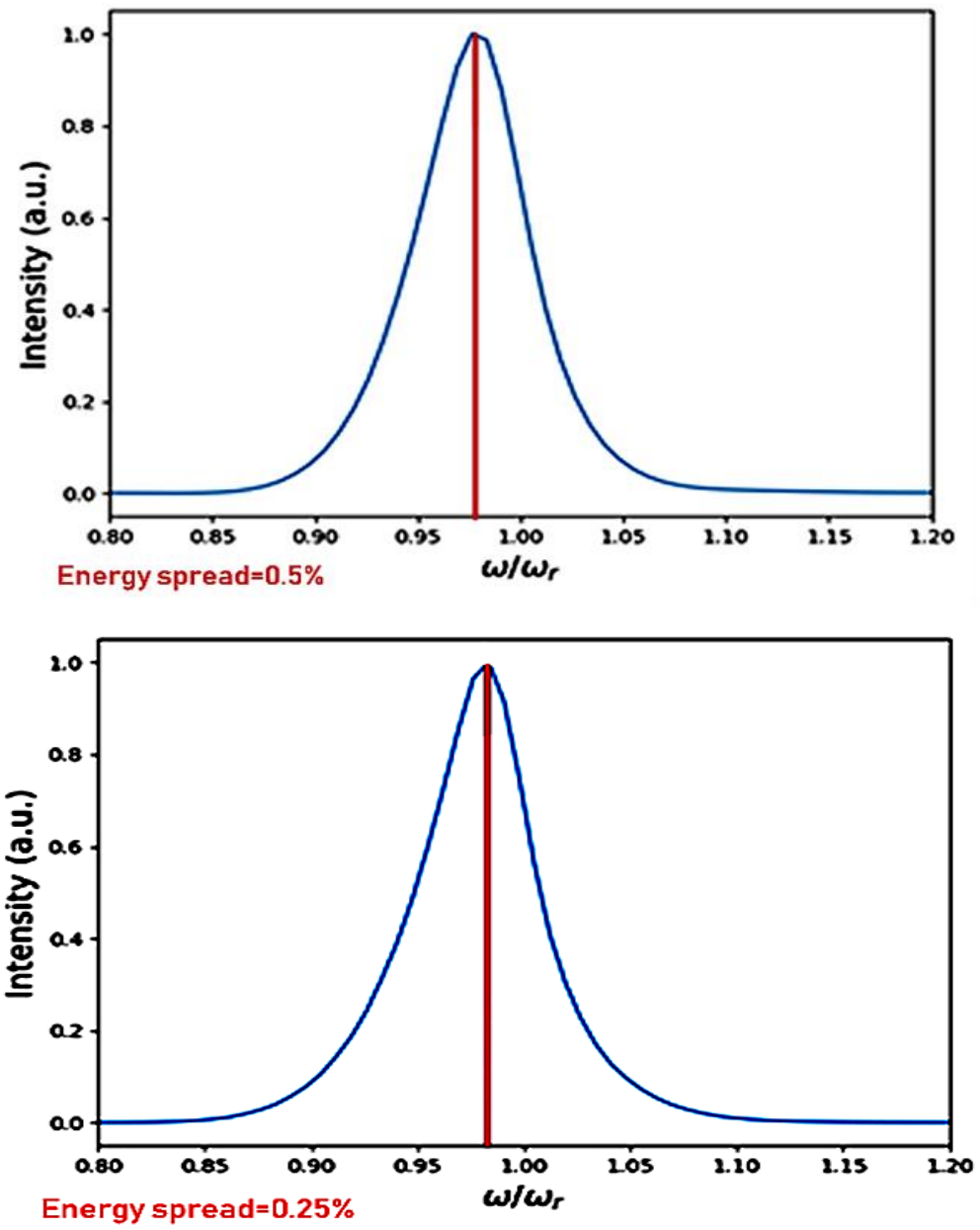

Figure 3.7: The scaled intensity spectrum ($|\tilde{A}|^2$) is plotted as function of scaled frequency $f = \omega / \omega_r$ for two values of energy spread σ_γ= 0.25% and 0.5%.

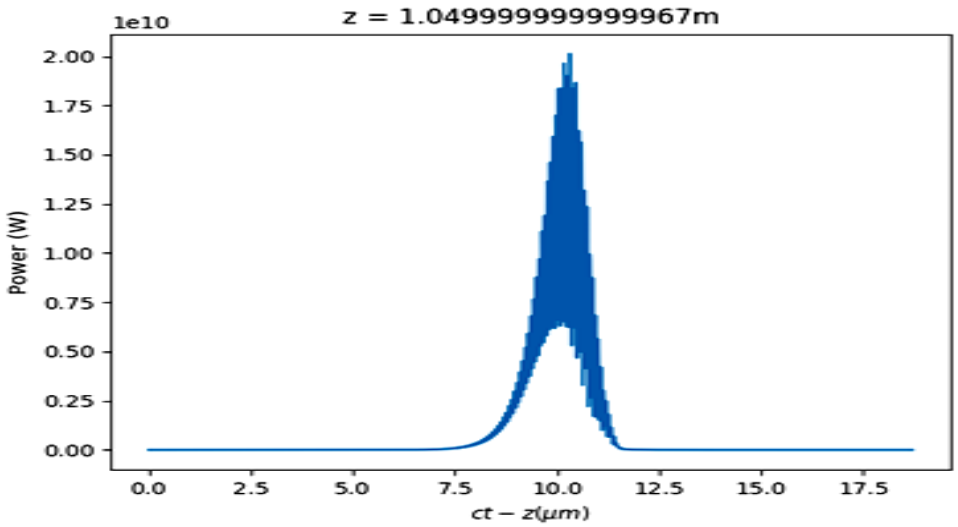

Energy spread=0.25%

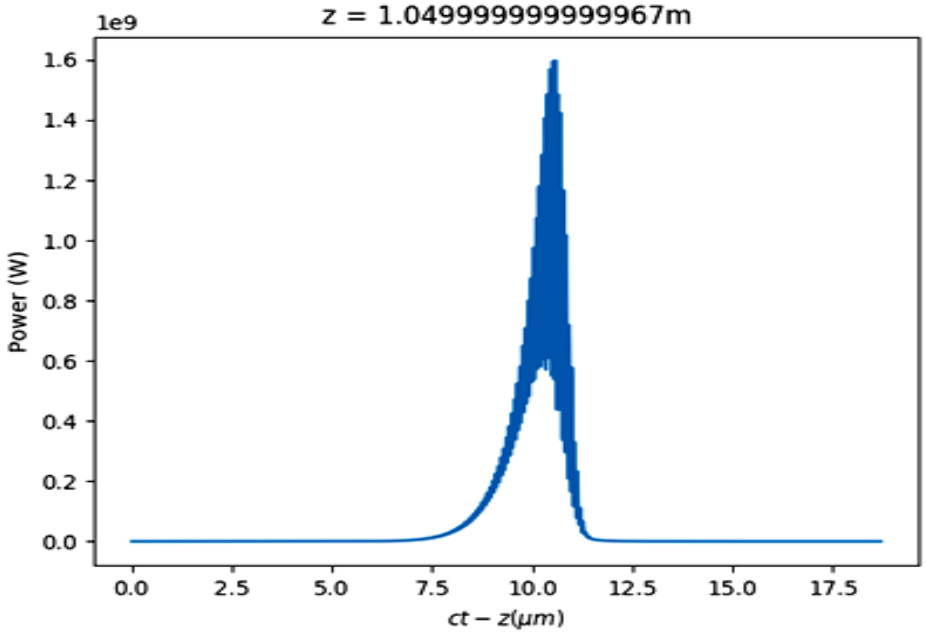

Energy spread=0. 5%

Figure 3.8: The temporal power of the pulse as a function of the scaled time coordinate $(ct - z)$ at saturation (z=1.05m) for energy spread σ_γ=0.25% and 0.5%.

After the energy spread simulation, we can conclude that the undulator length was too limited however, saturation can be achieved in a shorter distance of undulator for lower value of energy spread as seen from figure 3.5 with peak saturated output at 1 - 1.2 m. This may be great interest when considering modelling of a compact LPA Driven FEL.

To reach short radiation wavelength requires (i) large e-beam energy γ, or (ii) shorter undulator period λ_u. Radiation wavelength tuning is achieved by varying beam energy and/or undulator period, with the undulator parameter a_u.

In the case of steady-state simulations figure 3.4 we obtained the reasonable gain for Gaussian distributions as clear is from figure 3.5. The reduced gain is due pulse effects which reduce the peak power [50].

However, in the case of steady-state a higher order of energy gain is obtained compared to the Gaussian pulse mode where for the typical LWA parameters used here, a relatively short pulse was used of the order of the cooperation length. This generates a single superradiant pulse output [50] with a lower peak power output than in the steady state. This short, single pulse output is of interest in its own right where this output is often wanted by FEL users.

For lower energy spreads a higher peak energy is obtained at shorter distance along the undulator as expected. The best results were found when the energy spread $\sigma_\gamma$was below 0.5% and it is clear that the energy spread has large effect on the gain and output in the FEL and must be minimised to equation (2.62) in order to get acceptable FEL output efficiency.

Lastly, the energy spread limit is the most important issue here. The FEL startup performance may be reduced when the energy spread exceeds a threshold. In this case, the radiation is weakened. Due to this factor, efforts must be made to conserve the high quality electron beam used for the next generation light source plus related applications by compensating the correlated energy spread (see chapter 5). An overview of FEL performance degradation is described in chapter (4). Additionally, the energy chirped beam induced degradation is presented in section (4.1). At the end of the chapter, a unique de-chirping method is described. Removing the energy chirp is critical because it acts like an energy spread.

Chapter 4

Review of Energy chirp impact on FEL performance

4.1 Introduction

In the global plasma accelerator community, there is currently much effort to drive a FEL by delivering sufficiently high quality electron bunches. One obstacle to this is the correlated energy spread, or energy chirp, on the bunches. The PWFA/LWFA community identifies this as a problem and a threat to the ability to demonstrate the operation of a plasma accelerator driven FEL. The energy chirp is of the form where the tail of the electron bunch has a higher energy than its head.

Here, the effect of the energy chirp of electron beams in FEL lasing is investigated. The effectiveness of the electron beam at FEL lasing following the removal of the chirp is also investigated.

4.2 Energy chirp impact on FEL performance

As indicated in Figure 4.1 [26], a sufficiently negative electron pulse energy chirp, as generated in plasma accelerators, shortens the pulse in longitudinal phase space as it propagates through an undulator. The pulse length minimizes after a sufficient propagation distance is reached. At this point, three things happen: (1) the energy chirp starts to become positive; (2) the pulse starts lengthening; and (3) a short pulse of coherent radiation is generated. This will occur under the condition that the minimum of the electron pulse length is of the order of a resonant FEL wavelength λ_r. The length of the electron pulse and the chirp's magnitude determine the number of undulator periods at which this process occurs. Hence, fewer undulator periods are needed for stronger chirps to produce coherent spontaneous emissions leading to shorter radiation pulse. The energy chirp causes the linear shortening of the electron pulse which leads to Coherent Spontaneous Emission effects, not FEL bunching. The Puffin code model of the FEL equations is able to self-consistently model both the electron pulse shortening and the subsequent emission of the CSE. Neither of these effects can be modelled by an averaged set FEL equations.

In this thesis, the coherent radiation output generated from such a chirped electron pulse is isolated in the 1D analytic solution and compared to 3D and 1D numerical simulation using Puffin, the unaveraged FEL code.

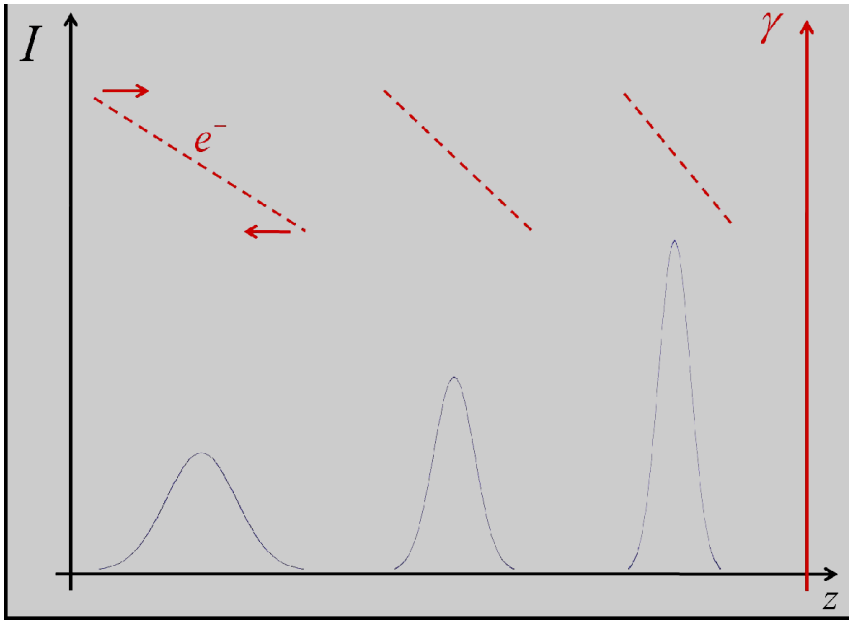

Figure 4.1: Schematic of the evolution of short negatively chirped electron pulse propagating through an undulator showing the current I and scaled energy [26].

4.3 Short Chirped Pulse

PWFA generated electron pulses can have longitudinal lengths of the order of a few resonant wavelengths. Strong chirped electron beams with small durations can invert in longitudinal phase space while propagating in the undulator. Consequently, the electron bunch length can become of the order of resonant wavelength, resulting in coherent spontaneous radiation for multiple undulator periods. It's important to note that this effect is dependent on the chirp's magnitude. Generally, broader radiation bandwidths (shorter pulses) are generated from stronger chirped electron pulses. This is not necessarily caused by the FEL interaction, rather it independently arises from the linear evolution of the chirped electron beam. The Puffin code is used to simulate this effect.

The following equations in reference [26] describe the analytical solution. An initial linear chirp α_0 , is defined in the electron beam such that

$$\alpha_0 = \frac{dv_j}{d\bar{z}_2} \qquad (4.1)$$

Where the j^{th} is the electron's phase velocity is v_j. Then we take the initial electron beam spread to be a Gaussian with rms spread σ_0, the resulting distribution after propagation distance $\bar{z}$ becomes

$$\sigma(\bar{z}) = \sigma_0 + \alpha_0\sigma_0\bar{z} \qquad (4.2)$$

$$\sigma(\bar{\bar{z}}) = \sigma_0(1 + \alpha_0\bar{\bar{z}}) \qquad (4.3)$$

A minimal intrinsic pulse length σ_i is added to convert $\sigma(\bar{\bar{z}})$ to zero from the perfect linear chirp:

$$(4.4)\ \ \sigma(\bar{z}) = \sqrt{\sigma_0^2(1 + \alpha_0\bar{z})^2 + \sigma_i^2}$$

When the initial chirp and electron distribution is determined with this method, the initial peak electron current $I_{peak} = \frac{Q}{\sqrt{2\pi}\sigma_0}$, and the electron weighting function in 1D , as a function of $\bar{z}$ can then be found to be

$$\chi(z,t) = \frac{I(\bar{z},\bar{z}_2)}{I_{pk}} \qquad (4.5)$$

Where χ is normalized current respect to the peak current I_{pk}.

$$\chi(z,t) = \frac{\sigma_0}{\sqrt{\sigma_0^2(1+\alpha_0 z)^2+\sigma_i^2}} \exp\left(-\frac{\bar{z}_2^2}{2(\sigma^2(1+\alpha_0 z)^2+\sigma_i^2}\right) \qquad (4.5)$$

An analytic solution for the field generated by this electron pulse evolution is possible. The solution is extracted from the Fourier space. The resulting expression for the scaled radiation envelope as a function of $f = \omega/\omega_r$ is:

$$(4.6)\ \ \tilde{A}(f) = \frac{4\pi\rho_{FEL}}{f} \exp\left(-i\frac{f-1}{2\rho_{FEL}\alpha_0}\right) \exp\left(-\frac{f^2\sigma_i^2}{8{\rho_{FEL}}^2}\right) \exp\left(-\frac{(f-1)^2}{2\sigma_0^2\alpha_0^2 f^2}\right)$$

In the following sections, the essential components of the dechirping technique used to remedy the negative effects of the energy chirp on the FEL is presented.

4.4 Review the energy chirp compensation methods of beam energy chirp

The process for producing one broadband radiation pulse from a strong electron chirp pulse is outlined. To reiterate, it's important to compensate for the effect of the energy chirp to conserve the quality of the beam before leaving the plasma acceleration stage. In an undulator, the chirp enables the generation of a pulse of coherent spontaneous radiation that has a shorter duration than the FEL cooperation length. In fact the energy spread and energy chirp are important effect in the application of plasma-based accelerators and compensation ("dechirping") techniques are important, due to the energy chirp represents an obstacle and dechirping techniques may provide key to obtain high quality of electron

beams. Dechirping allows to transform the ultrahigh 5D-brightness of plasma-photocathode-generated electron beams into beams with unprecedented 6D-brightness[18].There are many methods to compensate the energy chirp such as RF dephasing technique [37] . RF dephasing technique (off crest acceleration) in the downstream LINAC sections using beam self-induced wakefields in order to remove head to tail chirp or rotate the longitudinal phase space and passive dechirping. Also, there is another method to remove the energy chirp called beam loading. It is state-of-the-art methodology for removing head-to-tail chirp. It means perturbation of the wakefield into the plasma wakefield by injection of charged particles. In contrast to other methods of dechirping which depend on many stages and a reduction of energy chirp due to self-driven plasma wake fields [53-57] which is used at LCLS such as dielectric wakefield dechirpers, the method described in Ref [37], beam loading is capable of obtaining the lowest emittance values and highest 6D brightness. Using this method energy spreads will also be reduced [18].

A numerical simulation was used for removing the energy chirp and then compared to the emitted radiation pulse with the energy chirp. This further justifies the reasoning behind removing or minimizing the energy chirp effect as describe later in section (5.4.3).

In this thesis, my procedure was to simply remove the energy chirp numerically after the electron pulse was emitted from the plasma photocathode. This effectively rotated the beam in energy phase space to make it horizontal in energy so the chirp will be close to 0. However, in this method we removed the effect of energy chirp without any change in value of the energy spread or any parameters of electron beam. However, experimentaly these parameters can be expected to change a little while the main effect will be the energy spread reduction.

In the following chapter a 3D simulation is presented that matches the electron beam with the natural undulator focusing channel. A start-to-end simulation of the evolution in phase-space of the electron bunch and radiation in 3D is conducted both with and without the electron bunch energy chirp.

Chapter 5

Start –to-End Simulation

5.1 Introduction

This thesis explores the dynamics of a fs-scale and mm-mrad normalised emittance electron bunch from a plasma photocathode with natural negative energy chirp and at 250 MeV electron energies. Such a bunch combines ultrahigh (slice) brightness, which implies strong gain characteristics, with dispersive compression due to a rotation in longitudinal phase space, which gives rise to a current spike. Previous studies have shown that an electron beam energy chirp can have both detrimental and beneficial effects upon the FEL interaction depending upon the gradient of the chirp [58, 59].

One effect, which has not been modelled before with a PWFA plasma photocathode-generated energy chirped beam, is to induce the generation of Coherent Spontaneous Emission [26, 59]. CSE arises when the electron pulse has significant current gradients over a resonant radiation wavelength. It is shown that for the electron beam parameters used here, such current gradients can be realised when the energy chirped beam undergoes spatial dispersive compression in its propagation direction due to the correlated energy spread [26, 59]. CSE can have radiation power output orders of magnitude above normal spontaneous emission, and can therefore be a useful radiation source in its own right. By dominating any normal spontaneous emission, CSE can also self-seed the FEL interaction [60]. It has also been shown that CSE can help mitigate the effects of a homogeneous electron energy spread in beams without an energy chirp, significantly reducing the start-up time and enhancing the generation of high intensity, short, superradiant radiation pulses from a poor-quality electron pulse [61].

5.2 Electron beam generation and acceleration PIC modelling

The following section discusses the results of the modeling of a PWFA driven of FEL.

The PWFA stage and the subsequent controlled electron beam injection via the plasma photocathode method, are modeled with the fully explicit 3D Particle-In-Cell (PIC) code VSim [8]. The electron bunches generated were supplied by another PhD student, Reem Alturijri studying with Prof. Bernhard Hidding of Strathclyde.

The simulation box, moving with the speed of light, consists of 109 × 65 ×65 cells with one macroparticle per cell this leads to approximately 450 k of macroparticles modelling the background plasma. The size of the co-moving box is set to 345 μm ×205 μm ×205 μm to accommodate the plasma blowout structure. The PIC simulation runs for t_{sim}= 4.6

ps corresponding to a propagation distance of $z_{sim} = t_{sim}$ = 14mm. A bi-gaussian charge distribution driver beam of ultrarelativistic energy $W_d = 10$ GeV and relative energy spread of $\Delta W_{rms,d}/W_d$= 2% is shot into a uniformly distributed pre ionized hydrogen plasma of density n_p = 4.95 × 10^{16} cm^{-3} corresponding to a plasma wavelength of $\lambda_p = 2\pi c(m_e\varepsilon_0/n_p e^2)^{1/2}$= 150 μm , where c is the speed of light, m_e is the electron mass, e and ε_0 represent the electron charge and the vacuum permittivity, respectively. Driver beam charge is optimized to Q_d= 800 pC , and its longitudinal and transverse dimensions are matched to the plasma density with $\sigma_{z,d}$ = 20 μm and $\sigma_{(x,y),d}$= 3.5 μm, respectively, resulting in "cigar"-like electron beam of peak density n_d= 1.3 × 10^{18} cm^{-3}. The driver beam parameters are tailored to meet the blowout condition $n_d/n_p \gg 1$ and to excite a large amplitude plasma wave by expelling plasma electrons by means of its unipolar radial electric field $E_r(r) = Q_d/(2\pi)^{3/2}\,\varepsilon_0\sigma_z r[1+\exp(-r^2/2\sigma_r)]$ while keeping the heavy ions immobile. At the same time, the parameters are balanced towards dark-current-free PWFA operation such that the maximum radial electric field $E_{r,max}$ = 28GVm^{-1} is below the tunnel ionization threshold of the background helium gas of density n_{He} = 1.5×10^{17}cm^3 [59]. A moderate intensity laser pulse trailing the driver beam at the distance $\Delta\xi$= 115 μm with the normalized amplitude a_0= 0.018, FWHM pulse duration τ_0 = 30 fs, and rms spot size ω_0 = 7 μm, reaches its focal position at z_i= 2 mm where the laser pulse intensity is just above the tunnel-ionization threshold of the neutral helium. This results in localized ionization of helium gas directly inside the blowout cavity. The tunnel-ionized helium electrons are quickly accelerated to relativistic energies and are trapped inside the blowout structure. Note, that due to the moderate laser intensity the residual transverse momentum of the electrons is very small and combined with the confined ionization volume of the laser pulse the normalized emittances can be as low as nm-rad.

Driver parameters			Photocathode laser parameters		
Name	Symbol	Values	Name	Symbol	Values
Energy	W_d	10 GeV	Wavelength	λ_l	800 nm
Rel. energy spread	$\Delta W_{rms,d}/W$	2 %	Laser amplitude	a_0	0.018
RMS bunch length	$\sigma_{z,d}$	20 μm	Pulse duration	τ_0	30 fs
RMS bunch width	$\sigma_{x,y,d}$	3.5 μm	RMS spot size	w_0	7 μm
Norm. emittance	$\epsilon_{n,d}$	50 μm	Laser position	ξ_i	200 μm
Charge	Q_d	800 pC	Focal position	z_i	2 mm

Table 5. 1: 3-D PIC simulation PWFA driver beam and plasma photocathode laser parameters

Figure 5.1 shows PIC results of a dephasing-free plasma wakefield excited by an ultrarelativistic driver beam (green dots) with a peak current $I_{pk,d} \approx$ 4.5kA. The solid black line represents the on-axis accelerating electric field with maximum accelerating field

$E_{z,max}$= -24GVm^{-1} at the rare of the blowout. The solid blue line is the corresponding electrostatic wake potential in units of electronic rest energy ($em_e^{-1}c^2$). The transparent blue filling indicates the trapping potential which has to satisfy the trapping condition $\Delta\Psi < -1$ to support trapping of the released electrons inside the blowout structure. In (left) the laser pulse (not shown here) just released helium electrons via the plasma photocathode method at the co-moving position ξ_i=200 μm at the trapping potential minimum. This is a preferable position to obtain highest trapping efficiency due to the deep potential. The electrons are velocity bunching and are in the process of forming an electron bunch ("witness beam"). In (right) the witness beam of charge $Q_\omega = 3.6$ pC is accelerated to mean energy of $W_\omega \approx 247$ MeV after an acceleration distance of Δz = 12 mm. The projected normalized emittance of the witness beam is ϵ_n = 21nm rad combined with the peak current of $I_{pk,\omega} \approx 1.5$ kA this results in 5D brightness of $B_{5D} = 6.8 \times 10^{18}$ A/m^2/rad^2. The driver beam and injector laser parameters are summarized in Table 5.1 and output witness beam characteristics are highlighted in Table 5.2.

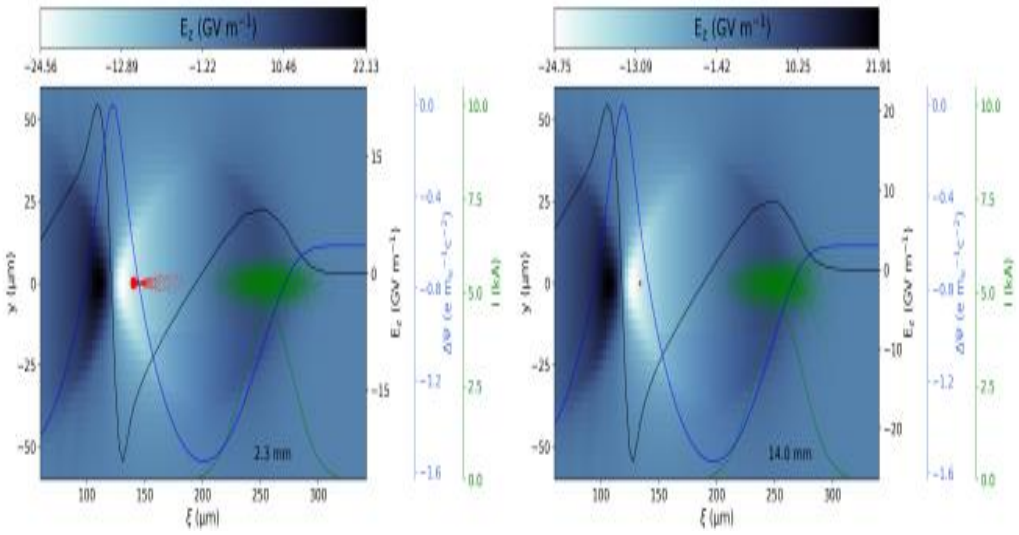

Figure 5.1: 3-D PIC simulation of the plasma photocathode beam-driven wake field acceleration. The green and red dots show drive and witness beam, respectively. The color map represents the accelerating gradient $E_z$while the solid black line is the electric field on-axis and the solid blue line represents the electrostatic trapping potential $\Delta\Psi$ .In (left) witness beam tapping process is shown at z = 2.3mm while in (right) the witness beam is trapped and already accelerated to the final energy

Name	Symbol	Values
Energy	W_{w}	247.3 MeV
Lorentz factor	γ	483.9
Slice energy spread	σ_γ/γ	0.3 %
Normalised emittance	$\epsilon_{\mathrm{n,w}}$	21 nm rad
RMS bunch length	σ_{w}	0.26 μm
Bunch charge	Q_{w}	3.6 pC
Peak current	$I_{\mathrm{pk,w}}$	1.5 kA
5D Brightness	B_{5D}	6.8×10^{18} A/m^2/rad^2

Table 5.2: Projected witness beam parameters from the 3D PIC simulation at the end of the acceleration z = 14 mm.

5.3 Transfer and conditioning of the simulation particles from the PWFA to the FEL

The macroparticle distribution from the VSim PWFA simulation has too sparse a phase-space distribution for accurate FEL simulation with the code Puffin. There are not enough *macroparticles* from VSim per resonant wavelength and it has unknown shot-noise statistics. It also has different format and units, and must hence be converted into a suitable format and units of a greater number of microparticles, for which the conversion script of [30] was used. The beam of macroparticles from VSim is 'up-sampled' to create a beam with a greater number of microparticles which have the correct shot-noise statistics as an equivalent beam of real electrons. The method of [31] uses cumulative distribution function approach together with an optional smoothing function to obtain such a beam of microparticles. The relevant parameters of the beam of microparticles are compared to the original beam of macroparticles from the VSim simulation in figure 5.2 (dashed). Here, key bunch characteristics such as normalise emittance ϵ_n, Lorentz factor γ, slice energy spread σ_γ and current I are plotted versus the co-moving coordinate $z_2 = (ct - z)$, such that the electron beam head is on the left and the electron beam tail is on the right. The microparticle distribution has also had the correct shot-noise statistics applied as described in [62]. This beam of microparticles can now be used to simulate longitudinal phase space rotation, self-seeding via shot noise spontaneous emission via Coherent Spontaneous Emission using the Puffin code.

A particularly prominent signature of the plasma photocathode-generated electron bunch are its very low normalized slice emittance ϵ_n around 10 nm rad throughout the electron beam (top panel). The beam further has a slice current exceeding 1 kA (bottom panel), and

average RMS slice energy spread width of $\sigma_\gamma \approx 1.5$ (third panel), corresponding to a relative slice energy spread of $\sigma_\gamma/\gamma \approx 0.3\%$. As can be seen in the second panel of figure 5.2 , the electron beam has a negative longitudinal energy chirp, which is the natural result of the beam being accelerated in the linear electric field of the strongly nonlinear plasma wave.

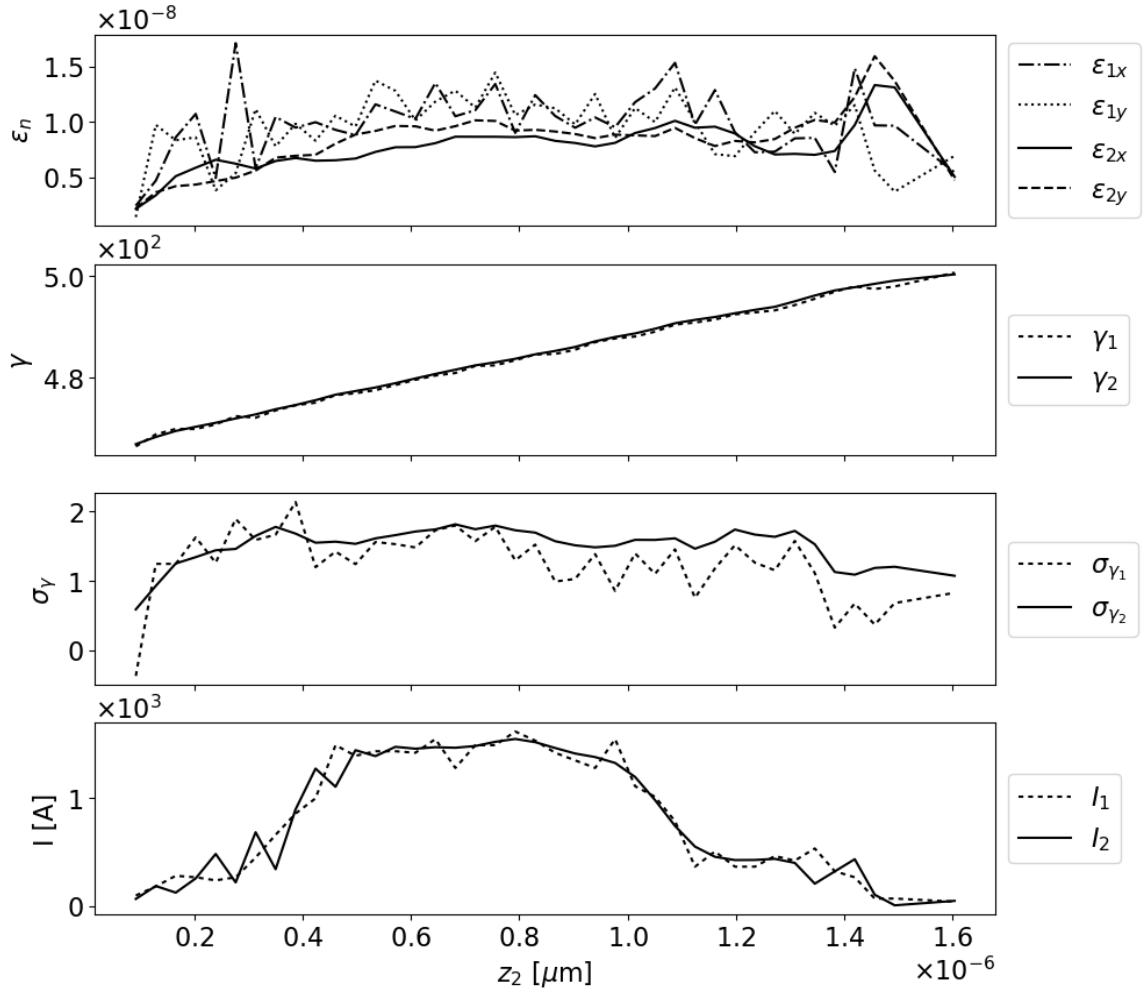

Figure 5.2: From top, the electron beam normalised emittance ϵ_n, localised Lorentz factor γ, current I, and RMS energy spread σ_γ as a function of window position $z_2 = (ct - z)$ of the beam. In this window, travelling at speed c along the z-axis of the undulator the head of the electron bunch is on the right, the tail on the left, and the beam will propagate to larger values of z_2 as the beam propagates through the undulator. The dashed plots (index 1) show the original macroparticle beam from the VSim simulation and the solid plots (index 2) show the beam following smoothing and up-sampling to a greater number of microparticles with the correct shot-noise statistics.

5.4 FEL simulation

In this work we used the Puffin code to model this simulation as it is able to model the effects of the macroscopic electron beam changes due to (correlated) electron beam energy

and any CSE and Self Amplified CSE (SACSE) that may arise. Before doing any simulations, suitable undulator parameters are chosen and FEL saturated power and undulator length estimates are also made for an electron beam with no energy chirp in the steady state regime using the analytical Ming Xie formalism [22, 23]

5.4.1 Analytical parameter study without beam energy chirp

In order to choose a suitable set of undulator parameters before any full simulation using Puffin and to estimate FEL performance from a hypothetical beam without an energy chirp for steady-state FEL operation (no pulse effects), the Ming Xie formalism of [22, 23] was used to vary the planar undulator period λ_u and undulator parameter a_u. The parameters of Table 5.3 were used as estimates of the unchirped parameters of figure 5.2. The estimated FEL saturation power and length in this steady state regime are plotted in figure 5.3.

Parameter	Value
Peak current I_{pk}	1500 A
Normalised emittance	0.01 mm mrad
Bunch Lorentz factor (γ)	486
RMS energy spread	0.3%
Bunch charge	3.6 pC

Table 5.3: The approximate output parameters from the PWFA used for the Ming Xie formalism parameters estimate.

The undulator parameters chosen for the full simulations were $\lambda_u = 0.015$ m and $a_u = 1.0$. With these values, the radiation wavelength is $\lambda_r = 64$ nm and the FEL Pierce parameter for the peak current is $\rho_{FEL} = 0.021$. Given that the average RMS slice energy spread is ${}^{\sigma_\gamma}/_{\gamma} \approx 3 \times 10^{-3}$ the energy spread condition for FEL lasing of $\sigma_\gamma/\gamma \leq \rho_{FEL}$ is well satisfied without the energy chirp. The steady state, Self Amplified Spontaneous Emission (SASE) saturation length is then approximated as $L_{sat} \approx 1.4$ m and saturation power $P_{sat} \approx 2.2$ GW The electron bunch does not , however , satisfy the steady-state approximation as it is only ~3 cooperation length long, where the cooperation length $l_c = \frac{\lambda_r}{4\pi\rho_{FEL}}$ [50]. This relatively short electron pulse length will result in the output of short, single pulses, at saturation. This type of short pulse operation is in the weak superradiant

regime of FEL operation [50] and also results in reduced saturation powers from that of the steady-state, Ming Xie approximation above.

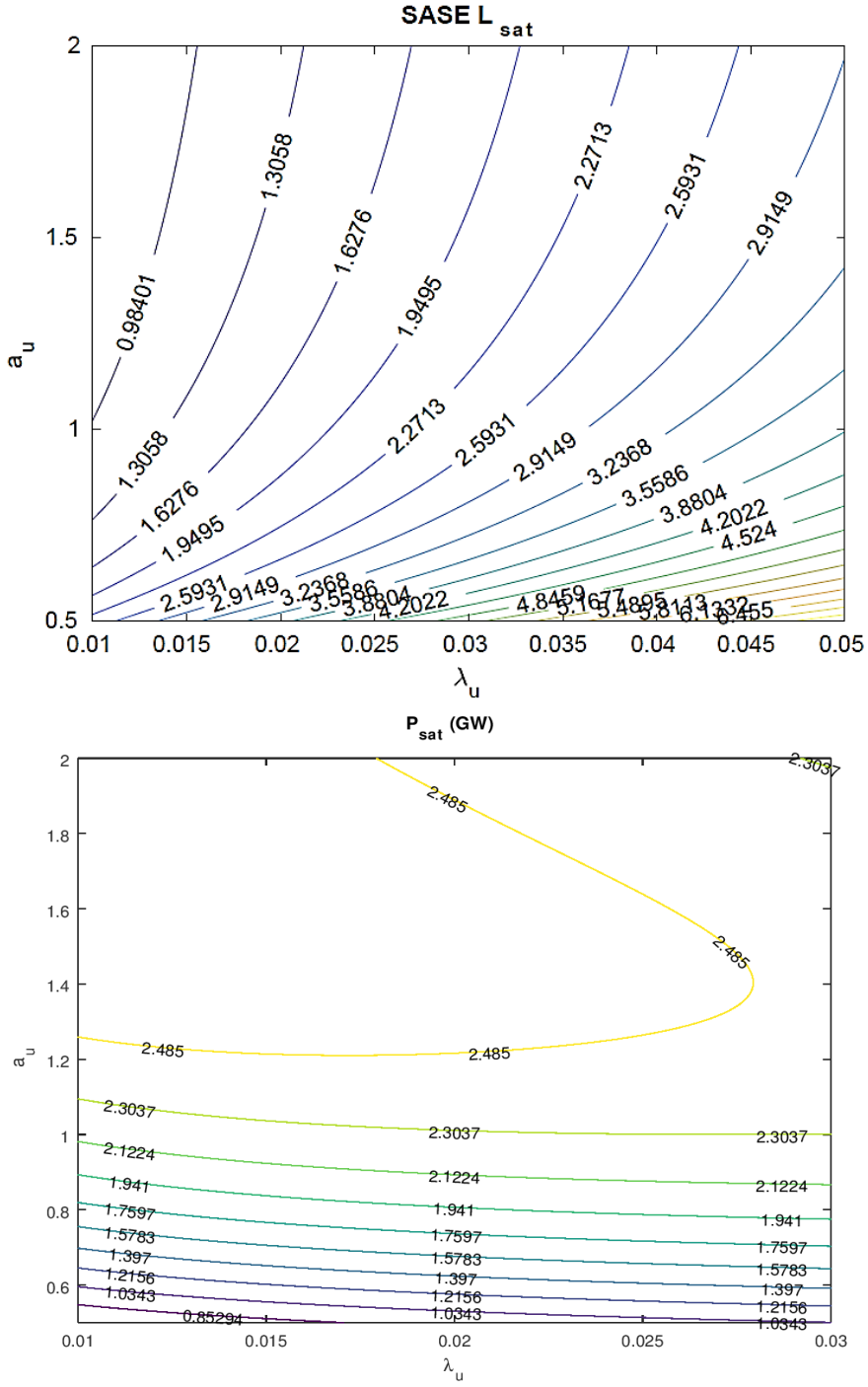

Figure 5.3: Contour plots of the saturation length L_{sat} (above) and the saturated power P_{sat}(bottom) as a function of undulator period λ_u and undulator parameter a_u using the electron beam parameters of Table 3 and SI units are used unless stated

5.4.2 Numerical simulation with an energy chirped beam

First, the Puffin simulation uses the energy chirped electron bunch distribution output converted from the VSim simulation of the PWFA as shown in figure5. 2. As discussed above, the macroparticle output from the VSim accelerator modelling was first up-sampled to generate an equivalent distribution of a greater number of microparticles with the correct shot-noise statistics. The beam of microparticles was matched to the natural focusing channel of the undulator lattice chosen for the simulation as above using the method of [29]. In figure 5.4 the red plots are for the chirped electron bunch and the blue for the unchirped bunch where the energy chirp was removed numerically under approximation of new experimental method under development [54-57].

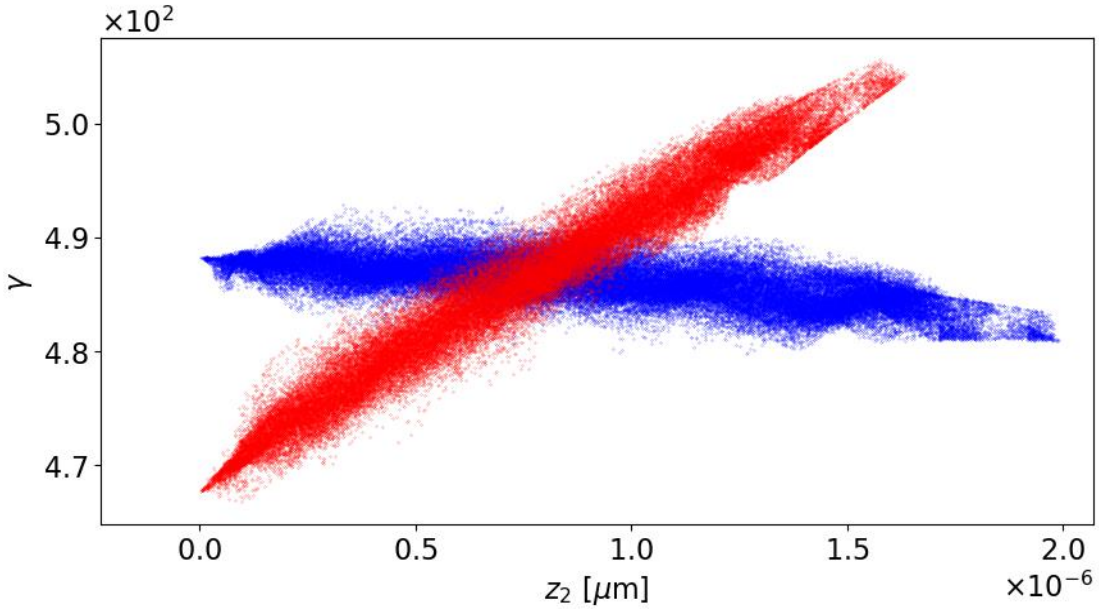

Figure 5.4: Shown in red is the accelerator electron beam phase-space output: Lorentz factor as a function of position $z_2$within the beam. The beam propagates along the positive z-axis. Also shown (blue) is the electron beam with the energy chirp artificially removed.

It is seen from the parameters of the chirped pulse, plotted in figure 5.2, that the electron pulse generated by the PWFA has a total length of $l_e \approx 24\lambda_r \approx 6l_c$ and has a negative energy chirp in z (positive energy chirp in z_2). During propagation through the undulator, dispersion will cause this short, energy chirped electron bunch to self-compress in z_2 due to rotation in longitudinal phase space, which is significant at these comparatively low energies, and it may even `flip over' the electron bunch in longitudinal phase space [26]. During this process, the electron bunch length may approach that of the resonant wavelength ($l_e \approx \lambda_r$) and consequently would be expected to radiate significant CSE. Note that this CSE is not due to the FEL interaction and can only be modeled using un-averaged FEL simulation codes such as Puffin.

In what follows the CSE generation due to energy chirped bunch shortening and any FEL processes were modelled self-consistently. It should be noted that the FEL interaction may also amplify CSE in addition to the spontaneous emission due to electron beam shot-noise in the process called SACSE process [60,61]. As with SASE, given the large energy chirp here, any SACSE would be expected to be significantly affected. The electron longitudinal phase space evolution and the corresponding transverse radiation intensities are plotted for different positions through the undulator in figures. 5.5 and 5.6.

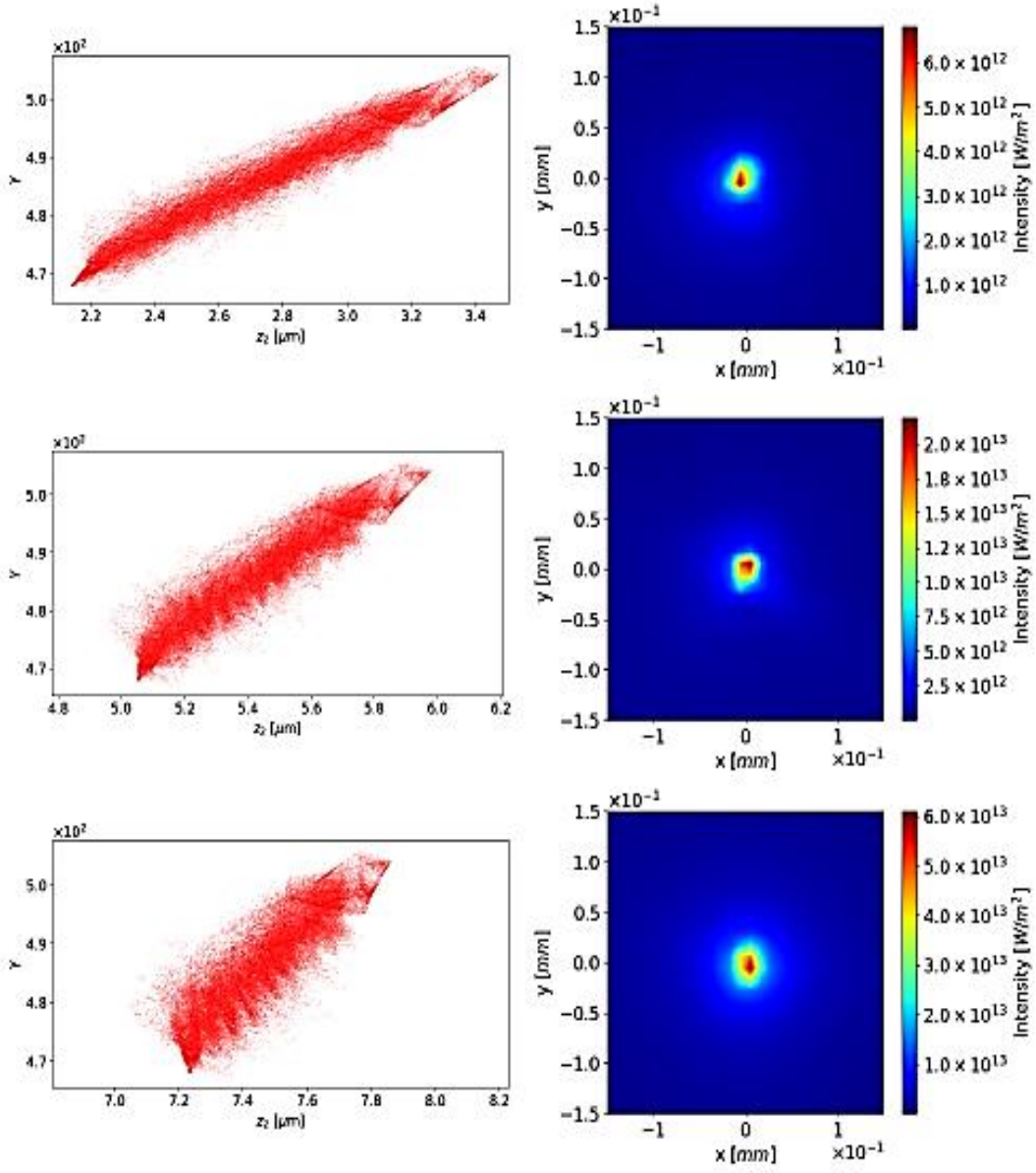

Figure 5.5: The electron beam longitudinal phase space (γ, z_2) and the corresponding transverse intensity, averaged over the pulse length, at 5 different positions along the undulator: z = 0.45, z = 1.05 and z = 1.50. The initial energy chirp at z = 0 is seen to cause the electron pulse to compress and then will decompress longitudinally.

It is seen from the electron phase space of figures. 5.6 that the electron energy chirp causes the electron bunch to compress longitudinally in phase space and shorten as it propagates through the undulator. At saturation, $z = 1.95\text{m}$, the electron bunch is only$\sim$9 resonant radiation wavelengths long.

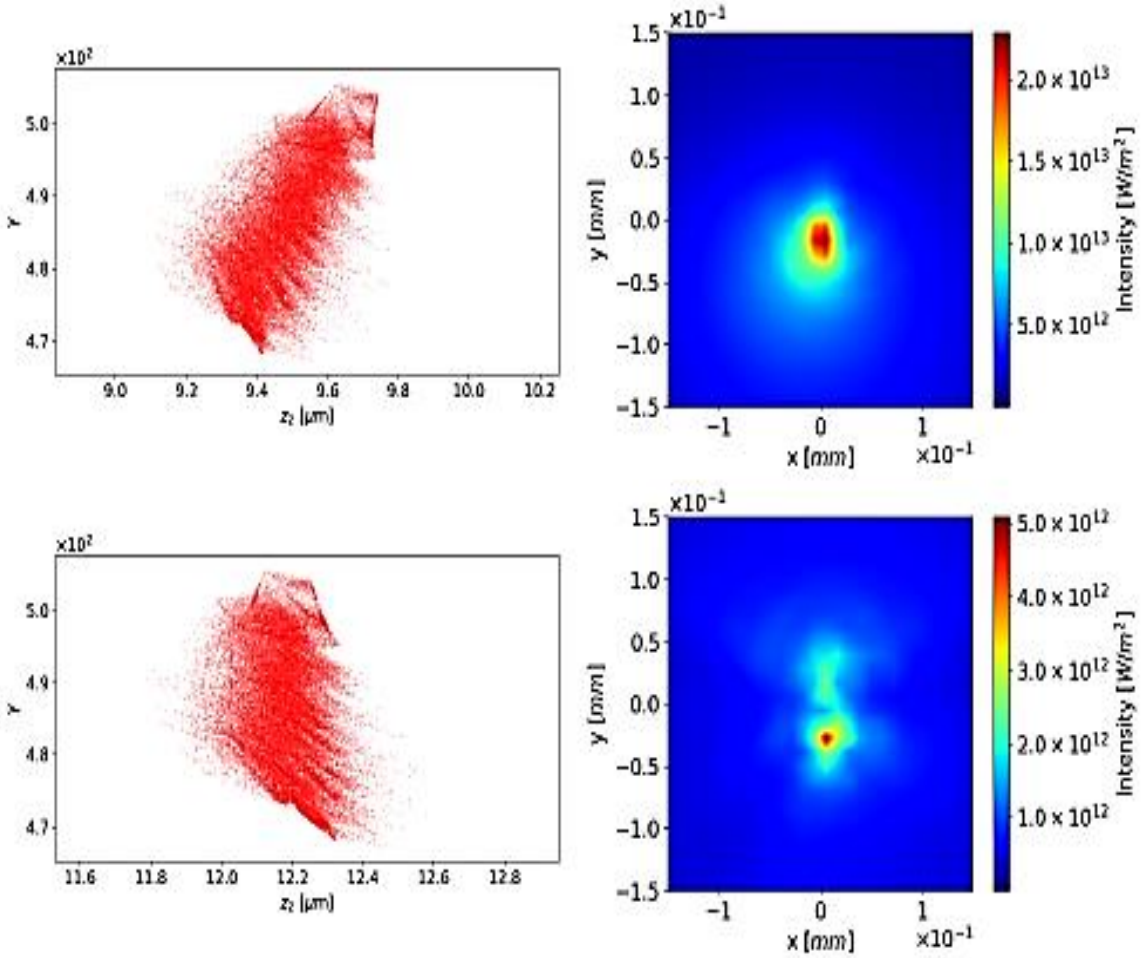

Figure 5.6: The electron beam longitudinal phase space (γ, z_2) and the corresponding transverse intensity, averaged over the pulse length, at 5 different positions along the undulator: $z = z_{sat} = 1.95$ and z = 2.55 m. The initial energy chirp at z = 0 is seen to cause the electron pulse to compress and then decompress longitudinally.

The energy of the radiation pulse through the undulator is shown in figure 5.7. Also shown is the spontaneous radiation without any FEL interaction i.e. the radiation from both shot-noise and CSE, for both the chirped and un-chirped bunches of figure 5.4. Also, the average bunching parameters $|\bar{b}|$, for both the chirped and un-chirped electron pulses are shown in figure 5.8. The radiation pulse instant power (i.e. unaveraged over a radiation wavelength [14]) and electron bunching parameter $|b|$ at saturation for case of energy chirp or without , are shown in figures 5.9 ,5.10 as a function of local position z_2

In what follows, the FEL interaction can be ‘switched off' in the Puffin simulation by artificially stopping the electrons interacting with the radiation field. Then the electrons only emit spontaneous emission due to both shot-noise and CSE. The radiation energy growth from the chirped electron pulse, with and without the FEL interaction, is shown in figure 5.7. This allows to see the different between the case of FEL interaction and without. The growth is not exponential but has a growth which is proportional to $\sim z^{2}$, more like that from CSE [26]. Because the radiation energy emitted in the absence of the FEL interaction is nearly the same as with the FEL on, shows that the radiation in both cases comes mainly from CSE. Also plotted is the radiation energy emitted from the electron pulse in the without any energy chirp. Here, there is no shortening of the electron pulse and the CSE emission is much smaller. In fact, the energy growth is nearly linear going through the undulator, which is incoherent spontaneous emission due to shot-noise. The evolution of the mean electron bunching parameter $|\bar{b}|$ of figure 5.8 increases nearly linearly with distance through the undulator until $z \approx 1.2$. This is in good agreement with the increased bunching due to the dispersive shortening of the electron pulse which causes larger current gradients across a radiation wavelength. This type of bunching drives the Coherent Spontaneous Emission [26] and can act as a self-generated seed field which can be amplified as SACSE [60,61].

Also plotted is the electron bunching of the electron pulse without energy chirp. As described above, there is no shortening of the electron pulse and the bunching remains approximately constant and at a much smaller value, mainly due to shot-noise, than when the pulse shortens and significant current gradients occur at the radiation wavelength which lead to significant CSE. The differences of the radiation emission and electron bunching, between the spontaneous-only case, when the FEL interaction is switched off, and when the FEL interaction is included in the simulation, is probably due to a small extra bunching due to SACSE. Some small bunching about the radiation wavelength $\lambda_r \approx 64$ nm due to SACSE, can be seen from figures. 5.5 and 5.6 in the electron phase-space evolution going through the undulator. The lack of any real FEL gain is agree with the work of [59] where for negative values of their chirp parameter $\hat{\alpha}$, here $\hat{\alpha} \approx -2$ at $z = 0$, FEL power output is greatly reduced from that expected from an un-chirped beam. So while some increased bunching is seen due to the FEL interaction between radiation and electrons, it is not operating in the high-gain, and greatly reducing the power emitted. Following the minimum of its length, the electron bunch continues to disperse as it propagates through the undulator, ‘flipping over’ in phase space and then re-absorbing some of the emitted radiation. This agrees with previous simplified models [26].

Figure 5.9 plots both the radiation power and electron bunching as a function of local position at saturation. It is seen that the electron pulse bunching, corresponding to the electron pulse at saturation of figures 5.5 and 5.6, is within a small local interval around

$z \sim 9.5\mu$ m. The radiation pulse power for $z_2 < 9.5\mu$m has propagated ahead of the electron bunch and is propagating into vacuum.

Figure 5.10 is the same simulation as for figure 5.9, but with the FEL interaction switched off. The radiation is then that due to spontaneous radiation from shot-noise and CSE only. The difference in the power emitted between the two is then due to the FEL interaction as seen from the extra electron bunching of figures 5.8 and figures 5.5 - 5.6. The small increase in output power shows that the FEL is not working in the high-gain. These results are not as good as a normal FEL as discussed in section 5.4.3.

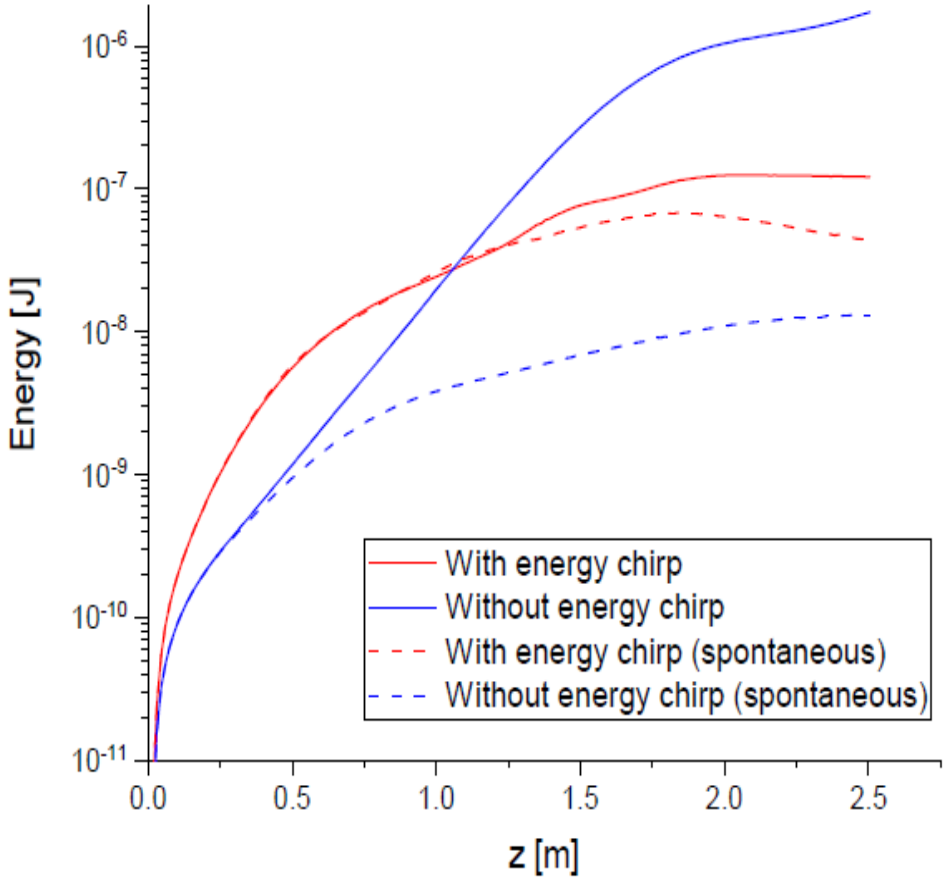

Figure 5.7: Radiation energy as a function of distance z through the undulator in particles distribution with and without energy chirp chirping in the case of spontaneous (no FEL interaction) and unspontaneous (with FEL interaction).

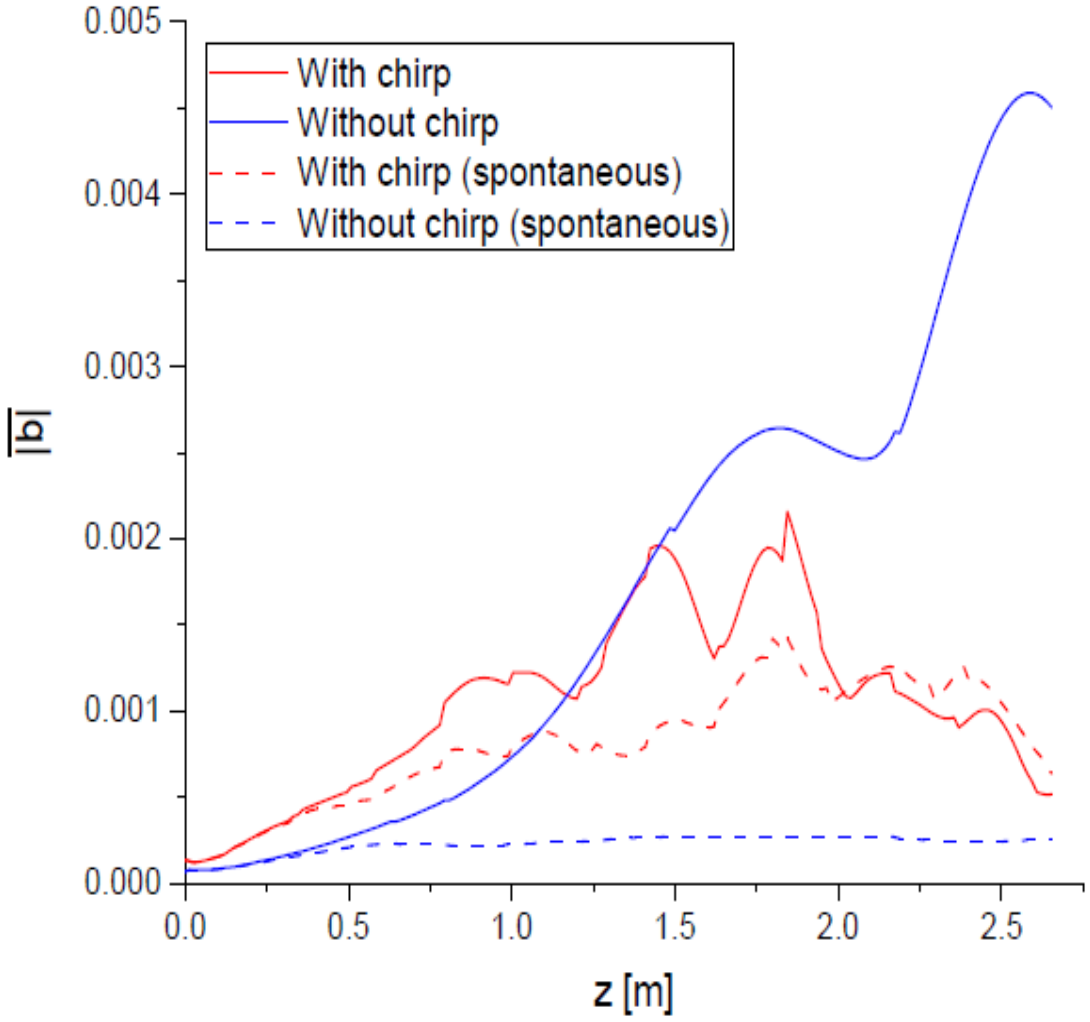

Figure 5.8: Average bunching parameter evolution for the electron beam as a function of distance through the undulator both with and without the energy chirp.

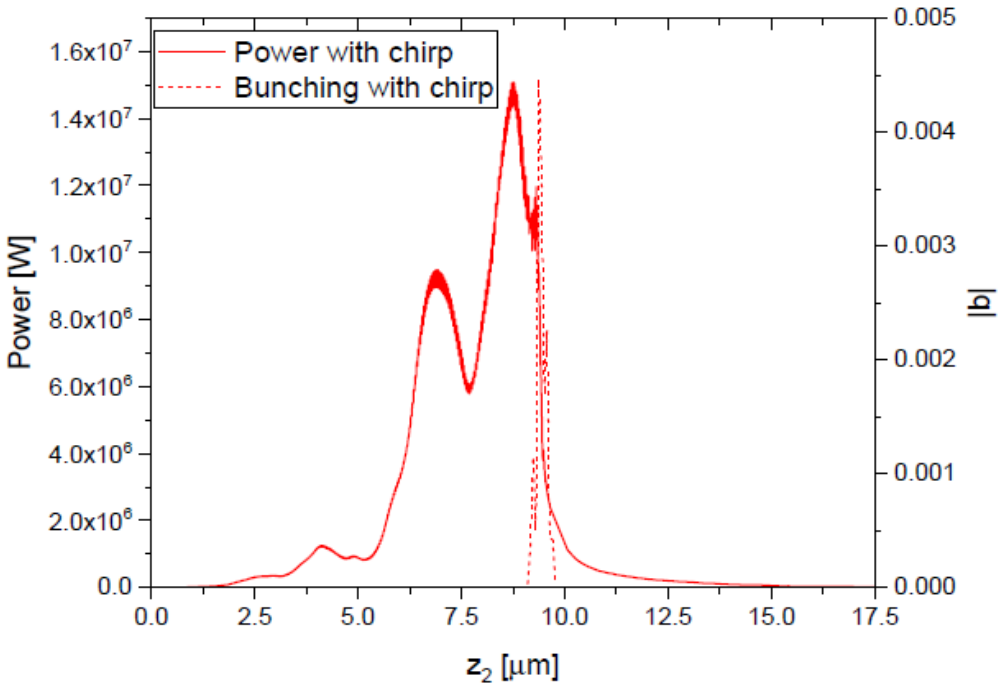

Figure 5.9: The radiation power profile (solid red) and the electron bunching parameter (dashed red) as a function of $z_2 = (ct - z)$ at $z = z_{sat} = 1.95\text{m}$ through the undulator for the energy chirped case.

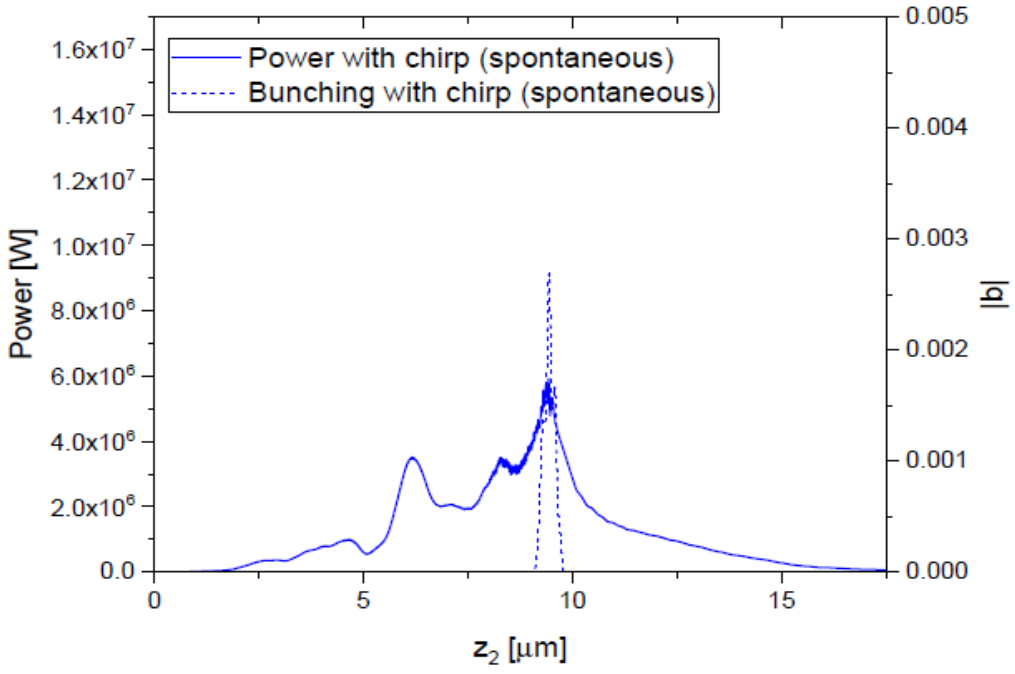

Figure 5.10: As Fig. 5.9, but with no FEL interaction (spontaneous only.) The radiation power profile (solid blue) and the electron bunching parameter (dashed blue) as a function of $z_2 = (ct - z)$ at $z = z_{sat} = 1.95\text{m}$ through the undulator for the energy chirp.

5.4.3 Without energy chirped beam

It was seen above that in the presence of an energy chirp in the electron beam there was no clearly observable exponential FEL gain, and that radiation emission from the bunch was primarily due to CSE as the electron bunch shortened due to dispersion. Furthermore, the energy chirp disrupts the FEL lasing process, firstly because the different parts of the electron bunch emit radiation at a different wavelength and secondly, the electron bunch dispersion inhibits the FEL bunching process. In order to remove these deleterious effects, the energy chirp in the electron bunch is now removed and the FEL interaction is simulated as above. While methods already exist to de-chirp electron beams [53-57], here the energy chirp is removed from the beam by using a simple geometrical approach. The energy chirp is approximated by a linear function in z and this is then used to rotate the electron beam in phase space to minimize any chirp in the microparticle energy as shown in figure 5.4. Given the homogeneous energy spread requirement of $\sigma_\gamma/\gamma \leq \rho_{FEL}$is satisfied, the FEL should now lase. There will also be less CSE as the electron pulse remains at its original length and does not shorten due to dispersion. The de-chirped beam was used in a Puffin simulation, matched to the same undulator parameters (λ_u and a_u) as the chirped beam simulation above. Comparing to the previous chirped simulation's figures. 5.5,5.6, the unchirped beam of figure 5.12 shows a clear electron bunching at the resonant radiation wavelength at the head of the electron pulse, indicative of FEL lasing. Both the radiation energy of figure 5.7 , the radiation power from figure 5.11 and the electron bunching of figures 5. 8 or 5. 11 also show exponential gain as a function of distance z through the undulator. Figure 5.11 plots both the radiation power and electron bunching as a function of local position at saturation. It is seen that the electron pulse bunching, corresponding to the electron pulse at saturation of figure 5.12, is within a small local z interval around $z\sim12.5\mu$m. The radiation pulse power for $z >12.5\ \mu$m is propagating in vacuum.

Unlike the chirped case, this is attributed to SASE effect rather than SACSE as the spontaneous radiation emission for the unchirped beam of figure 5.7 shows a linear growth in z consistent with spontaneous emission due to electron beam shot-noise rather than CSE. From figure 5.12, the peak of the transverse radiation intensity is seen to be more than one order of magnitude higher than in the chirped beam simulation of figures 5.5,5.6 where only CSE effect was present. Again, this is indicative of the FEL interaction where optical guiding effects, absent in CSE, reduce diffraction, so increasing the intensity [63]. Saturated peak power output is seen from figure 5.12 to be $P_{sat}\sim100$ MW with a single pulse duration of ~8 fs FWHM. As with the chirped case, the radiation pulse is seen to have propagated out of the bunched electron beam into vacuum on propagating through the undulator. This peak power is less than that estimated from simple theory [1], where the saturated power output $P_{sat}\sim\rho_{FEL}P_{beam}$ where P_{beam} is the electron beam power. Approximating $P_{beam} \approx 1$ kA $\times$250 MeV, then $P_{sat}\sim$5GW. This reduced power can be attributed to non-ideal beam quality and an electron pulse of only a few cooperation lengths long, where the cooperation length $l_c = \frac{\lambda_r}{4\pi\rho_{FEL}}$ [50]. This relatively short electron pulse

length also reduces the peak radiation power and results in the output of short, single pulses, as observed here, in the weak superradiant regime of FEL operation [50].

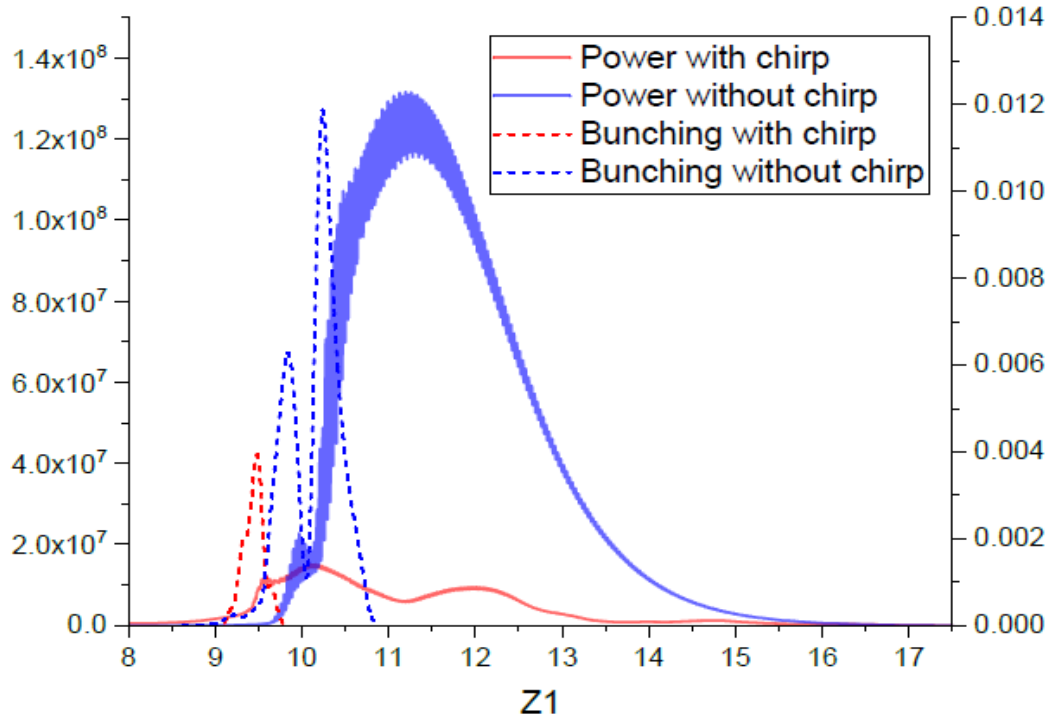

Figure 5.11: The bunching and power profile as a function of window of electron ($z_1 = \frac{Z - v_z t}{l_c}$) for both the energy chirped case (red) where z_{sat} = 1.95m and the unchirped case (black) where z_{sat}= 1.95m.

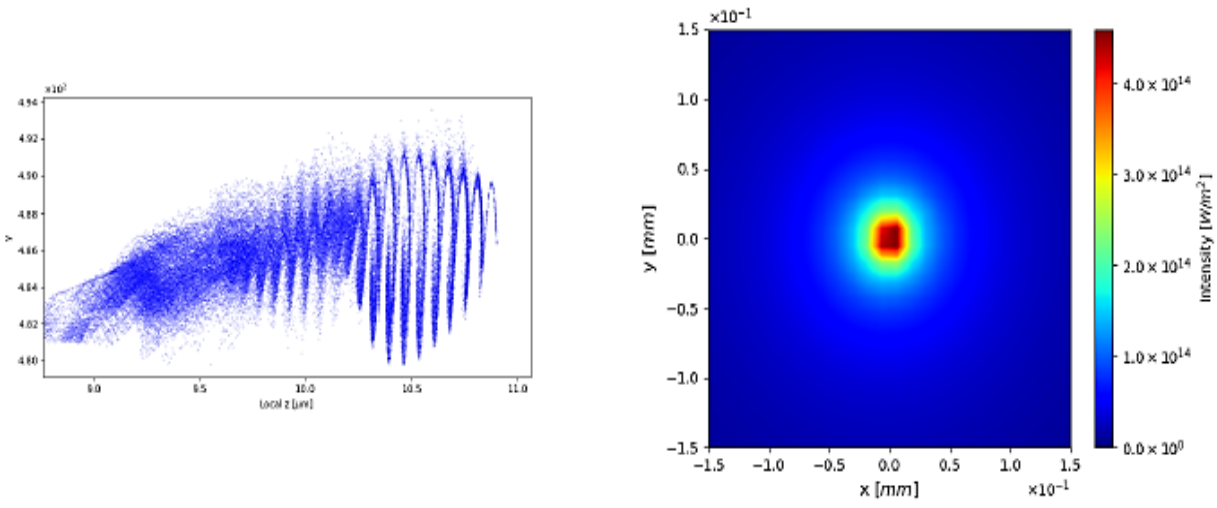

Figure 5.12: Bunching and transverse intensity of the FEL (SASE) effect in the case of removing the energy chirp at saturation $z = z_{sat}$= 1.95m

5.4.4 Numerical simulation with a quadraticly energy chirped beam

In this section the removal of the energy chirp is made, but a quadratic energy dependence remains as seen in figure 5.13. This quadratic dependence of the energy represents a more realistic pulse than the simple removal of the linear chirp as shown above. While the quadratic energy dependence was introduced numerically, as with the removal of the linear chirp above, it has the same scaling as the quadratic dependence seen from the full 3D accelerator simulations conducted in reference [37] (see its *Witness bunch longitudinal phase space* of Fig. 3). So the following FEL simulations represent the most realistic simulations presented in this thesis.

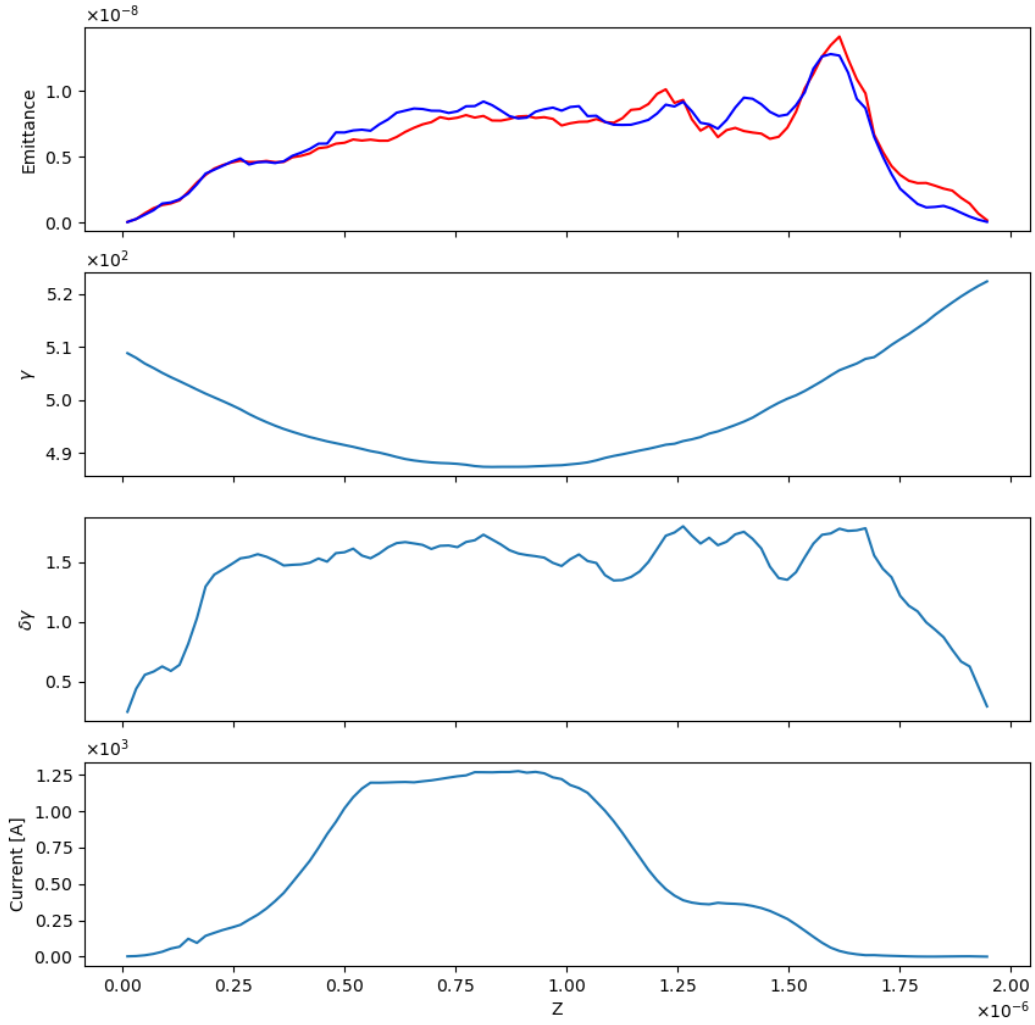

Figure 5.13: The properties of electron beam with a more realistic quadratic energy dependence, following the removal of the linear energy chirp. As with Fig 5.2 from top: electron beam normalised emittance ϵ_n; the localised Lorentz factor γ; the RMS energy spread σ_γ; and the current I as a function of window position $z_2 = (ct - z)$ of the beam.

It can be seen from Figs 5.14-5.16 that following propagation through the undulator the quadratically chirped electron pulse has evolved with the higher energy electrons moving forward in the local *z* coordinate with respect to the lower energy electrons as expected. It is probable that the electrons around 9.5µm in the figure have emitted significant CSE which has assisted seeding and enhancing the FEL interaction over the un-chirped case above which has less CSE emission. It is seen that the FEL interaction is significant over approximately ten radiation wavelengths with strong electron beam bunching between 9.8µm and 10.5µm.

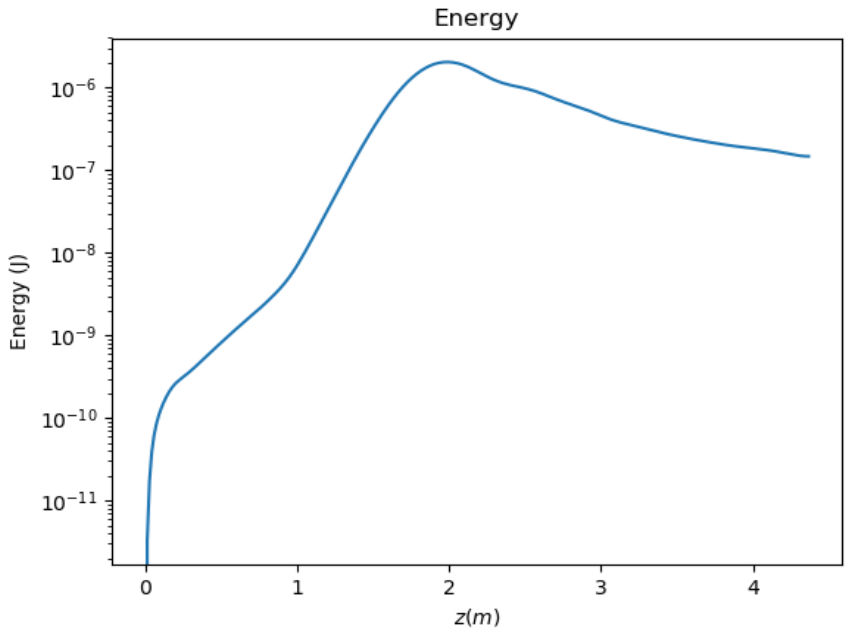

Figure 5.14: Radiation energy as a function of distance z through the undulator in particles distribution with a quadraticly energy chirped beam

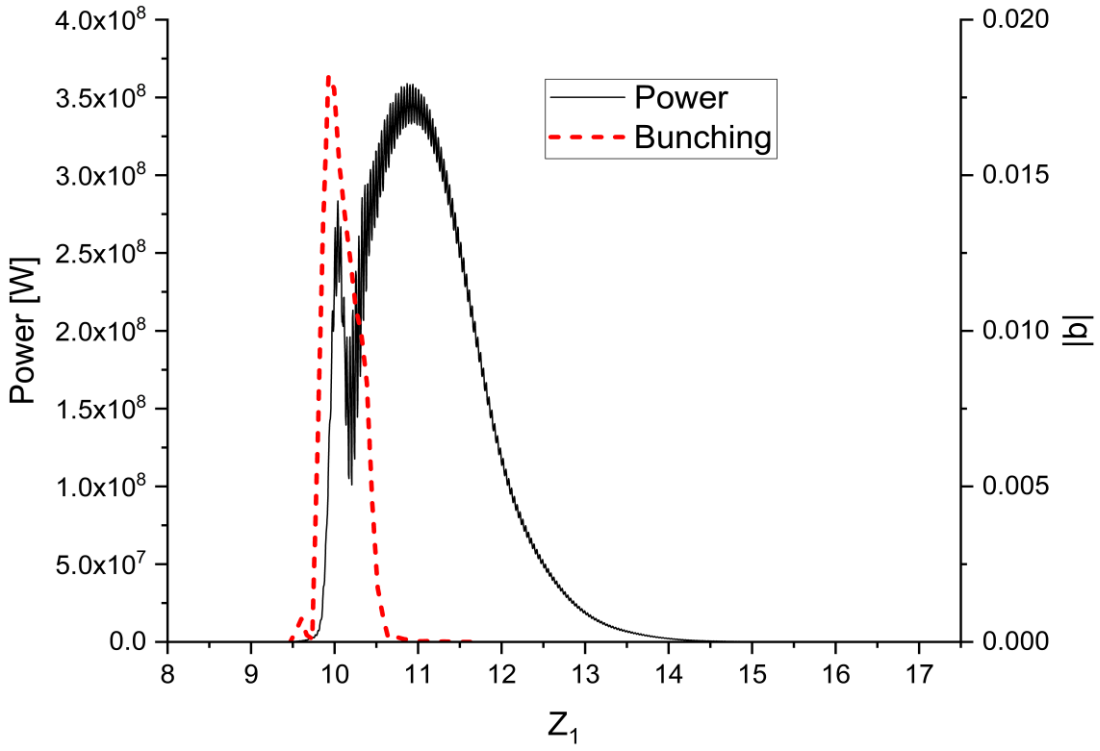

Figure 5.15: The bunching and power profile as a function of window of electron ($z_1 = \frac{Z - v_z t}{l_c}$) for a quadraticly energy chirped beam where z_{sat} = 1.95m

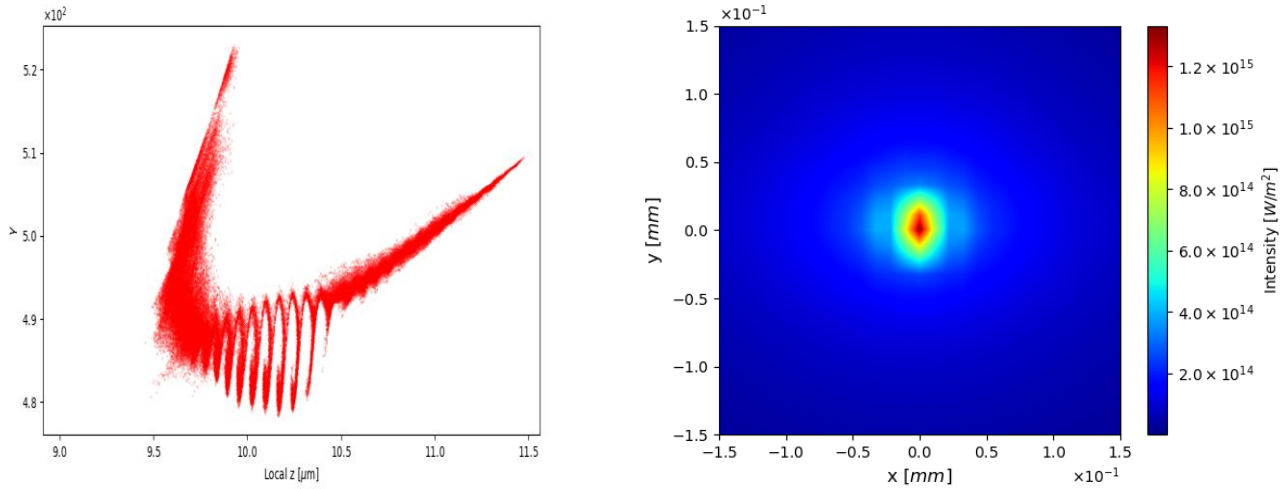

Figure 5.16: Bunching and transverse intensity of the FEL (SASE) effect around saturation at $z = z_{sat}$= 1.95m for the case of energy chirp removal, but including a more realistic quadratic energy dependence than that of Fig 5.12

Chapter 6

6.1 Conclusion

As outlined in prior chapters, the various obstacles associated with a laser-plasma accelerator driven FEL are well understood. For this reason, relevant optimization concepts to allow FEL lasing are examined.

The concept of Plasma Acceleration (PA) is to generate a high peak current, high energy electron beam, and low normalized emittance within a very short distance.

The Free Electron Laser (FEL) is a vital application of the PA. However, there are two primary problems that may not allow FEL operation. One is that there is a large correlated energy spread of the electron beams along the beam (energy chirp). Secondly, there's also a large localised energy spread at the plasma exit that is positioned to trap beams in the undulator. For lower values of energy spread a higher peak energy is obtained at a shorter distance along the undulator as expected. We found that the best results were obtained when the energy spread σ_γ was below 0.5% and it is clear that the energy spread has large impact on the energy gain and output in the FEL and must be minimized to $\sigma_\gamma/\gamma \leq \rho_{FEL}$ in order to achieve acceptable FEL output efficiency.

The challenge of the plasma accelerator energy chirp or correlated energy spread has been recognized in the PWFA/LWFA and that this energy spread may hinder the amplification of the FEL. We can define the energy chirp as the tail of the bunch having more energy than its head. This additional issue from the plasma accelerator further compromises the FEL's performance and supports the need to minimize, if not eliminate, the energy chirp.

The most important outcome of this thesis is to the Start-to-End Simulation of the effect of the energy chirp of electron beams in lasing. Another important message from this thesis is that removing the energy chirp is key to enable the high quality beams for applications. We decided to demonstrate application of PA beam in FEL. The beam is first used as delivered – with relatively high chirp and then with the chirp removed. We also considered the case where the chirp removal was not perfect and left a quadratic electron energy dependence in *z* in agreement with the scaling of the full 3D plasma accelerator simulation of [37].

We obtained the parameters of the electron beams from a research team at Strathclyde University. We worked on a special type of plasma accelerator, the Trojan Horse method, or 'plasma photocathode'. It is one of the promising schemes in plasma acceleration mechanism to produce electron bunches with high brightness and ultra-low emittance. This method is based on injecting electrons (driver beam) inside the plasma blowout by a tightly

focused laser to produce a witness bunch which has a small energy spread and can then accelerate in multi-GV/m fields. The code VSim was used for the PWFA simulation.

They made new Trojan Horse PIC simulations where the aim was to optimize the witness bunch properties for FEL performance. Although the new runs produced bunches with peak current at kA level, normalized emittance at ~10^{-8} m rad range and slice energy spread at $\sigma_\gamma \sim 0.25\%$ level such bunch properties could be promising as input for FEL.

This thesis uses a start-to-end simulation. First of all, we have to prepare the output file from VSim simulation after going through multiple steps into suitable file for the FEL simulation using the Puffin code. We choose Puffin as it is better able to model the interaction for any complex beam structures occur such as the energy chirp. The code is unaveraged over the radiation wavelength. Another example of this is useful is where Coherent Spontaneous Emission occurs due to an electron bunch that has significant current gradients over a resonant radiation wavelength. This may typically occur in PA output which generate short, high current bunches. Here, Puffin would be a more accurate FEL modelling tool. Similarly, where significant beam energy chirps occur, or in multi-colour operation, averaged simulation codes are not as able to model the resultant effects. Before any full simulation using Puffin we have to choose the suitable undulator parameters such as λ_u undulator period and a_u undulator parameter for TH FEL target radiation wavelength of $\lambda_r = 64nm$ and at the same time we have taken the gain length into account to ensure small gain length l_g. It was also considered that the following condition $\sigma_\gamma/\gamma \leq \rho_{FEL}$ is met, where σ_γ is the slice energy spread an.

Using the full start-to-end approach the Free Electron Laser (FEL) operation on a self-amplified spontaneous emission (SASE) was studied analytically and numerically using a 3D model. We have studied the influence of a quasi -linear energy chirp in the electron pulse from plasma photocathode. For the beam energy used here, this chirp causes the electron pulse to shorten as it propagates through the undulator and emit a large CSE power. This CSE was seen to drive the electrons to give some weak periodic bunching at the resonant radiation wavelength, but not to enter into the high-gain regime where analysis in the steady-state regime (no pulse effects) predicts output powers approximately two orders of magnitude greater.

The dynamic shortening of the electron pulse and so the emission of CSE as it propagates through the undulator is an effect that has never been modeled in plasma accelerator driven FEL simulations before. The CSE seeding of the high gain FEL interaction (SACSE) is a mechanism that may prove useful to future plasma accelerator driven FEL designs.

As the next step we decided to remove the chirp by simple mathematical procedure thus getting a beam without an energy chirp. The interesting point was the difference between the two cases. The un-chirped case resulted in the generating of a high-gain microbunching effect of the FEL as shown on figures 5. 7 and 5. 12. The result showed that by removing chirp we can get higher energy gain and higher intensity. The experiment showed that the

PA generated beams can prove to be a good source of electron beam for FEL after finding a way to efficiently remove the chirp.

When the plasma accelerator methods of [37] are used to remove the chirp, a nearly quadratic energy dependence of the electron pulse remains. This was also modelled using a similar numerical method to the removal of the linear chirp and using the same scaling as the full plasma accelerator modelling of [37]. This electron pulse with the remaining quadratic energy chirp still lased strongly in the FEL with strong electron bunching probably seeded by higher power CSE than when the energy chirp is completely removed. This will require further investigation and optimization and may, in fact, be a method to further enhance FEL operation.

Further methods to remove the electron beam energy chirp that would allow a PWFA FEL, are the subject of on-going research and, if possible, are expected to allow the high gain FEL interaction to develop, possibly in a SACSE mode of operation and for the first time, to generate experimental output of short coherent pulses of high power coherent radiation from a plasma accelerator.

6.2 Future work

One of the most important applications of plasma-based accelerators may be the FEL. Today, most leading researchers in the plasma accelerators field are working on generating high quality electron bunches that are able to drive an FEL.

The correlated energy spread, or the energy chirp, represents a potential obstacle and energy chirp reduction ('dechirping') techniques will provide a key contribution towards high quality electron beams. Moving forward, this chirp effect should be removed before exiting the plasma acceleration stage as in [37] so as to conserve the high quality electron beam for use in the free electron FEL and any other applications. These methods need further investigation and optimization.

Other dechirping methods outside the plasma are possible. For example, decelerating a passive corrugated metal structure by an RF dephasing technique. This rotates the longitudinal phase space. Dechirping using beam generated wakefields to remove the head-to-tail chirp may also be possible.

TH-injection produced witness beams with consideration to the maximized relative energy spread value of σ_{rms}~1.2 % for the FEL-application, this is an indicator that the first value is likely too large and needs to be reduced. The main component of the relative energy spread is derived from the energy time correlation, or energy chirp, in the phase space running lengthwise. Hence, removing the energy chirp is essential for maintaining the high quality beams necessary in the applications. We need to recalculate the work of [61] in 3D by using Puffin code.

The high-power, high-frequency capabilities of the free-electron laser have found interesting applications in fusion-energy research and high energy physics: the auxiliary heating of plasmas at cyclotron frequencies, and the high-power drive for a two-beam, high-energy-gradient linear accelerator.

6.3 Publications from this thesis

Different forms of the work in this thesis have been published. Posters were presented at Sciences@ FEL conferences in Stockholm June 25-27 ,2018, at the 3rd international conferences on Nuclear and Plasma Physics and submitted into IOP science with the following DOI https://doi.org/10.1088/2399-6528/ab291b. The paper is in appendix A. The second paper submitted to New Journal of Physics and also, presented as a Poster at FEL2019 (https://fel2019.vrws.de/papers/tup051.pdf) and as a paper are attached in Appendices B and C. The third paper, on which I will be a co-author and is currently in preparation, is to be submitted to the journal Nature Photonics and shows the results of a method of removing the chirp which allows FEL lasing as shown in this thesis.

Bibliography

[1] B.W.J. McNeil and N.R. Thompson. X-ray Free-electron Lasers. *Nature Photonics*, 4:814-821, 2010.

[2] Z. Huang and K. J. Kim. Review of X-ray Free-Electron Laser Theory. *Phys. Rev. ST-AB* 10, 034801, 2007

[3] T. Tajima and J. M. Dawson. Laser Electron Accelerator. *Phys. Rev. Lett.*, 43(4):267–270, 1979 .

[4] H. P. Schlenvoigt, K. Haupt, A. Debus, F. Budde, O. Jäckel, S. Pfotenhauer, H. Schwoerer, E. Rohwer, J. G. Gallacher, E. Brunetti, R. P. Shanks, S. M. Wiggins & D. A. Jaroszynski. A compact synchrotron radiation source driven by a laser plasma wakefield accelerator. *Nat. Phys*. **4**, 130–133, 2008.

[5] M Fuchs, R Weingartner, A Popp, Z Major, S Becker. Laser-driven soft-X-ray undulator source .*Nat. Phys.* **5**, 826–829,2009.

[6] F. Grüner, S. Becker, U. Schramm, T. Eichner, M. Fuchs, R. Weingartner, D. Habs, J. Meyer-ter-Vehn, M. Geissler, M. Ferrario, L. Serafini, B. van der Geer, H. Backe, W. Lauth, S. Reiche .Design considerations for table-top, laser-based VUV and X-ray free electron lasers, *App. Phys. B* **86**, 431–435, 2007.

[7] K. Nakajima. Compact x-ray sources: Towards a table-top free-electron laser. *Nat. Phys.* **4**, 92–93, 2008.

[8] C. Nieter and J. R. Cary, J. Comput. VORPN, a versatile plasma simulation code. *J. Comp. Phys*. 196, 448, 2004.

[9] B. Hidding, G. Pretzler, J. B. Rosenzweig, T. Königstein, D. Schiller, and D. L. Bruhwiler. Ultracold electron bunch generation via plasma photocathode emission and acceleration in a beam-driven plasma blowout. *Phys. Rev. Lett.*, 108:035001, 2012.

[10] B Hidding, G G Manahan, O Karger, A Knetsch, G Wittig, D A Jaroszynski, ZM Sheng, Y Xi, A Deng, J B Rosenzweig, G Andonian, A Murokh, G Pretzler, D L Bruhwiler, and J Smith. Ultrahigh brightness bunches from hybrid plasma accelerators as drivers of 5th generation light sources. *J. Phy. B: Atomic, Molecular and Opt. Phy.*, 47(23):234010, 2014.

[11] S. Reichem. GENESIS: A Fully 3D Time-Dependant FEL Simulation Code. *Nucl. Instr. and Meth. in Phys. Res. A*, **429**:243-248, 1999.

[12] W.M. Fawley, 2006. An Enhanced GINGER Simulation Code With Harmonic Emission and HDF5 Capabilities, Proceedings of FEL 2006, BESSY, Berlin, Germany, 218-221, 2006.

[13] E.L. Saldin, E.A. Schneidmiller, M.V. Yurkov. FAST: A Three-Dimensional Time-Dependant FEL Simulation Code. *Nucl. Instr. and Meth. in Phys. Res. A* **429** 233-237, 1999.

[14] L. T. Campbell, and B. W. J. McNeil. Puffin: A Three Dimensional Unaveraged Free Electron Laser Simulation Code. *Phys. of Plasmas*,19:093119, 2012.

[15] L.T. Campbell, J.D.A. Smith, P. Traczykowski and B.W.J. McNeil, Updated Description of the FEL Simulation Code Puffin, in Proceedings of IPAC2018, Vancouver, BC, Canada, 02 Photon Sources and Electron Accelerators, A06 Free Electron Lasers, THPMK112 , 2018.

[16] James Robert Henderson. *Novel techniques in Free Electron Lasers*. PhD thesis, University of Strathclyde, 2015.

[17] Lawrence Thomas Campbell. *The physics of a 4th generation light source*. PhD thesis, University of Strathclyde, 2011.

[18] Ahmad Fahim Habib, et al. Plasma accelerator-based ultrabright x-ray beams from ultrabright electron beams. SPIE Optical Engineering Applications, 2019, San Diego, California,United States, 2019.

[19] P. Schmuser, M. Dohlus, J. Rossbach, C. Behrens. Free-Electron Laser in the Ultraviolet and X-Ray Regime. *Springer Tracts in Modern Physics*, 229, 2008.

[20] R. Bonifacio, L. De Salvo, P. Pierini, N. Piovella, and C. Pellegrini. Spectrum,Temporal structure, and fluctuations in a High-Gain Free-Electron Laser Starting from Noise. *Phys. Rev. Lett.*, 73:70, 1994.

[21] R. Bonifacio, L. De Salvo Souza and B.W.J. McNeil. Emittance Limitations in the Free Electron Laser. *Optics Comm.*, 93,179, 1992.

[22] M. Xie. Exact and Variational Solutions of 3D Eigenmodes in High Gain FELs. *Nucl. Instr. and Meth. in Phys. Res. A* **445**-59, 2000.

[23] M.Xie. Design optimization for an x-ray free electron laser driven by slac linac. *Proc. Of 1995 Part. Accel. Conf.*, 183, 1996.

[24] J.R. Henderson, L.T. Campbell and B.W.J. McNeil. Free Electron Laser Using Beam by Design. *New J. Phys. p.*17-083017, 2015.

[25] Bilel Hadri, Samuel Kortas, Saber Feki, Rooh Khurram. Overview of the KAUST's Cray X40 system–Shaheen II. Greg Newby, Cray User Group Proceedings, 2015.

[26] L.T. Campbell and B.W.J. McNeil, A Simple Model For The Generation Of Ultra-Short Radiation Pulses, FEL2012: Proceedings of the 34th International Free-Electron Laser Conference, 26–31 August 2012, Paper THPD41, Nara, Japan .

[27] J.R. Henderson, H. P. Freund, L.T. Campbell and B.W.J. McNeil .Modelling elliptically polarised free electron lasers . *New J. Phys. p*. 18 062003 , 2016.

[28] https://github.com/UKFELs/Puffin.
[29] https://github.com/UKFELs/Paraffin
[30] https://github.com/UKFELs/FXFEL/
[31] https://github.com/UKFELs/JDF

[32] A. Loulergue, M. Labat, C. Evain, C. Benabderrahmane, V. Malka and M. E. Couprie. Beam manipulation for compact laser wakefield accelerator based free-electron lasers. *New J. Phys. p.* 17, 2015.

[33] M.E. Couprie, , et al.,. An application of laser–plasma acceleration: towards a free-electron laser amplification. *Plasma Physics and Controlled Fusion*,**58**, 2015.

[34] V. Malka et al. Electron Acceleration by a Wake Field Forced by an Intense Ultrashort Laser Pulse. *Science* 298, 1596 , 2002.

[35] B. Hidding et al. Beyond Injection: Trojan Horse Underdense Photocathode Plasma Wakefield Acceleration. *AIP Conference Proceedings* ,**1507**, 570 , 2012.

[36] A. Deng , O. Karger and et al. Generation and acceleration of electron bunches from a plasma photocathode. *Nat. Phys.* accepted, arXiv:1907.00875v1, 2019.

[37] G. G. Manahan, A. F. Habib, P. Scherkl, P. Delinikolas, A. Beaton, A. Knetsch, O. Karger, G. Wittig, T. Heinemann, Z. M. Sheng, J. R. Cary, D. L. Bruhwiler, J. B. Rosenzweig and B. Hidding. Single-stage plasma-based correlated energy spread compensation for ultrahigh 6D brightness electron beams. *Nat. Commun*. **8** 15705, 2017.

[38] B. Hidding, T. KÃ nigstein, J. Osterholz, S. Karsch, O. Willi, and G. Pretzler. Monoenergetic energy doubling in a hybrid laser-plasma wakefield accelerator. *Phys.Rev. Lett.*, 104(19):195002, 2010.

[39] Zhirong Huang,Yuantao Ding and , Carl B Schroeder. Free-Electron Laser from a Laser-Plasma Accelerator Using a Transverse-Gradient Undulator. *Phys.Rev. Lett.*, 109(20):204801, 2012.

[40] A. R. Maier, A. Meseck, S. Reiche, C. B. Schroeder, T. Seggebrock, and F. Grüner. Demonstration Scheme for a Laser-Plasma-Driven Free-Electron Laser *Phys. Rev.* X**2** 031019, 2012.

[41] T. Seggebrock, A. R. Maier, I. Dornmair, and F. Grüner. Bunch decompression for laser-plasma driven free-electron laser demonstration schemes. *Phys. Rev. ST Accel. Beams* **16**-070703, 2013.

[42] M. E. Couprie , A. Loulergue , M. Labat , R. Lehe and V. Malka , Towards a free electron laser based on laser plasma accelerators, *J. Phys. B: Atomic, Molecular and Opt. ics*,47,234001, 2014.

[43] A. Loulergue, M, Labat, C. Evain, C. Benabderrahmane, V. Malka and M.E. Couprie. Beam manipulation for compact laser wakefield accelerator based free-electron lasers . *New J. Phys.* ,17-023028, 2015.

[44] E.L. Saldin, E.A. Schneidmiller and M.V. Yurkov,. On a linear theory of an FEL amplifier with an axisymmetric electron beam. *Optics Comm.*, 97, 272, 1993.

[45] A.R. Maier, A. Meseck, S. Reiche, C.B. Schroeder, T. Seggebrock and F. Gruner, Demonstration Scheme for a Laser-plasma-driven free-electron Laser, Phys. Rev., X 2, 031019, 2012.

[46] B. M. Alotaibi, Sh. M. Khalil, B.W.J. McNeil, and P. Traczykowski. Modelling a laser plasma accelerator driven free electron laser. *J. Phys. Commun.* 3 , 065007, 2019.

[47] M. E. Couprie and M. Valléau 2012 Synchrotron radiation,polarisation, devices, new sources Proc. 6th Int. School on‘Magnetism and Synchrotron Radiation: Towards the Fourth Generation Light Sources’ (Mittelwihr, France), 2012.

[48] I. Dornmair, L.T. Campbell, J.T. Henderson, S. Jalas, O. Karger, M. Kirchen, A. Knetsch, G.G. Manhan, G. Wittig, B. Hidding, B.W.J. McNeil, A.R. Maier. Towards Plasma-driven Free Electron Laser. *NIC Symposium*, 48 :401, 2016.

[49] Marco Venturini. Basics on FEL Physics; Undulators; High-Level Machine-Design Parameters.Course Materials, Lecture Mo2 - Rutgers University - New Jersey, 2015.

[50] R. Bonifacio, B.W.J. McNeil and P. Pierini. Superradiance in the High-Gain Free Electron Laser. *Phys. Rev. A,* 40:4467, 1989.

[51] L.T. Campbell and A.R. Maier. Velocity dispersion of correlated energy spread electron beams in the free electron laser. *New J. Phys.*, 19 :033037, 2017.

[52] M. Khojoyan, F. Briquez, M. Labat, A. L oulergue, O.Marcouille, F. Marteau, G. Sharma, M. E. Couprie. Transport Studided Of LPA Electron Beam Towards The FEL Amplification At COXINEL, *Nucl, Instr. and Meth. in Phys. Res A*, 829 -260, 2016.

[53] Feichao Fu, Rui Wang, Pengfei Zhu, Lingrong Zhao, Tao Jiang, Chao Lu, Shengguang Liu, Libin Shi, Lixin Yan, Haixiao Deng, Chao Feng, Qiang Gu, Dazhang Huang, Bo Liu, Dong Wang, Xingtao Wang, Meng Zhang, Zhentang Zhao, Gennady Stupakov, Dao Xiang, and Jie Zhang. Demonstration of nonlinear-energy-spread compensation in relativistic electron bunches with corrugated structures. *Phys. Rev. Lett.*, 114:114801, 2015.

[54] Zhen Zhang, Karl Bane, Yuantao Ding, Zhirong Huang, Richard Iverson, Timothy Maxwell, Gennady Stupakov, and Lanfa Wang. Electron beam energy chirp control with a rectangular corrugated structure at the linac coherent light source. *Phys. Rev. ST Accel. Beams*, 18:010702, 2015.

[55] Y. P. Wu, J. F. Hua, Z. Zhou, J. Zhang, S. Liu, B. Peng, Y. Fang, Z. Nie, X. N. Ning, C.-H. Pai, Y. C. Du, W. Lu, C. J. Zhang, W. B. Mori, and C. Joshi, . Phase space dynamics of a plasma wakeeld dechirper for energy spread reduction. *Phys. Rev. Lett.* 122, 204804, 2019.

[56] R. D'Arcy, S. Wesch, A. Aschikhin, S. Bohlen, C. Behrens, M. J. Garland, L. Goldberg, P. Gonzalez, A. Knetsch, V. Libov, A. M. de la Ossa, M. Meisel, T. J. Mehrling, P. Niknejadi, K. Poder, J.-H. R.ockemann, L. Schaper, B. Schmidt, S. Schroder, C. Palmer, J.-P. Schwinkendorf, B. Sheeran, M. J. V. Streeter, G. Tauscher, V. Wacker, and J. Osterho. Tunable plasma-based energy dechirper. *Phys. Rev. Lett.* 122, 034801, 2019.

[57] V. Shpakov, M. P. Anania, M. Bellaveglia, A. Biagioni, F. Bisesto, F. Cardelli, M. Cesarini, E. Chiadroni, A. Cianchi, G. Costa, M. Croia, A. Del Dotto, D. Di Giovenale, M. Diomede, M. Ferrario, F. Filippi, A. Giribono, V. Lollo, M. Marongiu, V. Martinelli, A. Mostacci, L. Piersanti, G. Di Pirro, R. Pompili, S. Romeo, J. Scifo, C. Vaccarezza, F. Villa, and A. Zigler. Longitudinal phase-space manipulation with beam-driven plasma wake_fields,*Phys. Rev. Lett*. 122,114801, Mar 2019.

[58] E. L. Saldin, E. A. Schneidmiller, and M. V. Yurkov. Self-Amplified Spontaneous Emission FEL with Energy-Chirped Electron Beam and its Application for Generation of Attosecond X-ray Pulses. *Phys. Rev. ST-Accel. Beams*, 9:050702, 2006.

[59] J. R. Henderson, L. T. Campbell and B. W. J. McNeil. Chirped and Modulated Electron Pulse Free Electron Laser Techniques. *Proceedings of FEL 2014, Basel, Switzerland*, MOC04, 2014.

[60] B.W.J. McNeil, G. R. M. Robb and D. A. Jaroszynski. Self-Amplification of Coherent Spontaneous Emission in the Free Electron Laser. *Opt. Commun.*,165:65-70, 1999.

[61] B. W. J. McNeil, G. R. M. Robb, and D. A. Jaroszynski. SACSE in a FEL Amplifier with Energy Spread. *Nucl, Instr. and Meth. in Phys. Res. A* 445:72-76, 2000.

[62] B. W. J. McNeil, M. W. Poole, and G. R. M. Robb. Unified Model of ElectronBeam Shot Noise and Coherent Spontaneous Emission in the Helical Wiggler Free Electron Laser. *Phys. Rev. ST-Accel. Beams*, 6:070701, 2003.

[63] Scharlemann E T, Sessler A M and Wurtele. Optical guiding in a free-electron laser. *Phys. Rev. Lett.*, 54 1925-1928, 1985.

Appendix

Appendix A
Paper 1

IOP Publishing J. Phys. Commun. 3 (2019) 065007 https://doi.org/10.1088/2399-6528/ab291b

Journal of Physics Communications

PAPER

Modelling a laser plasma accelerator driven free electron laser

B M Alotaibi[1,3], Sh M Khalil[1,2], B W J McNeil[3,4] and Piotr Traczykowski[3,4]

[1] Physics Department, Faculty of Science, Princess Nourah Bint Abdulrahman University, Riyadh, Kingdom of Saudi Arabia
[2] Plasma Physics & Nuclear Fusion Department, NRC, Atomic Energy Authority, Cairo, Egypt
[3] Department of Physics, University of Strathclyde, Glasgow, G4 0NG United Kingdom
[4] Cockcroft Institute, Warrington, WA4 4AD, United Kingdom

E-mail: bmalotaibi@pnu.edu.sa

Keywords: free-electron lasers, laser-plasma accelerator, puffin code, undulator

OPEN ACCESS

RECEIVED
10 May 2019

REVISED
17 May 2019

ACCEPTED FOR PUBLICATION
12 June 2019

PUBLISHED
24 June 2019

Abstract

Free-electron lasers (FEL) are the brightest, coherent sources of short wavelength radiation from the VUV into the x-ray. There is much research interest in reducing the cost and the size of FELs by utilising new accelerator techniques. Laser-plasma accelerator (LPA) are a promising accelerator for next generation compact FEL light sources with many potential advantages due to the high acceleration gradient and large peak currents they offer. The electron beams of a LPA typically have a smaller transverse emittance, a large energy spread and tend to be of shorter duration and higher current than conventional Radio Frequency (RF) accelerators. In this paper, a FEL driven by an electron beam from a typical LPA was simulated using the 3D FEL simulation code Puffin. It is shown that lowering the homogenous electron beam energy spread increases the radiation energy output in a short undulator and , as become less than the FEL, or Pierce parameter (ρ), then the peak radiation energy increases and the saturation length reduces significantly as expected.

Introduction

The FEL can create tunable, high-power sources from the hard x-ray to far infrared (FIR) with high brightness, coherent radiation, as has been demonstrated at many facilities worldwide [1]. Figure 1 shows a typical high gain FEL configuration with a highly relativistic electron beam propagating through an undulator or (wiggler) characterised by the dimensionless undulator parameter, $a_u = \frac{eB_u\lambda_u}{2\pi mc}$, where, B_u is the RMS undulator magnetic field strength, λ_u is the undulator period, e and m are the electron charge and rest-mass respectively. The resonant FEL wavelength is then given by $\lambda_r = \frac{\lambda_u}{2\gamma_0^2}(1 + a_u^2)$, where γ_0 is the mean Lorentz factor.

A fundamental scaling parameter for a FEL that determines the strength of FEL interaction in the 1D is the dimensionless Pierce parameter(also called the FEL parameter), defined as [2]:

$$\rho = \left[\frac{a_u^2[JJ]^2}{16}\frac{k_p^2}{k_u^2}\right]^{1/3} = \left[\frac{1}{8}\frac{I_{peak}}{I_A}\frac{a_u^2[JJ]^2}{\gamma_0^3\sigma_x^2k_u^2}\right]^{1/3} \quad (1)$$

where a planer undulator trajectory is assumed [3] with a Bessel function factor $[JJ] = [J_0(\xi) - J_1(\xi)]$ where $\xi = a_u^2/2(1 + a_u^2)$. The gain length of the interaction is $l_g = \lambda_u/4\pi\rho$. $k_p = \sqrt{2I_{peak}/(\gamma_0^3 I_A\sigma_x^2)}$ is the longitudinal plasma oscillation, k_u is the undulator wavenumber, $I_A = ec/r_e \approx 17\ kA$ is the Alfven current , $r_e \approx 2.8 \times 10^{-15}m$ is the classical electron radius, I_{peak} is the peak current , and $\sigma_x = \sigma_y$ is the rms transverse radius of the electron beam for a circular cross-sectional beam[2, 3] .

The normalised beam emittance ε_n introduces an effective energy spread [4] in the resonant energies of the electron beam [2, 3] which may be written as:

$$\sigma_\epsilon = \frac{\epsilon_n a_u^2 k_u^2 \beta}{4\gamma_r(1 + a_u^2)} \quad (2)$$

where β is the betatron function and γ_r is the resonant energy for the radiation field. This may be combined with the homogenous electron beam energy spread σ_γ, to give a total effective energy spread of :

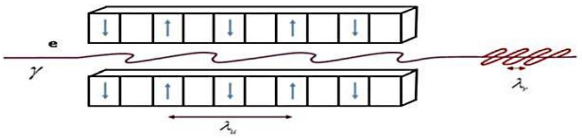

Figure 1. Schematic of an FEL amplifier with the electron passing through a planer undulator and emitting resonant undulator radiation.

Table 1. Output parameters from LPA.

Parameters	Value parameters
Normalised emittance (ε_n)	0.2 mm mrad
Normalised beam energy (γ)	600 MeV
Peak current (I_{peak})	9.6 kA
Bunch charge current (Q)	40 pC
RMS energy spread (σ_γ)	(0.0, 0.25, 0.5, 0.75, 1.0)%

$$\sigma_{eff} = \sqrt{\sigma_\epsilon^2 + \sigma_\gamma^2}. \tag{3}$$

Some conditions are required for high gain FEL operation [1, 3, 5]:

The homogeneous energy spread must be less than the FEL parameter $\sigma_\gamma \leqslant \rho$.

The conflicting requirements of transverse matched beam radius and radiation diffraction require that the normalised beam emittance $\epsilon_n \leqslant \lambda_r \gamma / 4\pi$.

To balance the a_u-dependent Pierce parameter ρ and the resulting gain length l_g, while minimizing λ_u and obtaining a practical undulator gap g, undulator parameters $a_u = 2.3$ and ($\lambda_u = 15mm$)were used [6]. An undulator length of 2 m (determined from the estimated saturation length and λ_u) was chosen to allow for a compact set-up and to avoid refocusing optics between undulator modules enhancing FEL performance with a planar undulator design [6].

The following simulations were carried out using the code Puffin [7, 8] which is a non-averaged FEL simulation code that may be used to simulate FEL parameters typical of those generated by LPA output . In contrast in [6] they used Genesis code. GENESIS and PUFFIN are considered as high gain FEL simulation codes, including clear differences between them.

In spite of the agreement between GENESIS and PUFFIN was in general excellent, it is shown that [9] for a relatively small energy modulations, the GENESIS is a sufficient tool for modeling both HGHG and EEHG beams. However in more extreme settings, such as those with very large energy modulations, the assumptions of GENESIS could cause inaccurate results [9].

Simulation results

A study was first carried out for a range of parameters using the Ming Xie formalism of [10, 11]. These analytical calculations of FEL performance, which does not require any significant computation, estimates important parameters, such as the gain length, while taking into account multiple electron beam and 3D effects, such as radiation diffraction of importance for short wavelength operation. The estimates so obtained are a quick and useful method for optimising FEL output and other parameters such as the gain length.

The FEL simulation code Puffin [7, 8] was also used in a steady-state mode, which has periodic boundary conditions applied over one wavelength of the radiation field/electron beam [12]. Full 3D-Puffin simulations were used to model a LPA driven FEL which assumed Gaussian distributions for the electron pulse duration and other electron parameters. An electron bunch with LPA–like parameters as given in table 1 was used for different values of uncorrelated energy spreads 0.0%–1.0% [6].

The- Ming Xie formalism was used to determine the effect of many beam parameters in table 1, such as electron beam emittance and energy spread on the undulator length to achieve high power saturated radiation output. Figure 2 shows contour plots of (**a**) Pierce parameter ρ (**b**) RMS transverse sizes of the electron beam $\sigma_{x,y}$

X

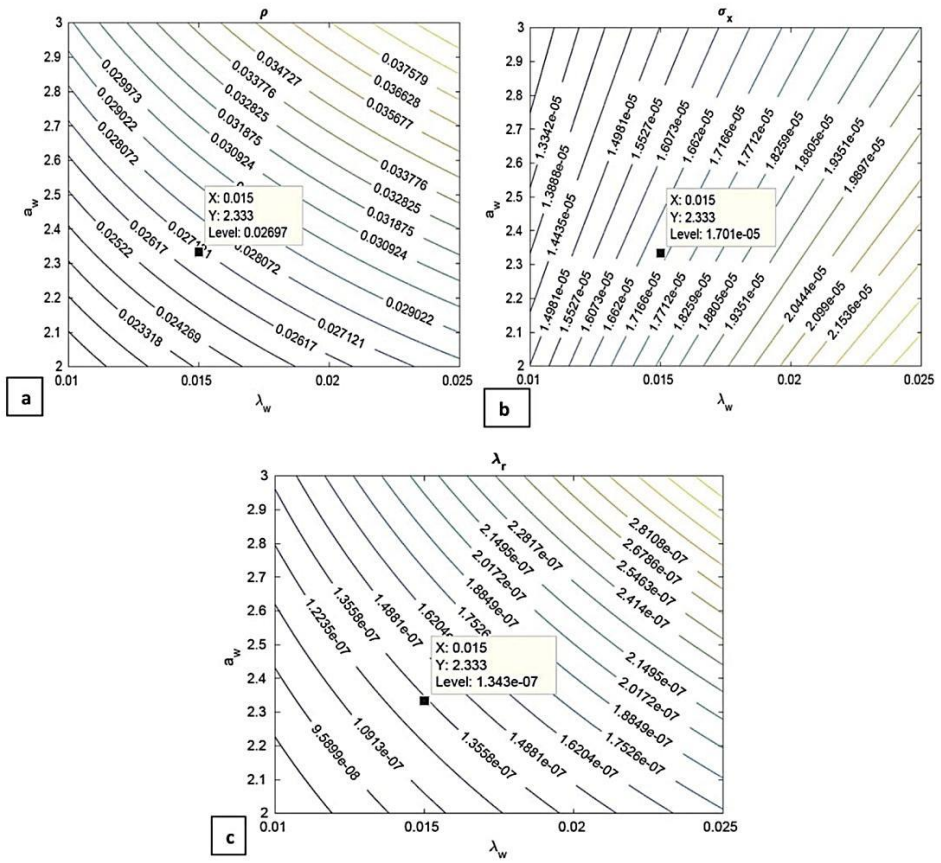

Figure 2. Contour plots of (a), (b) $\sigma_{x,y}$ and (c) λ_r against λ_u and a_u.

Table 2. Output parameters from Ming Xie formalism.

Parameters	Value parameters
ρ	0.0269
L_{sat}	0.83 m
λ_r	1.34×10^{-7} m = 134 nm
σ_x, σ_y	1.7×10^{-5} m

and (**c**) resonant wavelength against λ_u and a_u using the parameters of table 1. This resulted in the parameters of table 2 being chosen.

These parameters were then used in the Puffin simulation code in steady-state mode.

L_{sat} is the saturation length, which can be approximated by $L_{sat} \approx 20L_g$ [13]. Figure 3 shows a comparison between the radiation energy of different values of energy spreads σ_γ in steady state mode .

3D laser-wakefield accelerator (LWA) driven FEL

After running Puffin in periodic (steady state) mode as above, it is seen that beam energy spreads of $\sigma_\gamma = (0.25\%–0.5\%)$ give a reasonable gain. A full Gaussian current electron pulse beam for these values of energy spreads are now simulated. A beam of peak current $I_{peak} = 9.6$ kA , charge of $Q = 40$ pC, and unchirped energy of 600 MeV was used [6]. A planar undulator period of $\lambda_u = 15$ mm with an undulator pole gap of

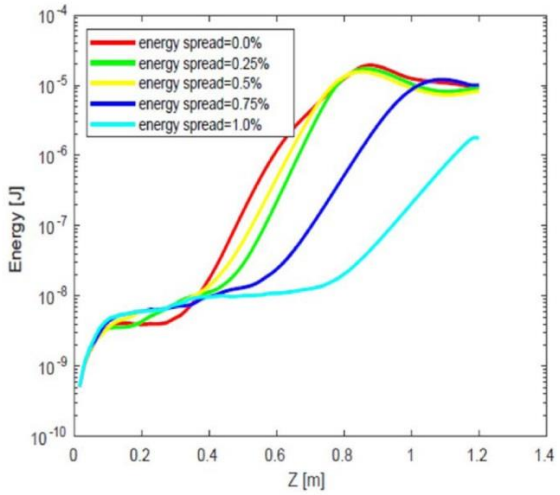

Figure 3. The radiation energy as a function of distance z through the undulator for different values of energy spread.

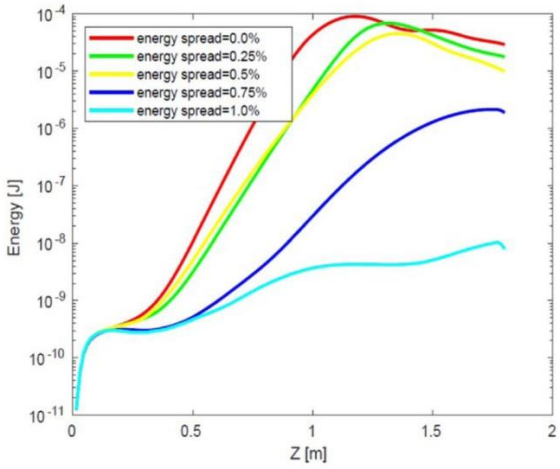

Figure 4. 3D Puffin simulation showing radiation energy as a function of distance z through the undulator in Gaussian distribution.

$g = 2.5$ mm was chosen to give an undulator parameter of $a_u = 2.3$ [6]. These beam and undulator parameters give an FEL parameter of $\rho = 0.0269$ as above with a resonant wavelength $\lambda_r = 134\ nm$.

The electron bunch length is calculated as $\sigma_e = \frac{cQ}{\sqrt{2\pi}I_{peak}} = 0.5\mu m$ which is similar to that of one cooperation length $l_c = \frac{\lambda_r}{4\pi\rho} = 0.4\ \mu m$ [7], so that the radiation output will then be in the weak superradiant mode of operation to give a single, short radiation pulse output [14]. Figure 4 shows the total radiated energy in the FEL for the Gaussian electron bunch. Figure 5 shows that if we have a sufficiently low value of energy spread then a relatively high peak energy can be achieved in a short undulator. Note that as the energy spread approaches the criterion $\sigma_\gamma \geqslant \rho$, then the peak energy reduces and the saturation length increases significantly as expected.

Figure 6 shows the intensity spectrum ($|\tilde{A}|^2$) plotted as function of scaled frequency ω/ω_r for two values of energy spread=0.25% and 0.5% , for z=1.05 m through the undulator . It is seen that the maximum gain is at $\omega/\omega r \approx 0.99$ for 0.25% and $\omega/\omega_r \approx 0.97$ for 0.5%. This is in broad agreement with small shift from resonance ($\omega/\omega_r = 1$) for the peak that occurs due to the effect of the emittance ($\epsilon_n = \beta\gamma\varepsilon_{rms}$) [13], where $\varepsilon_{rms} = \frac{\lambda_r}{4\pi}$ is the geomertric rms emittance [4].

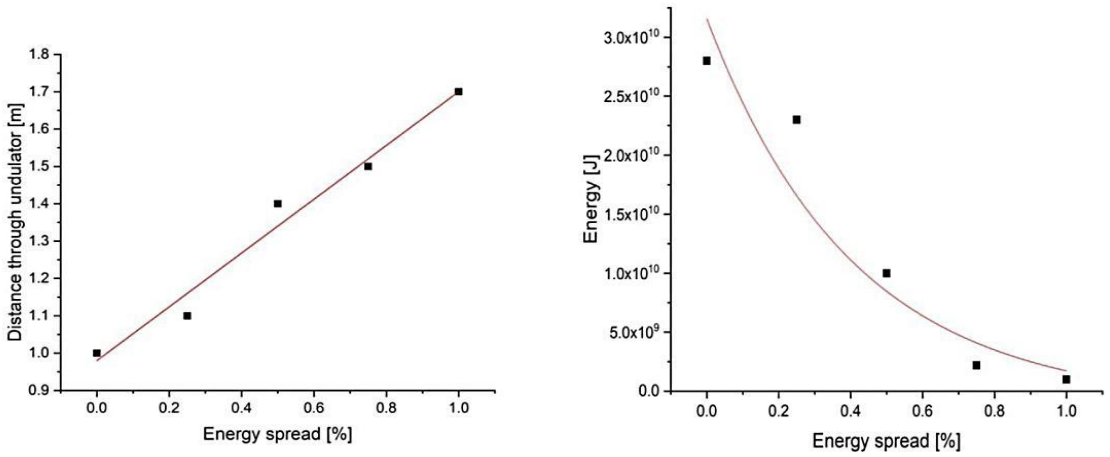

Figure 5. Energy [J] as a function of energy spread and undulator distance as a function of energy spread through the undulator in Gaussian distribution.

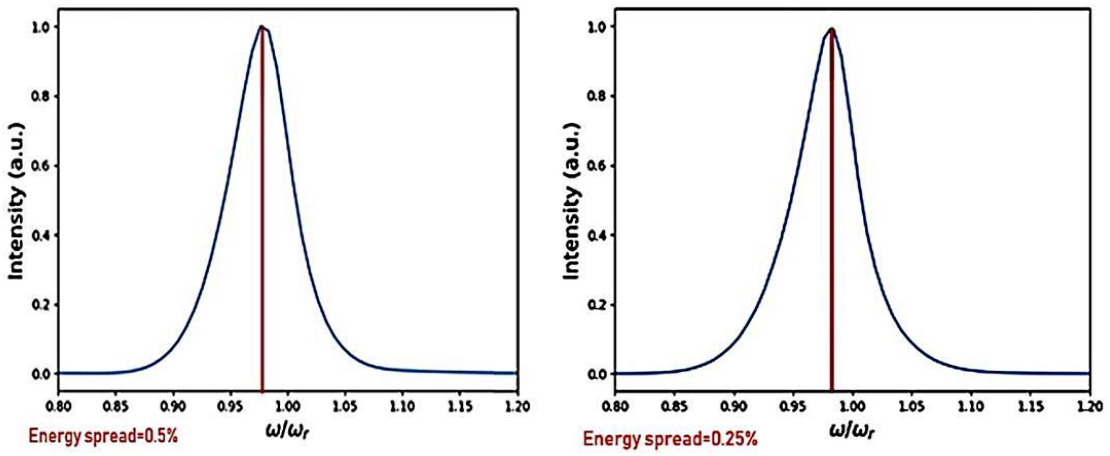

Figure 6. The intensity spectrum ($|\tilde{A}|^2$) is plotted as function of scaled frequency $f = \omega/\omega_r$ for two values of energy spread $\sigma_\gamma = 0.25\%$ and 0.5%.

Figure 7 shows the temporal power of the pulse as a function of $(ct - z)$ at saturation (z=1.05 m) for energy spread $\sigma_\gamma =$ (0.25% and 0.5%), clearly showing the reduced power when $\sigma_\gamma \geqslant \rho$.

Future work , will look to start-to-end FELs simulations using LPA in the range of soft x-ray (XFEL) between 1–10 nm [15, 16]. This will requrie high quality beam with high peak current, high energy and small transverse emittance within a relatively short undulator. This can be challenging in propagating, conditioning and matching the electron beams into the undulator due to , relatively large energy spreads and divergence of the electrons at the LPA exit [17].

Conclusions

The work on plasma accelerators is not only limited to optimisation of the qualities of electron beams; FEL performance benefits from beams with a high current, small transverse emittance and small energy spread. The undulator design is based on recent achievements in the development of undulators to optimise the FEL performance.

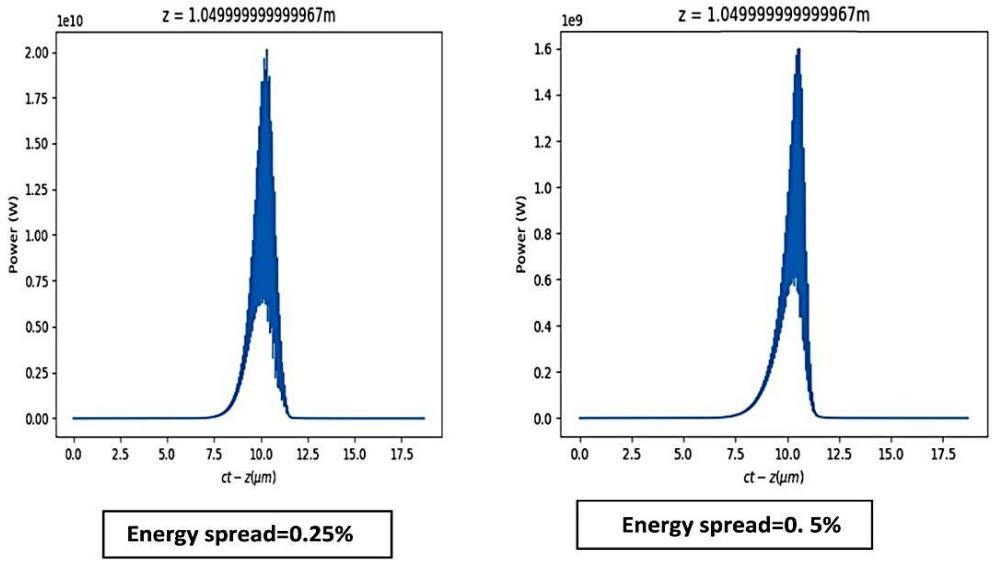

Figure 7. The temporal power of the pulse as a function of the scaled time coordinate ($ct-z$) at saturation (z = 1.05 m) for energy spread $\sigma_\gamma = 0.25\%$ and 0.5%.

The undulator length was limited however, saturation can be achieved in a shorter distance as seen from figure 4 with peak saturated output at 1–1.2 m. This may be great interest when considering modelling of a compact LPA Driven FEL.

To reach short radiation wavelength requires (i) shorter undulator period λ_u, or (ii) large e-beam energy γ. Radiation wavelength tuning is achieved by varying beam energy and/or undulator period, with the undulator parameter a_u.

In case of steady-state simulations (figure 4) we obtained the reasonable gain for Gaussian distributions as clear from (figure 5). However, in case of steady-state a higher order of energy gain is obtained compared to the Gaussian pulse mode where for the typical LWA parameters used here, a relatively short pulse was used of the order of the cooperation length. This generates a single superradiant pulse output [18] with a lower peak power output than in the steady state. This short, single pulse output is of interest in its own right where such output is often sought by FEL users.

For lower values of energy spread a higher peak energy is obtained at shorter distance along the undulator as expected .

The best results of were obtained when the energy spread σ_γ was below 0.5% and it is clear that the energy spread has large impact on the energy gain and output in the FEL and must be minimised to $\sigma_\gamma < \rho$ in order to achieve acceptable FEL output efficiency.

ORCID iDs

B M Alotaibi https://orcid.org/0000-0002-9499-2711

References

[1] McNeil B W J and Thompson N R 2010 Review article: x-ray free-electron lasers *Nat. Photonics* **4** 814
[2] Bonifacio R, Pellegrini C and Narducci L 1984 Collective instabilities and high-gain regime in a free electron laser *Optics Commun.* **50** 373
[3] Huang Z and Kim K-J 2007 Review of x-ray free electron laser theory *Physical Review Special Topics, AB* **10** 034801
[4] Bonifacio R, Souza L D S and McNeil B W J 1992 Emittance limitations in the free electron laser *Optics Comm.* **93** 179
[5] Henderson J R, Campbell L T and McNeil B W J 2015 Free electron laser using 'beam by design *New J. Phys.* **17** 083017
[6] Maier A R, Meseck A, Reiche S, Schroeder C B, Seggebrock T and Gruner F 2012 Demonstration scheme for a laser-plasma-driven free-electron laser *Physical Review,* X **2** 031019
[7] Campbell L T and McNeil B W J 2012 Puffin: a three dimensional, unaveraged free electron laser simulation code *Phys. Plasmas* 19093119

[8] Campbell L T, Smith J D A, Traczykowski P and McNeil B W J 2018 Updated description of the FEL simulation code puffin *Proc. of IPAC2018, Vancouver, BC, Canada, 02 Photon Sources and Electron Accelerators, A06 Free Electron Lasers, THPMK112* http://ipac2018.vrws.de/papers/thpmk112.pdf
[9] Brian *et al* 2017 Comparing FEL codes for advanced configuration *38th Int. Free Electron Laser Conf., FEL (Santa Fe, NM, USA)* http://accelconf.web.cern.ch/AccelConf/fel2017/papers/mop016.pdf
[10] Xie M 2000 Exact and variational solutions of 3D eigenmodes in high gain FELs *Nuclear Instruments and Methods in Physics Research, section* A **445** 59
[11] Xie M 1995 Design optimization for an x-ray free electron laser driven by SLAC linac *Proc. of the 1995 Particle Accelerator Conf. (JACoW, Geneva)* https://accelconf.web.cern.ch/accelconf/p95/ARTICLES/TPG/TPG10.PDF
[12] Dornmair I *et al* 2016 Towards plasma-driven free electron laser *NIC Symposium* **48** 401
[13] Marco Venturini, Basics on FEL Physics; Undulators; High-Level Machine-Design Parameters, Course Materials, Lecture Mo2 - Rutgers University - New Jersey, 21-06-2015 http://uspas.fnal.gov/materials/15Rutgers/Lecture_Mo2.pdf
[14] Campbell L T and McNeil B W J 2012 A simple model for the generation of ultra-short radiation pulses *FEL2012: Proc. of the 34th Int. Free-Electron Laser Conf.* paper THPD41 26–31*(Nara, Japan)* https://accelconf.web.cern.ch/accelconf/FEL2012/papers/thpd41.pdf
[15] Campbell L T and Maier A R 2017 Velocity dispersion of correlated energy spread electron beams in the free electron laser *New J. Phys.* **19** 033037 http://iopscience.iop.org/article/10.1088/1367-2630/aa6205
[16] Pellegrini C 2012 The history of x-ray free-electron lasers *Eur. Phys. J.* H **37** 659
[17] Khojoyan M, Briquez F, Labat M, Oulergue A L, Marcouille O, Marteau F, Sharma G and Couprie M E 2016 Transport studided of LPA electron beam towards the FEL amplification at COXINEL *Nuclear Instruments and Methods in Physics Research section* A **829** 260
[18] Bonifacio R, McNeil B W J and Pierini P 1989 Superradiance in the high-gain free electron laser *Phys. Rev.* A **40** 4467

Appendix B
FEL2019 Poster

Plasma Accelerator Driven Coherent Spontaneous Emission

[1,4]B.M. Alotaibi, [1,4]R. Altuijri, [1,2]A.F. Habib, [1,2]B. Hidding, [1,2]Brian McNeil and [1,2,3]Piotr Traczykowski

[1]SUPA, Department of Physics, University of Strathclyde, Glasgow, G4 0NG
[2]The Cockcroft Institute Daresbury Laboratory, Daresbury, Warrington, WA4 4AD
[3]ASTeC, STFC Daresbury Laboratory, Daresbury, Warrington, WA4 4AD
[4]Physics Department, Faculty of Science, Princess Nourah Bint Abdulrahman University, Riyadh, KSA

- Novel plasma photocathodes [1,2] may offer improvement to the normalised emittance and brightness of electron beams compared to Radio Frequency-driven accelerators, a challenge is the energy spread and chirp of beams, which can make FEL operation impossible.
- Here, we show that an energy-chirped with dynamically evolving current profile due to ballistic bunching can generate significant coherent radiation output via the process of Coherent Spontaneous Emission (CSE) [3].
- While this CSE is seen to cause some FEL-induced electron bunching at the radiation wavelength, the dynamic evolution of the energy chirped pulse dampens out any high-gain FEL interaction.

- The initial macroparticle distribution was taken from the VSim PWFA simulation and was converted into suitable format for Puffin[10], for this process the conversion [4] and upsampling [5] scripts were used.
- The relevant parameters of the beam of microparticles are compared to the original beam of macroparticles from the VSim simulation in **Fig.1**. The microparticle distribution has also had the correct shot-noise statistics applied as described in [6].

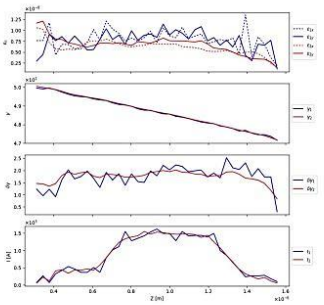

Fig.1 Beam parameters before and after upsampling. The electron pulse generated by the PWFA has a length of l_e~24λ_r~6l_c and has a negative energy chirp in z (positive energy chirp in z_2).

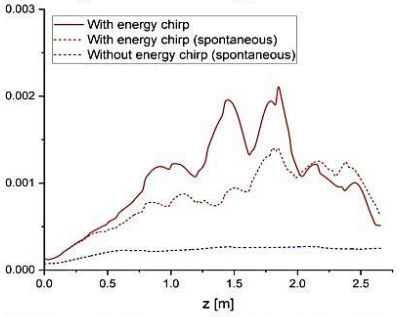

Fig.2 Average bunching parameter evolution for the electron pulse as a function of distance through the undulator.

PARAMETER	VALUE
Peak current	1500 A
Normalised emittance	0.01 mm mrad
Energy (γ)	486
RMS energy spread	0.3 %
Bunch charge	3.6 pC

- The undulator parameters selected for simulations: λ_u= **0.015m, a_u = 1.0**.
- The resulting radiation wavelength is λ_r**~67nm** and the FEL parameter at peak current is **ρ=0.021**.
- Given that the average slice energy spread σ_γ**=0.003** the energy spread condition for FEL lasing of $\sigma_\gamma/\gamma<\rho$ is well satisfied in the absence of an energy chirp.
- The steady state, Self Amplified Spontaneous Emission (SASE) saturation length is then approximated as L_{sat}**~ 1.4m. <u>The electron bunch does not, however, conform to the steady-state approximation as it is only 6 cooperation lengths long.</u>**

- During propagation through the undulator, dispersion will cause this short, energy chirped electron bunch to **<u>self-compress longitudinally</u>** due to rotation in longitudinal phase space, which is significant at these relatively low energies, and it may even *'flip over'* in longitudinal phase space [3] (**Fig.3**). During this process, the electron bunch length may approach that of the resonant wavelength (l_e~λ_r) and consequently **<u>would be expected to radiate significant CSE</u>**.
- It should be noted that the FEL interaction may also amplify CSE in addition to the spontaneous emission due to electron beam shot-noise in a process called **<u>Self Amplified Coherent Spontaneous Emission (SACSE)</u>** [7]. As with SASE, given the large energy chirp here, any **<u>SACSE</u>** process would be expected to be significantly affected.

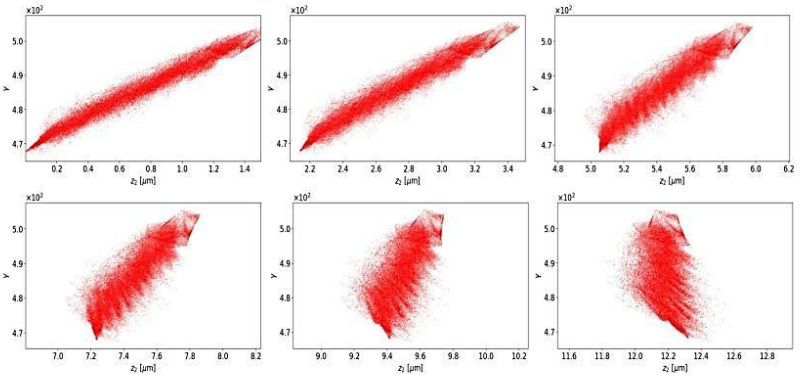

Fig.3 The electron beam evolution plotted for z=0m, 0.45m, 1.05m, 1.50m, 1.95m and 2.25m. The electron energy chirp causes the electron bunch to longitudinally compress in phase space and shorten as it propagates through the undulator. At saturation, z=1.95m, the electron bunch is only ~10 resonant radiation wavelengths long.

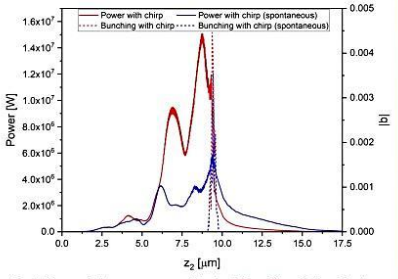

Fig.4 The radiation power profile (solid red) and the electron bunching parameter (dashed red) as a function of z_2=(ct−z) at $z=z_{sat}$=1.95m through the undulator for the energy chirped case and corresponding case for the FEL interaction 'switched off' (solid blue and dashed blue).

- The growth is not exponential but is **<u>proportional to ~z^2</u>**, more consistent with **<u>CSE</u>** [3].
- That the radiation energy emitted in the absence of the FEL interaction is similar to that with the FEL interaction, confirms that the emission in both cases arises mainly from CSE.
- The FEL interaction can be *'switched off'* in the Puffin simulation by artificially de-coupling the electrons from the radiation field. The electrons then only emit spontaneous emission due to both shot-noise and CSE. The radiation energy growth from the chirped electron pulse, both with and without the FEL interaction, is shown in **Fig.5.** Here, there is no shortening of the electron pulse and the CSE emission is greatly reduced. The energy growth is quasi-linear with distance z through the undulator, consistent with incoherent spontaneous emission due to **shot-noise only**. The evolution of the mean electron bunching parameter (**Fig.2**) increases quasi-linearly with distance through the undulator until z~1.2m. This is in broad agreement with the increased bunching due to the dispersive shortening of the electron pulse which causes significant current gradients with respect to the radiation wavelength. It is this type of bunching which drives the Coherent Spontaneous Emission [3] and which may act as a self-generated seed field which can be amplified as SACSE [7,9].

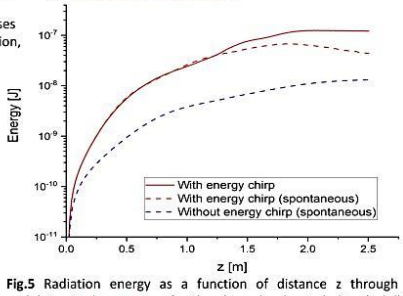

Fig.5 Radiation energy as a function of distance z through the undulator. Red curves are for the chirped pulse including (solid) the FEL interaction and (dashed) without the FEL interaction. The case without energy chirp or FEL interaction (blue) demonstrates an energy growth with a quasi-linear dependence with z, corresponding to shot-noise spontaneous emission without significant CSE contribution.

[1] Esary E et al 2009 Rev. Mod. Phys. 81 1229; [2] Hidding B, et al 2012, Phys. Rev. Lett. 108 035001; [3] Campbell L T and McNeil B W J 2012 Proc. FEL2012 (Nara, Japan); [4] https://github.com/UKFELs/FXFEL/ ; [5] https://github.com/UKFELs/IDF ; [6] McNeil B W J, Poole M W, and Robb G R M, 2003 Phys. Rev. ST Accel. Beam; [7] McNeil B W J, Robb G R M and Jaroszynski D A 1999 Opt. Commun. 165 65; [8] Campbell L T and McNeil B W J 2012 Phy. Plasmas. 19 093119; [9] McNeil B W J, Robb G R M and Jaroszynski D A 2000 Nucl. Inst .Meth. Phys. Res. A 445 72-76; [10] LT Campbell & BWJ McNeil, Phys. Plasmas 19, 093119 (2012)

Appendix C
FEL2019 Paper

PLASMA ACCELERATOR DRIVEN COHERENT SPONTANEOUS EMISSION

B.M. Alotaibi[1,2], R. Altuijri[1,2], A. F. Habib[2,3], B. Hidding[2,3], B.W.J. M^{c}Neil[2,3], P. Traczykowski[2,3]
[1]Physics Department, Faculty of Science,
Princess Nourah Bint Abdulrahman University, Riyadh, KSA
[2]SUPA, Department of Physics, University of Strathclyde, Glasgow, UK
[3]Cockcroft Institute, Warrington, UK

Abstract

Plasma accelerators [1] are a potentially important source of high energy, low emittance electron beams with high peak currents and generated within a relatively short distance. While novel plasma photocathodes [2] may offer improvement to the normalised emittance and brightness of electron beams compared to Radio Frequency-driven accelerators, a challenge is the energy spread and chirp of the beams, which can make FEL operation impossible. In this paper it is shown that such an energy-chirped beam, with a dynamically evolving current profile due to ballistic bunching, can generate significant coherent radiation output via the process of Coherent Spontaneous Emission (CSE) [3]. While this CSE is seen to cause some FEL-induced electron bunching at the radiation wavelength, the dynamic evolution of the energy chirped pulse dampens out any high-gain FEL interaction.

INTRODUCTION

Significant effort have been dedicated to demonstrating a plasma-based accelerator driven FEL [4–6]. However, next to stability challenges, the inherent by-product of plasma-based accelerators is a relatively large slice energy spread ($\sigma_\gamma/\gamma > \rho$) and a correlated energy spread ('chirp') when compared with RF linacs. In this paper, the dynamics of the electron bunch from a plasma photocathode [2], which can have an inherent negative energy chirp, is explored. One effect, which to the authors knowledge has not been modelled before with such a PWFA plasma photocathode-generated energy chirped beam, is to induce the generation of Coherent Spontaneous Emission (CSE) [3, 7]. CSE arises when the electron pulse has significant *current* gradients over a resonant radiation wavelength. It is shown that for the electron beam parameters used here, such current gradients can be realised when the energy chirped beam undergoes spatial dispersive compression in its propagation direction due to the correlated energy spread [3, 7]. By dominating any normal spontaneous emission, it has been shown in 1D simulations that CSE can also self-seed the FEL interaction in a process called Self Amplified Coherent Spontaneous Emission (SACSE) [8]. The CSE was also shown in 1D to help mitigate the effects of a homogeneous electron energy spread in beams without an energy chirp, significantly reducing the start-up time and enhancing the generation of high intensity, short, superradiant radiation pulses from a poor-quality electron pulse [9].

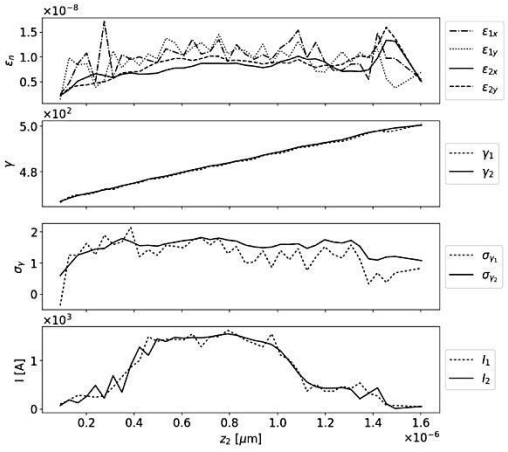

Figure 1: From top, the electron beam normalised emittance ϵ_n, localised Lorentz factor γ, RMS energy spread σ_γ and current I, as a function of window position $z_2 = (ct - z)$ of the beam. In this window, travelling at speed c along the z-axis of the undulator, the head of the electron bunch is on the left, the tail on the right, and the beam will propagate to larger values of z_2 as the beam propagates through the undulator. The dashed plots (index 1) show the original macroparticle beam from the VSim simulation and the solid plots (index 2) show the beam following smoothing and up-sampling to a greater number of microparticles with the correct shot-noise statistics.

ELECTRON BUNCH SIMULATION

A macroparticle distribution is taken from a VSim simulation of a PWFA. These macroparticles have too sparse a phase-space distribution for an accurate FEL simulation as there are too few macroparticles per resonant wavelength and they have unrealistic shot-noise statistics. These macroparticles are converted into a suitable distribution of *microparticles* using the scripts [10] and [11]. The relevant bunch parameters of a microparticle beam are compared to the original beam of macroparticles in Fig. 1. The microparticle distribution has had the correct shot-noise statistics applied as described in [12]. It is seen that the electron beam has a negative longitudinal energy chirp, which is the result of the beam acceleration in the electric field of the nonlinear plasma wave.

UNAVERAGED FEL SIMULATION

The unaveraged 3D FEL simulation code Puffin was used [13, 14] as it is able to model both macroscopic electron beam changes due to the electron beam energy chirp and any CSE and SACSE that may arise. The Ming Xie formalism of [15, 16] was used to chose the planar undulator period λ_u and undulator parameter a_u. The estimated beam parameters of the unchirped beam of Fig. 1 are: $I_{pk} = 1500\,\mathrm{A}$, $\epsilon_{xy} = 0.01\,\mathrm{mm\,mrad}$, $\gamma = 486$, $\sigma_\gamma = 0.3\,\%$, $Q = 3.6\,\mathrm{pC}$.

The undulator parameters selected for simulations were $\lambda_u = 0.015\,\mathrm{m}$ and $a_u = 1.0$. The resulting radiation wavelength is $\lambda_r \approx 67\,\mathrm{nm}$ and the FEL parameter at peak current is $\rho = 0.021$. Given that the average slice energy spread is $\sigma_\gamma/\gamma \approx 3 \times 10^{-3}$ the energy spread condition for FEL lasing of $\sigma_\gamma/\gamma \lesssim \rho$ is well satisfied in the absence of an energy chirp. The steady state, Self Amplified Spontaneous Emission (SASE) saturation length is then approximated as $L_{sat} \approx 1.4\,\mathrm{m}$ and saturation power $P_{sat} \approx 2.2\,\mathrm{GW}$. The electron bunch does not, however, conform to the steady-state approximation as it is only ~ 6 cooperation lengths long, where the cooperation length $l_c = \lambda_r/4\pi\rho$ [17]. This relatively short electron pulse length will result in the output of short, single pulses, at saturation. This type of short pulse operation is in the weak superradiant regime of FEL operation [17] and also results in reduced saturation powers from that of the steady-state, Ming Xie approximation above. The Puffin simulation uses the energy chirped electron bunch distribution output from the PWFA as shown in Fig. 1. The beam of microparticles was matched to the natural focusing channel of the undulator lattice chosen for the simulation as above using the method of [18]. It is seen from the parameters of the chirped pulse, plotted in Fig. 1, that the electron pulse generated by the PWFA has a length of $l_e \approx 24\lambda_r \approx 6l_c$ and has a negative energy chirp in z (positive energy chirp in z_2). During propagation through the undulator, dispersion will cause this short, energy chirped electron bunch to self-compress longitudinally due to rotation in longitudinal phase space, which is significant at these relatively low energies, and it may even 'flip over' in longitudinal phase space [3]. During this process, the electron bunch length may approach that of the resonant wavelength ($l_e \sim \lambda_r$) and consequently would be expected to radiate significant CSE. In what follows the CSE generation due to energy chirped bunch shortening and any FEL processes were modelled self-consistently. The FEL interaction may also amplify CSE in addition to the spontaneous emission due to electron beam shot-noise in the SACSE [8]. As with SASE, given the large energy chirp here, any SACSE process would be expected to be significantly affected. The electron bunch length is plotted as a function of position through the undulator in Fig. 2, and is seen to shorten and flip over before lengthening again.

The energy of the radiation pulse as a function of distance through the undulator emitted by the chirped bunch is shown in Fig. 3 both with and without the FEL interaction included in the simulation. The FEL interaction is 'switched off' in the

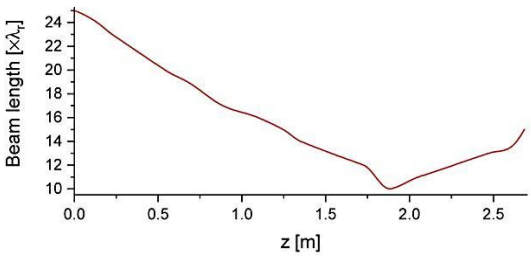

Figure 2: The full electron bunch length in units of resonant wavelentgh. The initial energy chirp at $z = 0\,\mathrm{m}$ is seen to cause the electron pulse to compress and then will decompress longitudinally.

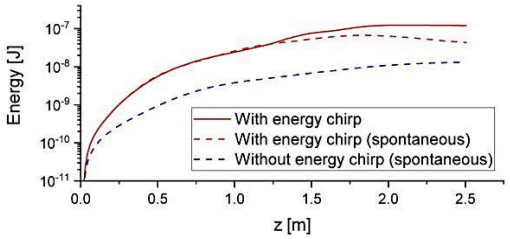

Figure 3: Radiation energy as a function of distance z through the undulator. Two of the plots (red) are for the chirped pulse including (solid) the FEL interaction and (dashed) without the FEL interaction. The case without energy chirp or FEL interaction (blue dashed) gives an energy growth with a quasi-linear dependence with z, corresponding to shot-noise spontaneous emission without significant CSE contribution.

Puffin simulation by artificially de-coupling the electrons from the radiation field. Also shown is the sponteneous emission with the energy chirp artificially removed from the electron bunch. The corresponding average bunching parameters $|\bar{b}|$, for both the chirped and un-chirped electron pulses are shown in Fig. 4.

The radiation pulse 'instantaneous' power (i.e. unaveraged over a radiation wavelength [13]) and electron bunching parameter $|b|$ at saturation, is shown in Fig. 5 as a function of local position z_2. It is seen from the Fig. 2 that the elec-

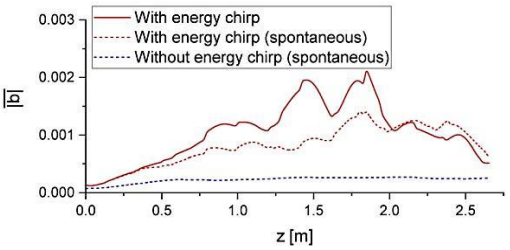

Figure 4: Average bunching parameter evolution for the electron pulse as a function of distance through the undulator both with (solid red) and without (dashed red) the FEL interaction. Also shown is the average bunching for the case of no energy chirp (dashed blue).

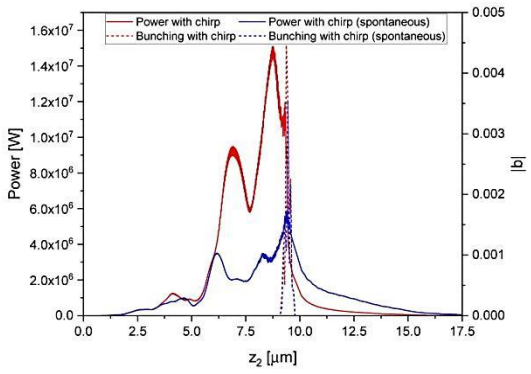

Figure 5: The radiation power profile (solid red) and the electron bunching parameter (dashed red) as a function of $z_2 = (ct - z)$ at $z = z_{sat} = 1.95$ m through the undulator for the energy chirped case and corresponding case for the FEL interaction 'switched off' (solid blue and dashed blue).

tron energy chirp causes the electron bunch to longitudinally compress in phase space and shorten as it propagates through the undulator. At saturation, $z = 1.95$ m, the electron bunch is only $\sim$ 10 resonant radiation wavelengths long. When the FEL interaction is switched off, the electrons then only emit spontaneous emission due to both shot-noise and CSE. Figure 3 shows that the energy growth is not exponential but is proportional to $\sim z^2$, more consistent with CSE [3]. That the radiation energy emitted in the absence of the FEL interaction is similar to that with the FEL interaction, confirms that the emission in both cases arise mainly from CSE. In the absence of any energy chirp or FEL interaction, there is no shortening of the electron pulse and the CSE emission is greatly reduced. The energy growth is then quasi-linear with distance z through the undulator, consistent with incoherent spontaneous emission due to shot-noise only.

The evolution of the mean electron bunching parameter $|\bar{b}|$ of Fig. 4 increases quasi-linearly with distance through the undulator until $z \approx 1.2$ m. This is in broad agreement with the increased bunching due to the dispersive shortening of the electron pulse which causes significant current gradients with respect to the radiation wavelength. It is this type of bunching which drives the Coherent Spontaneous Emission [3] and which may act as a self-generated seed field which can be amplified as SACSE [8,9]. Also plotted is the electron bunching of the electron pulse in the absence of any energy chirp. As described above, there is no shortening of the electron pulse and the bunching remains approximately constant and at a much smaller value, mainly due to shot-noise, than when the pulse shortens and significant current gradients occur at the radiation wavelength scale. The differences of the radiation emission and electron bunching, between the spontaneous-only case, when the FEL interaction is switched off, and that where the FEL interaction is included in the simulation, can be attributed to a small additional bunching due to SACSE. Some small periodic bunching about the radiation wavelength $\lambda_r \approx 67\,nm$ due to SACSE, can be seen in the evolution of the electron phase-space through the undulator. The lack of any significant FEL gain is consistent with the work of [19] where for negative values of their chirp parameter $\hat{a}$, here $\hat{a} \approx -2$ at $z = 0$ m, FEL power output is greatly reduced from that expected from an un-chirped beam. So while some increased bunching is evident due to the FEL interaction between radiation and electrons, it is not operating in the collective, high-gain mode, significantly reducing the power emitted. Following the minimum of its length, the electron bunch continues to disperse as it propagates through the undulator, flipping over in phase space and indeed re-absorbing some of the emitted radiation and is consistent with that of previous simplified models [3]. Figure 5 (red) plots both the radiation power and electron bunching as a function of local position at saturation. It is seen that the electron pulse bunching, corresponding to the electron pulse at saturation of Fig. 2, is within a small local interval around $z \sim 9.5$ μm. The radiation pulse power for $z_2 < 9.5$ μm has propagated ahead of the electron bunch and is propagating in vacuum.

Figure 5 show results for both simulations with the FEL interaction switched on (red) and off (blue). The radiation is then that due to spontaneous radiation from shot-noise and CSE only. The difference in the power emitted between the two is then due to the FEL interaction as observed from the additional electron bunching of Figs. 4 and 2. The modest increase in output power demonstrates that the FEL is not, however, operating the in the high-gain regime.

CONCLUSION

Using a start-to-end approach, PWFA driven FEL operation was studied numerically using an unaveraged 3D model. The PWFA electron pulse output had a significant quasi-linear energy chirp. This chirp causes the electron pulse to shorten as it propagates through the undulator and emit significant CSE power. This CSE was seen to drive the electrons to give some weak periodic bunching at the resonant radiation wavelength, but not to enter into a collective, high-gain regime where analysis in the steady-state regime (no pulse effects) predicts output powers approximately two orders of magnitude greater. The dynamic shortening of the electron pulse and subsequent emission of CSE as it propagates through the undulator is an effect that is not normally modelled in FEL simulations. Methods to remove the electron beam energy chirp are the subject of on-going research and, if possible, are expected to allow the high gain FEL interaction to develop and output short coherent pulses of high power radiation.

ACKNOWLEDGMENTS

The authors wish to thank (i) KAUST Supercomputing Laboratory (KSL) Thuwal, Saudi Arabia, (ii) STFC's ASTeC, using the STFC HPC Hartree Centre, (iii) The Science and Technology Facilities Council Agreement Number 4163192 Release #3, (iv) and the John von Neumann Institute for Computing on JUROPA at Jülich Supercomputing Centre, under project HHH20.

REFERENCES

[1] E. Esary *et al.*, "Physics of laser-driven plasma-based electron accelerators", *Rev. Mod. Phys.*, vol. 81, pp. 1229, 2009. doi:10.1103/RevModPhys.81.1229

[2] B. Hidding *et al.*, "Ultracold Electron Bunch Generation via Plasma Photocathode Emission and Acceleration in a Beam-Driven Plasma Blowout", *Phys. Rev. Lett.*, vol. 108, pp. 035001, 2012. doi:10.1103/PhysRevLett.108.035001

[3] L. T. Campbell and B. W. J. McNeil, "Puffin: A Three Dimensional, Unaveraged Free Electron Laser Simulation Code", in *Proc. FEL'12*, Nara, Japan, Aug. 2012, paper MOPD12, pp. 73–76.

[4] M. Pittman, S. Ferré, J.P. Rousseau, L. Notebaert, J.P. Chambaret, and G. Chériaux, "Design and characterization of a near-diffraction-limited femtosecond 100-TW 10-Hz high-intensity laser system", *Appl. Phys. B*, vol. 74, pp. 529-535, Apr. 2002. doi:10.1007/s003400200838

[5] Z. Huang, Y. Ding, and C.B. Schroeder, "Compact X-ray Free-Electron Laser from a Laser-Plasma Accelerator Using a Transverse-Gradient Undulator", *Phys. Rev. Lett.*, vol. 109, pp. 204801, Nov. 2012. doi:10.1103/PhysRevLett.109.204801

[6] H.P. Schlenvoigt *et al.*, "A compact synchrotron radiation source driven by a laser-plasma wakefield accelerator", *Nat. Phys.*, vol. 4, pp. 130-133, 2008. doi:10.1038/nphys811

[7] J. Henderson, L.T. Campbell, and B.W.J. McNeil, "Chirped and Modulated Electron Pulse Free Electron Laser Techniques", in *Proc. FEL'14*, Basel, Switzerland, Aug. 2014, paper MOC04, pp. 303–309.

[8] B.W.J. McNeil,, G.R.M. Robb, D.A. Jaroszynski, "Self-amplification of coherent spontaneous emission in the free electron laser", *Opt. Commun.*, vol. 165, pp. 65-70, 1999. doi:10.1016/S0030-4018(99)00222-9

[9] B.W.J. McNeil, G.R.M. Robb, D.A. Jaroszynski, "SACSE in a FEL amplifier with energy spread", *Nucl. Inst .Meth. Phys. Res. A*, vol. 445, pp. 72-76, 2000. doi:10.1016/S0168-9002(00)00116-9

[10] https://github.com/UKFELs/FXFEL

[11] https://github.com/UKFELs/JDF

[12] B.W.J. McNeil, M.W. Poole, G.R.M. Robb, "Unified model of electron beam shot noise and coherent spontaneous emission in the helical wiggler free electron laser", *Phys. Rev. ST Accel. Beams.*, vol. 6, pp. 070701, 2003. doi:10.1103/PhysRevSTAB.6.070701

[13] L.T. Campbell and B.W.J. McNeil, "Puffin: A three dimensional, unaveraged free electron laser simulation code", *Phy. Plasmas.*, vol. 19, pp. 093119, 2012. doi:10.1063/1.4752743

[14] L.T. Campbell, B.W.J. McNeil,, P.T. Traczykowski, and J.D.A. Smith, "An Updated Description of the FEL Simulation Code Puffin", in *Proc. IPAC'18*, Vancouver, Canada, Apr.-May 2018, pp. 4579–4582. doi:10.18429/JACoW-IPAC2018-THPMK112

[15] M. Xie, "Design Optimization for an X-Ray Free Electron Laser Driven by SLAC Linac", *Proc. the Particle Accelerator Conference 1995 (Geneva)* in *Proc. PAC'95*, Dallas, TX, USA, May 1995, paper TPG10, pp. 183-185.

[16] M. Xie, "Exact and variational solutions of 3D eigenmodes in high gain FELs", *Nucl. Instrum. and Methods Phys. Res. A*, vol. 445, pp. 59-66, 2000. doi:10.1016/S0168-9002(00)00114-5

[17] R. Bonifacio, B.W.J. McNeil,, and P. Pierini, "Superradiance in the high-gain free-electron laser", *Phys. Rev. A*, vol. 40, pp. 4467-4475, 1989. doi:10.1103/PhysRevA.40.4467

[18] https://github.com/UKFELs/Paraffin

[19] E.L. Saldin, E.A. Schneidmiller, and M.V. Yurkov, "Self-amplified spontaneous emission FEL with energy-chirped electron beam and its application for generation of attosecond x-ray pulses", *Phys. Rev. Special Topics Accel. Beams.*, vol. 9, pp. 050702, 2006. doi:10.1103/PhysRevSTAB.9.050702

Appendix D
Puffin input files

D.1 Beam file

```
! PUFFIN BEAM FILE

!

!Describes electron beams for input into puffin. Multiple beams with

!different parameters can be used. Please refer to POP-REF for an

!explanation of the scaled variables used, such as z2 and p2.

!

! BEAM PARAMETERS - namelist NBLIST

!

! nbeams - number of electron beams

! dtype - Input type - simple, distribution, or macroparticle

!

! BEAM PARAMETERS - namelist BLIST

!=====================================================================

! sSigmaE - gaussian std dev in each dimension - x, y, z2, px, py, gamma, then for additional beams

! sLenE - Total length of beam modelled in each dimension - x, y, z2, px, py, gamma...

! bcenter - Center of beam in z2

! iNumElectrons - Number of macroparticles in each dimension used to model the beam

! sEmit_n - Scaled transverse beam emittance

! sQe - Beam charge
```

```
! gammaf - Ratio of average beam energy to reference beam energy gamma / gamma_r

! chirp - Energy chirp in z2 i.e. dgamma/dz2

! mag - magnitude of energy oscillation on beam

! freq - frequency in z2 of beam energy oscillation

! qRndEj_G - Round edge of flat top?

! sSigEj_G - Gaussian sigma of tail-off if used

! qMatched_A - Automatically match beam to focusing channel??

!=========================================================================

&NBLIST

nbeams = 1

dtype = 'h5'

/

&BH5LIST

dist_f='ch8nc_beam.h5'
```

D.2 Main input file

```
!
! The main input parameters are described below - Puffin takes the namelist blocks at the
! bottom of this file as input. This is the 'main' input file, containing info about the
! wiggler, field sampling, and general flags and other numerical instructions for the
! simulation. This file also points to a beam file, seed file, and optionally a lattice
! file.
!-----------------------------------------------------------------------------------------!
! NAME DESCRIPTION
!-----------------------------------------------------------------------------------------!
!
! FLAGS
!
!
! qOneD If TRUE, model 1D FEL, with only 1 field node and 1 macroparticle in transverse dimensions
! qFieldEvolve if letting the radiation field evolve
! qElectronsEvolve if integrating electron equations
! qElectronFieldCoupling if allowing field to feedback onto the electron equations
! qFocussing if focussing is included in the transverse plane
```

! qMatchedBeam if matching beam to undulator. If TRUE, electron pulse sigma and length in x,y,px,py are automatically calculated

! qDiffraction if modelling diffraction

! qFilter TRUE to filter, if FALSE the low frequencies will just be ignored during diffraction

! q_noise Shot noise in initial electron beam distribution

! qDump Do you wish to dump data so the run can be resumed if anything goes wrong? .TRUE. for yes.

! qResume If resuming from dump files left from a previous run

! qSeparateFiles Write data to separate SDDS files at each step

! qFormattedFiles Write data as formatted text(TRUE) or binary(FALSE)

! qWriteZ Write out Z data

! qWriteA Write out A data

! qWritePperp Write out Pperp data

! qWriteP2 Write out P2 data

! qWriteZ2 Write out Z2 data

! qWriteX Write out X data

! qWriteY Write out Y data

!

! ELECTRON MACROPARTICLE SAMPLING

!

!

! beam_file Name of the beam file

! sElectronThreshold Beyond the threshold level(%) * the average of real electrons are removed(ignored)

!

!

!

! FIELD NODE SAMPLING

!

!

! iNumNodesX Number of nodes to sample radiation field in x direction

! iNumNodesY Number of nodes to sample radiation field in y direction

! nodesPerLambdar Number of nodes per resonant wavelength

! sFModelLengthX Length of radiation field model in x direction

! sFModelLengthY Length of radiation field model in y direction

! sWigglerLengthZ2 Length of field model in z2-bar direction

! iRedNodesX Length of central field section in x where electrons will not leave

! iRedNodesY Length of central field section in y where electrons will not leave

! sFiltFrac Specifies cutoff for high pass filter as fraction of resonant frequency - used in diffraction step

! sDiffFrac Specifies diffraction step size as fraction of the undulator period

! beta Absorption coefficient

! seed_file Name of the seed file

!

!

! INDEPENDANT VARIABLES

!

! Input the scaled independant variables from [1] here

!

! srho Pierce or FEL parameter, describing the strength of the interaction (or efficiency)

! sux Normalised magnitude of wiggler magnetic field x-vector: H=1 is helical, H=0 is planar

! suy Normalised magnitude of wiggler magnetic field y-vector: H=1 is helical, H=0 is planar

! saw peak undulator parameter

! sgamma_r Resonant, or reference, beam energy

! lambda_w Undulator period

! Dfact Dispersive strength factor for chicane

! zundType Undulator type - 'curved' , 'planepole' , else 1D (no off axis variation of aw)

! taper gradient of taper - d/dz of alpha

!

! INTEGRATION AND OUTPUT

! Here,a lattice file can be input to specify an undulator-chicane lattice.

```
! If it is specified, then the value of nPeriods and stepsPerPeriod supplied

! here is ignored. Otherwise the values below are used in a basic single undulator

! setup.

!

! lattFile Name of lattice file (optional).

! stepsPerPeriod Number of steps per wiggler period

! nPeriods Number of wiggler periods

! sZ0 Starting zbar position

! zDataFileName Data file name

! iWriteNthSteps Steps to write data at

! iWriteIntNthSteps Steps to write integrated data at

! iDumpNthSteps Steps to dump data at (0 for no dumping)

! sPEOut Percentage of macroparticles to write out

!

! Begin input:-

&MDATA

! meshtype = 1

! sperwaves = 1

qFMesh_G = .false.

qScaled = .true.
```

qOneD = .false.

qFieldEvolve = .true.

qElectronsEvolve = .true.

qElectronFieldCoupling = .true.

qFocussing = .false.

qDiffraction = .true.

qFilter = .true.

q_noise = .true.

qDump = .false.

qResume = .false.

qSeparateFiles = .false.

qFormattedFiles = .false.

qWriteZ = .true.

qWriteA = .true.

qWritePperp = .true.

qWriteP2 = .true.

qWriteZ2 = .true.

qWriteX = .true.

qWriteY = .true.

qsdds = .false.

qhdf5=.true.

qUndEnds = .true.

beam_file = 'beam_file.in'

sElectronThreshold = 0.05

iNumNodesX = 240

iNumNodesY = 240

nodesPerLambdar = 20

sFModelLengthX = 7.5

sFModelLengthY = 7.5

sFModelLengthZ2 = 140

iRedNodesX = 20

iRedNodesY = 20

sFiltFrac = 0.3

sDiffFrac = 1.0

sBeta = 1.0

seed_file = ''

srho = 0.02078

sux = 0.0

suy = 1.0

saw = 1.5

sgamma_r = 486.13

lambda_w = 0.015

Dfact = 0.0

zundType = 'planepole'

taper = 0.0

lattFile = ''

stepsPerPeriod = 30

nPeriods = 300

sZ0 = 0.0

zDataFileName = 'DataFile.dat'

iWriteNthSteps = 300

iWriteIntNthSteps = 30

iDumpNthSteps = 3000

sPEOut = 100.0

! sKBetaXSF = 1.15

! sKBetaYSF = 1.15

D.3 -3D Puffin variable

Variable	Mathematical Definition	Description
$\bar{z}$	$\frac{z}{l_g} = 2k_w\rho z$	Scaled propagation distance
$\bar{z}_2$	$\frac{(ct-z)}{l_c} = 2k\rho z$	Scaled time coordinate
l_g	$\frac{\lambda_w}{4\pi\rho}$	Exponential gain length
l_c	$\frac{\lambda_r}{4\pi\rho}$	Cooperation length
$E_\perp$	$E_x - iE_y$	Perpendicular radiation field
$p_\perp$	$p_x - ip_y$	Perpendicular electron momentum
$A_\perp$	$\frac{e\sqrt{f_x^2+f_y^2}}{\sqrt{2}mc\omega_p\sqrt{\gamma_r\rho}}E_\perp$	Scaled perpendicular field
A	$\frac{e\sqrt{f_x^2+f_y^2}}{\sqrt{2}mc\omega_p\sqrt{\gamma_r\rho}}\xi_0$	Scaled field envelope
η	$\frac{1-\beta_z}{\bar{\beta}_z}$	Scaled average z velocity of electrons
p_{2j}	$\frac{1}{\eta}\frac{1-\beta_{zj}}{\beta_{zj}}$	Scaled instantaneous energy
$\bar{p}_\perp$	$\frac{p_\perp}{mc}$	Scaled perpendicular electron momentum
$\bar{x}$	$\frac{x}{\sqrt{l_g l_c}}$	Scaled x coordinate
$\bar{y}$	$\frac{y}{\sqrt{l_g l_c}}$	Scaled y coordinate